Indoor Cooperative Localization for Ultra Wideband Wireless Sensor Networks

A Dissertation
Submitted to the Faculty
of the
WORCESTER POLYTECHNIC INSTITUTE
in partial fulfillment of the requirements for the
Degree of Doctor of Philosophy
in
Electrical and Computer Engineering

by

Nayef Alsindi

April 2008

APPROVED

_____

Prof. Kaveh Pahlavan, Advisor

_____

Prof. Fred J. Looft, Head, ECE Department

To My Wife

Abstract

In recent years there has been growing interest in ad-hoc and wireless sensor networks (WSNs) for a variety of indoor applications. Localization information in these networks is an enabling technology and in some applications it is the main sought after parameter. The cooperative localization performance of WSNs is ultimately constrained by the behavior of the utilized ranging technology in dense cluttered indoor environments. Recently, ultra-wideband (UWB) Time-of-Arrival (TOA) based ranging has exhibited potential due to its large bandwidth and high time resolution. However, the performance of its ranging and cooperative localization capabilities in dense indoor multipath environments needs to be further investigated. Of main concern is the high probability of non-line of sight (NLOS) and Direct Path (DP) blockage between sensor nodes, which biases the TOA estimation and degrades the localization performance.

In this dissertation, we first present the results of measurement and modeling of UWB TOA-based ranging in different indoor multipath environments. We provide detailed characterization of the spatial behavior of ranging, where we focus on the statistics of the ranging error in the presence and absence of the DP and evaluate the pathloss behavior in the former case which is important for indoor geolocation coverage characterization. Parameters of the ranging error probability distributions and pathloss models are provided for different environments: traditional office, modern office, residential and manufacturing floor; and different ranging scenarios: indoor-to-indoor (ITI), outdoor-to-indoor (OTI) and roof-to-indoor (RTI).

Based on the developed empirical models of UWB TOA-based OTI and ITI ranging, we derive and analyze cooperative localization bounds for WSNs in the different indoor multipath environments. First, we highlight the need for cooperative localization in indoor applications. Then we provide comprehensive analysis of the factors affecting localization accuracy such as network and ranging model parameters.

Finally we introduce a novel distributed cooperative localization algorithm for indoor WSNs. The Cooperative LOcalization with Quality of estimation (CLOQ) algorithm integrates and disseminates the quality of the TOA ranging and position information in order to improve the localization performance for the entire WSN. The algorithm has the ability to reduce the effects of the cluttered indoor environments by identifying and mitigating the associated ranging errors. In addition the information regarding the integrity of the position estimate is further incorporated in the iterative distributed localization process which further reduces error escalation in the network. The simulation results of CLOQ algorithm are then compared against the derived G-CRLB, which shows substantial improvements in the localization performance.

Acknowledgements

I am extremely grateful to Professor Kaveh Pahlavan for his support and guidance throughout my graduate studies. What I have learned from him was truly beyond academics and research for he has spurred the growth of my professional career. I have learned from his experiences and stories that carry many lessons in dealing with life's choices and struggles. I am sure that I will always revisit them to seek inspiration.

I would like to thank my dissertation committee members, Professor John Orr, Professor Allen Levesque, Professor Alexander Wyglinski and Professor Xinrong Li for their valuable suggestions, comments and encouragements.

My graduate experience at WPI was simply remarkable and for that I have to thank and acknowledge my best friends who shared with me all my setbacks and successes throughout the last 6 years. They are Engin Ayturk, Mohammad Heidari, Hamid Ghadyani, Bardia Alavi, Erdinc Ozturk, and Ferit Akgul.

Finally, my accomplishments were only possible because of my wife's continuous support, encouragement and motivation. Dr. Abeer Al-naqbi has provided me with the strength to persevere and succeed in the face of many adversities. I am also indebted to my father, Dr. Ali Alsindi and mother Mrs. Manar Fakhri for their support and investment in my upbringing and education. Also I would like to thank my brother and sisters who are also my best friends: Dr. Fahad Alsindi, Noora Alsindi and Muneera Alsindi.

Table of Contents

List of Figures

List of Tables

Chapter 1 Introduction

1.1. Localization in Wireless Sensor Networks

In recent years there has been growing interest in ad-hoc and wireless sensor networks (WSNs) for a variety of applications. The development of microelectromechanical systems (MEMS) technology as well as the advancement in digital electronics and wireless communications has made it possible to design small size, low-cost energy efficient sensor nodes that could be deployed in different environments for a variety of applications [Aky02]. Node localization is an enabling technology for WSNs because sensor nodes deployed in an area of interest usually need position information for routing and application-specific tasks, such as temperature and pressure monitoring [Pat05]. In many applications, a WSN is deployed to help improve localization accuracy in environments where the channel condition poses a challenge to range estimation [Pah06]. In such environments, cooperative localization provides a potential for many applications in the commercial, public safety and military sectors [Pah06, Pah02]. In commercial applications, there is a need for localizing and tracking inventory items in warehouses, materials and equipment in manufacturing floors, elderly in nursing homes, medical equipment in hospitals, and objects in residential homes. In public safety and military applications, however, indoor localization systems are needed to track inmates in prisons and navigate policemen, fire fighters and soldiers to complete their missions inside buildings [Pah02]. Node localization plays an important role in all these WSN applications.

In certain vital indoor cooperative localization applications, such as fire-fighting and military operations, a small number of sensors called anchors are deployed outside surrounding a building where they obtain their location information via GPS or are pre-programmed during setup. The un-localized sensor nodes are then deployed inside the building, e.g. carried by firefighters or soldiers entering a hostile building, who with the help of the anchors attempt to obtain their own location information. In traditional approaches, such as trilateration (triangulation) techniques, the exterior anchor nodes usually fail to cover a large building, which makes localization ineffective. In addition, the problems of indoor multipath and non-line-of-sight (NLOS) channel conditions further degrade the range estimates, yielding unreliable localization performance [Pah02]. Implementation of the cooperative localization approach *extends* the coverage of the outside anchors to the inside nodes and has the ability to enhance localization accuracy through the availability of more range measurements between the sensor nodes.

Effective cooperative localization in indoor WSNs does however hinge on the ranging technology. Among the emerging techniques, Ultra Wideband (UWB) Time of Arrival (TOA)-based ranging has recently received considerable attention [Gez05, Gha04, Opp04]. In addition to its high data rate communications, it has been selected as a viable candidate for precise ranging and localization. This is mainly due to its large system bandwidth which offers high resolution and signaling that allows for centimeter accuracies, low-power and low-cost implementation [Por03, Gez05]. The performance of this technique, nevertheless, depends on the availability of the direct path (DP) signal between a pair of sensor nodes [Lee02, Pah98]. In the presence of the DP, i.e. short distance line-of-sight (LOS) conditions, accurate UWB TOA estimates in the range of

centimeters are feasible due to the high time-domain resolution [Fon02, Chu03, Ala06, Tar06]. However, the challenge is UWB ranging in indoor NLOS conditions, which can be characterized as dense multipath environments [Lee02, Pah98]. In these conditions the DP between a pair of nodes can be blocked with high probability, substantially degrading the range and localization accuracy. Therefore, there is a need to analyze the impact of these channel limitations on the performance of cooperative localization in indoor WSNs.

This dissertation is concerned with the evaluation of cooperative localization in indoor WSNs from the radio propagation channel perspective. We intend to provide detailed analysis on the impact of the indoor multipath and NLOS conditions on the UWB TOA-based ranging and cooperative localization in WSNs. Next we provide detailed description of the motivation and contributions of the dissertation.

1.2. Background and Motivation

Indoor localization is one of the newly emerging technologies having potential for numerous applications in the commercial and public safety fields. The enabling of robust and accurate localization in harsh indoor environment faces real physical challenges, especially for TOA-based systems where the probability of NLOS and blockage of the DP between mobile nodes is very high [Pah98, Pah02]. The main challenges in these environments are multipath, NLOS propagation, DP blockage and insufficient signal coverage. Several techniques have been proposed to combat multipath for low bandwidth systems [Dum94, Li04]. These techniques have the potential to increase the time-domain resolution of the received waveform, mitigate multipath in indoor environments and

improve TOA ranging accuracy. Recently, UWB signals have showed promising potential for accurate TOA-based ranging and localization due to the available excess system bandwidth [Fon02, Lee02, Mol05]. However, these algorithms and techniques still suffer in harsh NLOS propagation and DP blockage environments where the degradation of the DP signal causes substantial ranging errors [Pah06]. Fortunately, the majority of the current research thrust in NLOS localization has been towards NLOS or DP blockage identification and mitigation [Che99, Wei05, Gev07, Hei07, Ven07a, Ven07b, Als08c]. The localization performance using these techniques have showed promising potential, where the channel statistics and signal information are incorporated in a decision theoretic framework to mitigate "bad" estimates before incorporation into localization algorithms.

Although these algorithms and techniques can improve the localization performance, they still face further physical limitations specific to the indoor environment. In outdoor GPS applications the accuracy is directly related to the Geometric Dilution of Precision (GDOP) where the number of satellites in view and their locations relative to the mobile user can have significant impact on the performance [Kap96]. Similarly, in indoor environments a large number of Reference Points (RPs) or anchors are needed in order to achieve acceptable levels of accuracy [Pah06]. For the majority of indoor applications the limited radio coverage of RPs/anchors in large buildings implies that there exists a high probability of insufficient coverage to enable effective localization [Pah06]. More importantly for the outdoor-indoor applications such as the firefighting or military operations the radio coverage is further diminished due to the signal having to penetrate

external building structures. This then poses questions as to the reliability and accuracy of TOA-based localization systems under these constraints.

One promising alternative to these challenges in indoor environments is UWB TOA-based cooperative localization using WSNs [Pah06, Gez05]. Unlike traditional localization techniques, cooperative localization in WSNs allows for ranging information to be exchanged between nodes and anchors as well as nodes and other nodes in the network. Coupled with UWB TOA-based ranging, cooperative localization has the potential to remedy many of the problems and challenges plaguing indoor localization applications. The UWB signals will allow for high resolution and thus very accurate ranging capability. In addition, cooperative localization will provide the ability to combat the NLOS/DP-blockage and limited coverage problems due to the redundancy in TOA-range information connecting the network.

In 2005, the Center for Wireless Information Network Studies (CWINS) at WPI with Innovative Wireless Technologies (IWT) were awarded a research fund sponsored by DARPA/DoD SBIR: BAA 03-029 entitled: “Innovative Methods for Geolocation and Communication with Ultra Wideband Mobile Radio Networks”. The project spanned different aspects of UWB localization. IWT were responsible for the design and implementation of the UWB radios while CWINS took charge of characterizing the empirical behavior of TOA-based ranging using UWB. As a result the foundation of this dissertation is the UWB measurement campaign that was conducted in the summer of 2005. The measurements provided a platform for evaluating the behavior of the UWB TOA-based ranging in different indoor environments.

In order to asses the potential of UWB cooperative localization in indoor environments, however, it is important to develop an analytical framework that addresses the different layers of the problem. At the ranging layer, understanding the behavior of UWB TOA-based ranging in indoor environments is essential. This can be accomplished by conducting UWB measurements and modeling of the TOA-based ranging. Several indoor propagation experiments with a focus on indoor ranging, be it UWB or otherwise, have been reported in the literature [Fon02, Lee02, Pah98, Ala03a, Tar06, Den04, Fal06, Ala06, Pat03, Hat06, Ala05, Low05]. These experiments have usually been limited to a floor or several rooms but do not address modeling the spatial statistics of NLOS ranging nor ranging coverage. The only available ranging error models were provided in [Den04, Ala06] but are based on limited measurement data sets, and only the latter focuses on characterization of errors according to the availability of the DP. As a result, a comprehensive measurement and modeling of UWB TOA-based ranging in different indoor environments and scenarios is needed but is not available in the literature.

At the localization layer, these ranging models should be used to evaluate the impact of the radio propagation channel on cooperative localization in indoor WSNs. In turn this could be achieved by integrating the empirical models in developing theoretical performance bounds (e.g. CRLB-type bounds) and assessing the accuracy of cooperative localization algorithms. In the literature, localization bounds in multi-hop WSNs have been examined extensively [Lar04, Sav05, Cha06], where the focus has been on analyzing the impact of network parameters such as the number of anchors, node density and deployment topology affecting localization accuracy, etc. However, these localization bounds have been analyzed with unbiased generic ranging assumptions

between sensor nodes. In [Koo98, Bot04] the impact of biased TOA range measurements on the accuracy of location estimates is investigated for cellular network applications. Their approach assumes NLOS induced errors as small perturbations, which clearly is not the case in indoor environments. A comprehensive treatment of the impact of biases on the *traditional* wireless geolocation accuracy in NLOS environments is reported in [Qi06]. Recently, position error bounds for dense cluttered indoor environments have been reported in [Jou06a, Jou06b] where the impact of the channel condition on the localization error is further verified in traditional localization. As a result there is a need for the derivation and analysis of the theoretical performance bounds for UWB cooperative localization in indoor-specific WSNs.

Another important research direction in this emerging field is the development of cooperative localization algorithms for WSNs. Unfortunately, most of the algorithms in the literature are generic and they do not address the impact of the indoor propagation channel on the ranging and localization performance [Savr01, Savr02, Alb01, Nic01]. Although those algorithms might yield unacceptable performance in indoor environments, they provide practical ideas for localizing nodes in large sensor networks. Therefore, there is a need for novel cooperative localization algorithms that are specifically designed for the harsh indoor environment.

The principle goal of this research work is to develop an analytical framework for assessing the impact of the indoor propagation channel on the performance of UWB TOA-based cooperative localization in WSNs. Specifically we define three major objectives of this research work. The first is to conduct large-scale measurements and modeling of the UWB TOA-based ranging in indoor multipath environments. The second

is to incorporate these empirical measurements and models into an analytical framework that can be used to assess the impact of indoor ranging on cooperative localization. The third objective of this work is to develop a novel cooperative localization algorithm that has the ability to improve localization accuracy by incorporating the channel statistics in the estimation process. The algorithm takes advantage of the models and attempts to quantify the quality of ranging and localization in order to improve the performance.

1.3. Contributions of the Dissertation

In this dissertation we first provide an overview of the basics of cooperative localization and the challenges facing this emerging technology where the impact of the channel on the localization performance is highlighted and the major cooperative localization bounds and algorithms are discussed. This work is presented in Chapter 2 and has been published in [Als08d]. Then we present the research work which focuses on three contributions to the field of WSN localization:

- Analysis, measurement and modeling of UWB TOA-based ranging in indoor multipath environments. The work presents empirical results of the measurement campaign in four different building environments: residential, traditional office, modern office and a manufacturing floor; and three different ranging scenarios: Indoor-to-Indoor (ITI), Outdoor-to-Indoor (OTI) and Roof-to-Indoor (RTI) using two different UWB system bandwidths. These empirical measurements are used to develop novel models that characterize TOA-based ranging coverage and error. Specifically the former model provides a characterization for the feasible ranging distance in indoor environments; while the latter provides statistical

characterization of ranging error in the different conditions such as LOS, NLOS and DP blocked NLOS. This work is presented in Chapter 3 of the dissertation and has been published in [Als07a, Als07b, Als08a].

- Analytical derivation and performance evaluation of the cooperative localization in WSNs through the Generalized Cramer Rao Lower Bound (G-CRLB) in dense cluttered indoor environments. Using the empirical TOA-based ranging models, we provide a novel framework for analyzing the performance of cooperative localization for WSNs in different indoor environments using two different systems bandwidths, 500 MHz and 3 GHz. The work focuses on analyzing the impact of node density, anchor density, building dimension and probability of NLOS and probability of DP blockage on the cooperative localization performance. This research work is presented in Chapter 4 and has been published in [Als08b].
- Development of a novel cooperative localization algorithm for indoor WSNs. We introduce Cooperative LOcalization with Quality of estimation (CLOQ) which is a novel algorithm that integrates the quality of the range (channel information) and node position (anchor confidence) in a weighted least square technique to provide accurate location information. This work is presented in Chapter 5 and has been published in [Als06a, Als06b].

1.4. Outline of the Dissertation

This dissertation focuses on node localization in UWB WSNs. First we will introduce the fundamental concepts related to node localization, discuss the major challenges for

node localization in WSNs, and present the major node localization techniques proposed for WSNs. In Chapter 3 we discuss the basics of UWB TOA-based ranging and their application to ranging and localization. We then introduce a comprehensive measurement campaign to evaluate the UWB TOA based ranging in four different indoor building environments and three different ranging scenarios: ITI, OTI and RTI. Using these measurements we develop and introduce novel models that characterize empirically the behavior of ranging coverage and error in dense cluttered indoor environments. In Chapter 4, we derive and evaluate the G-CRLB for UWB TOA-based cooperative localization in indoor WSNs using the empirical models. We then analyze and compare the localization performance in different indoor environments. In Chapter 5, we introduce the novel cooperative localization algorithm (CLOQ) and evaluate its performance against the G-CRLB. Finally we conclude the dissertation in Chapter 6, where we provide the major conclusions and suggest future work.

Chapter 2 Node Localization in Indoor Environments: Concepts and Challenges

In this chapter, we first introduce the evolution of localization technologies, and then we describe the basics of localization in traditional network settings. Finally, we introduce the main approaches to cooperative localization in WSNs and discuss the major challenges affecting their performance.

2.1. Evolution of Localization Techniques

The problem of locating mobile radios originated with military operations during World War II, where it was critical to locate soldiers in emergency situations. About twenty years later, during the Vietnam conflict, the US Department of Defense launched a series of Global Positioning System (GPS) satellites to support military operations in combat areas. In 1990, the signals from GPS satellites were made accessible to the private sector for commercial applications such as fleet management, navigation, and emergency assistance. Today, GPS technology is widely available in the civilian market for personal navigation applications. Despite its success, however, the accuracy of GPS positioning is significantly impaired in urban and indoor areas, where received signals can suffer from blockage and multipath effects.

In 1996, the Federal Communications Commission (FCC) introduced regulations requiring wireless service providers to be able to locate mobile callers in emergency situations with specified accuracy, namely 100 meters accuracy 67% of the time. Such

emergency service is called E-911 in the U.S. and E-112 in many other countries. In a manner similar to the release of the ISM bands and subsequent emergence of the wireless local area network (WLAN) industry, the FCC mandate for E-911 services quickly gave rise to the development of the wireless geolocation industry. In time, technologies have been developed to implement the E-911 mandate [Caf98, McG02] including GPS assisted techniques, a variety of Time of Arrival (TOA), Angle of Arrival (AOA), and Received Signal Strength (RSS) techniques. A variety of TOA, time differential (TDOA) or extension of time differential (EOTD) techniques require special location-measurement hardware integrated in the base stations and in some cases accurate synchronization between the mobile terminals and base stations (for cellular applications). In contrast with those approaches, RSS systems provide a lower-cost solution that can avoid additional hardware installation but does require incorporating training functions into the system.

In the late 1990s, at about the same time that E-911 technologies were emerging, another initiative for accurate indoor geolocation began independently. It was motivated by a variety of envisioned applications for indoor location-sensing in commercial, public safety, and military settings [Pah02, Kos00, Pot00]. In commercial applications for residences and nursing homes, there is an increasing need for indoor location-sensing systems to track people with special needs, e.g., the elderly, as well as children who are away from visual supervision. In public safety and military applications, indoor location sensing systems are needed to track inmates in prisons and to guide policemen, fire-fighters, and soldiers in accomplishing their missions inside buildings. More recently, location sensing has found its applications in location-based handoffs in wireless

networks [Pah00], location-based ad-hoc network routing [Ko98, Jai01], and location-based authentication and security [Sma00]. These and other applications have stimulated interests in modeling the propagation environment to assess the accuracy of different sensing techniques [Pah98, Kri99] as well as in developing novel technologies to implement the systems [Fon02, Bah00a, Bah00b]. The implementation of the first generation of indoor positioning products using a variety of technologies has been reported in [Wer98, Roo02a, Roo02b].

The natural evolution of these ranging and localization technologies makes their integration into WSN applications possible. Understanding the fundamental concepts and challenges of these technologies in traditional localization is a necessary bridge to WSN localization.

2.2. Localization Systems

In general, a localization system incorporates range measurements to determine the location estimate. Figure 2.1 illustrates a block diagram of the main components in a traditional localization system.

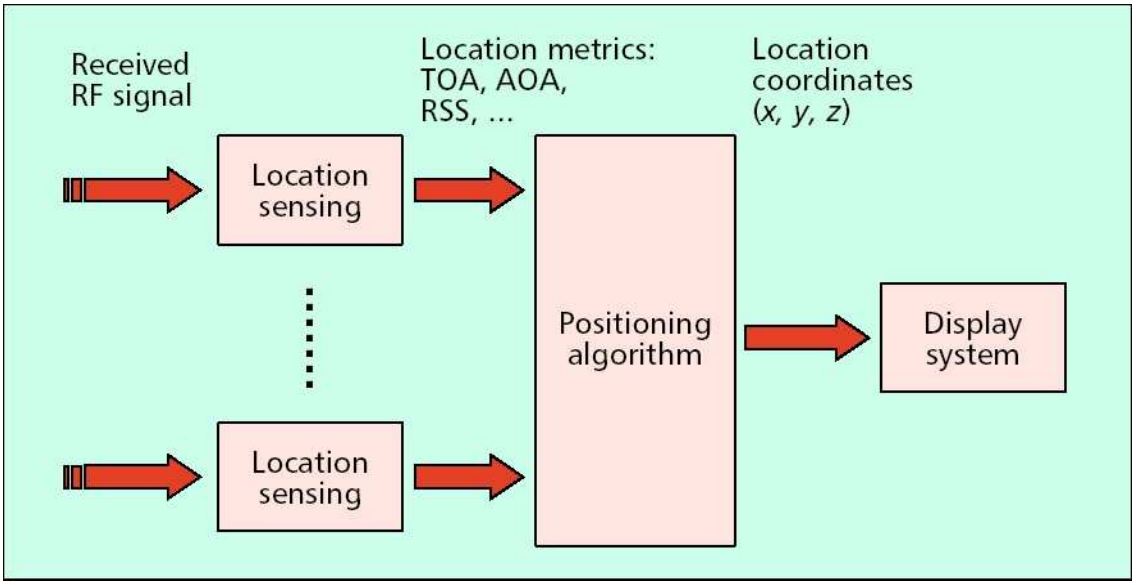

Figure 2.1: Localization block diagram.

The process for obtaining a location estimate involves different levels of complexities. At the physical layer, the mobile terminal (MT) or the sensor node receives a waveform from Reference Points (RP) or anchors. In the context of traditional localization an MT listens to ranging signals from at least 3 different RPs for 2-dimensinoal position. In WSNs cooperative localization MTs are usually referred to as nodes or *blind* nodes, while RPs are referred to as anchors. From this RF waveform, it is possible to extract the relevant range measurements.

In RSS systems, for example, the total signal energy that a node/MT receives from an anchor/RP can be used to estimate the distance. For a given received power, it is possible to estimate the corresponding distance with some certainty. The RSS technique is usually simple to implement but suffers from inaccuracies, especially in multipath rich environments. On the other hand, for TOA-based systems, the distance is estimated by

sending an RF signal and recording the time it takes to receive it. This approach is more accurate because the arrival time corresponds to the direct path distance.

Once 3(4) range measurements are obtained from different anchors/RPs, the node/MT passes this information to a positioning algorithm, where the 2(3)-dimensional position is then estimated. The range measurements essentially constrain the possible location of the MT. The area of uncertainty of a location estimate decreases as the accuracy of range measurements improves. Figure 2.2 shows an example of 2-dimensional localization, where a node/MT has 3 range measurements to different anchors/RPs. The positioning error, as will be described later in more detail, is affected by the accuracy of the range measurements, the number of anchors/RPs and their relative geometry to the sensor node/MT. Finally, the estimate of the location is displayed to the user with information regarding its quality or accuracy.

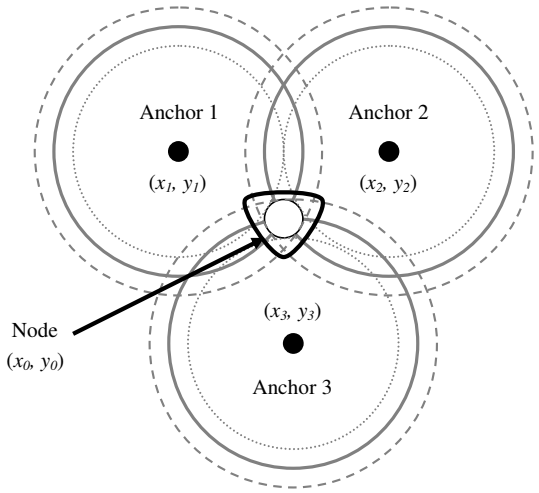

Figure 2.2: Localization with 3 anchors.

WSN localization is a general case of the traditional localization but it is fundamentally dependant on the building blocks in Figure 2.1. As a result, we will dedicate the first part of this chapter to ranging and localization techniques in traditional network settings and the second part to localization in WSNs. Understanding of ranging techniques and localization algorithms is essential in building a fundamental basis for WSN cooperative localization. First, we describe the two most popular ranging techniques that are used traditionally in wireless networks, which have a great potential for WSNs. Specifically, we show that the ranging accuracy and localization performance is directly related to the complexity of the wireless channel. Then we discuss popular localization algorithms commonly implemented in systems such as GPS and cellular geolocation. Finally, we relate these concepts to cooperative localization in WSNs, and describe some of the emerging centralized and distributed solutions to the problem.

2.3. Popular Ranging Techniques

2.3.1. TOA-based Ranging

In TOA-based ranging, a sensor node measures the distance to another node by estimating the signal propagation delay in free space, where radio signals travel at the constant speed of light. Figure 2.3 shows an example of TOA-based ranging between two sensors.

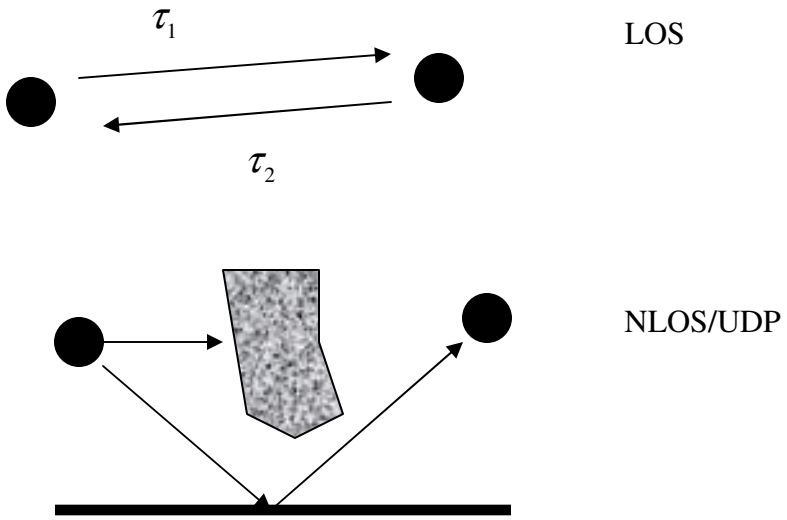

Figure 2.3: TOA ranging between sensors. The TOA can be measured by recording the time it takes to transmit and receive a packet between two nodes. If however, the direct path signal is block then the time delay or distance estimation is biased which can cause significant errors in the localization process.

The performance of TOA-based ranging depends on the availability of the DP signal [Pah98, Pah02]. In its presence, such as short distance LOS conditions, accurate estimates are feasible (see Figure 2.4).

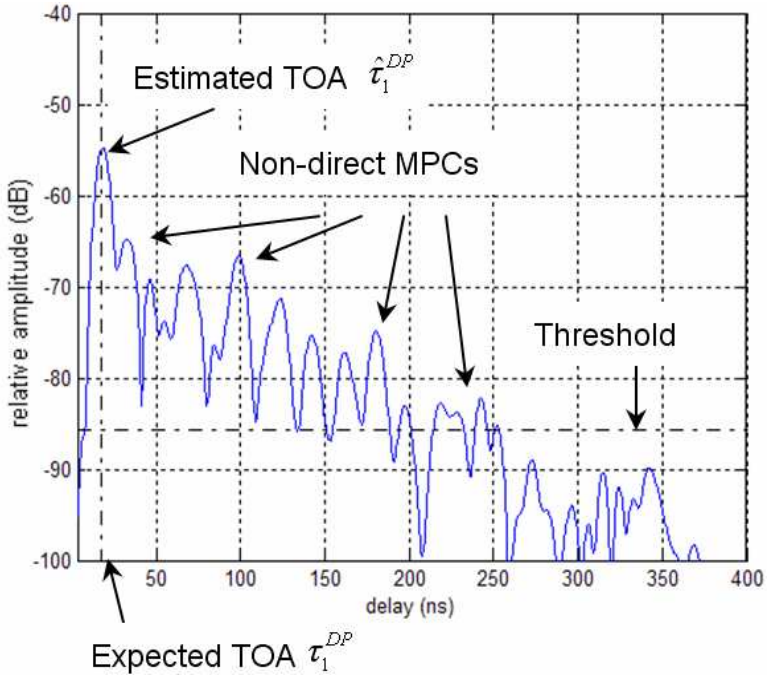

Figure 2.4: TOA estimation in the presence of DP. The accuracy of TOA estimation depends on the availability of the DP signal. In this case, the DP signal power is well above the detection threshold and thus can provide accurate distance estimation.

However, the challenge is ranging in NLOS conditions, which can be characterized as site-specific and dense multipath environments [Pah98, Lee02]. These environments introduce several challenges. The first, also present in LOS conditions, corrupts the TOA estimates due to the multipath components (MPCs). MPCs are delayed and attenuated replicas of the original signal, arriving and combining at the receiver thus shifting the estimate. The second is the propagation delay caused by the signal traveling through obstacles, which adds a positive bias to the TOA estimates. The third is the absence of the DP due to blockage, also known as Undetected Direct Path (UDP) [Pah98]. The bias imposed by this type of error is usually much larger than the first two and has a significant probability of occurrence due to cabinets, elevator shafts, or doors that are

usually cluttering the indoor environment. A sample measurement profile of this condition is illustrated in Figure 2.5 which illustrates TOA ranging in the absence of the DP.

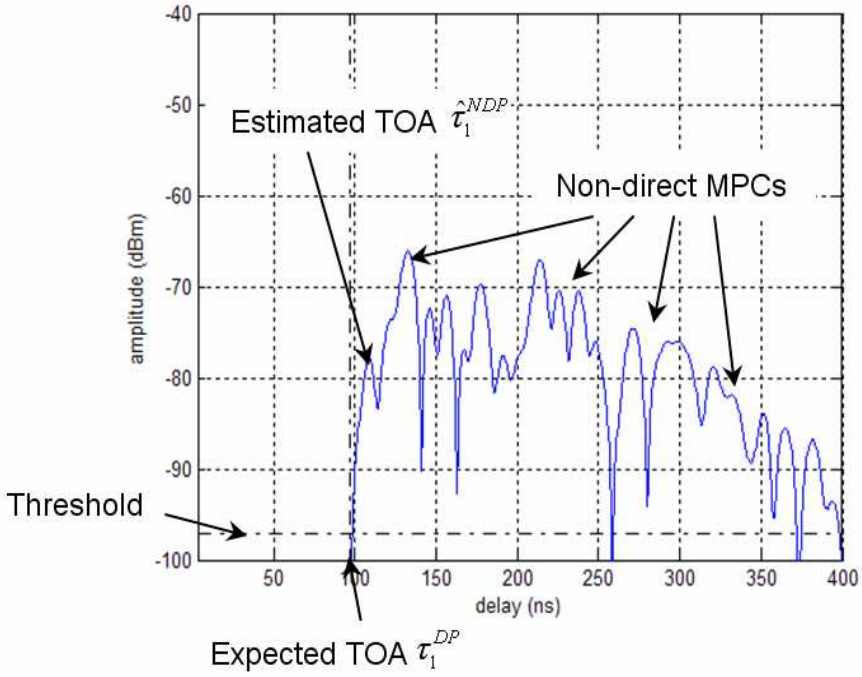

Figure 2.5: TOA estimation in the absence of the DP. In this condition, the DP signal power is attenuated and cannot be detected. As a result the first arriving path is used for TOA ranging instead causing significant estimation errors.

As a result for effective TOA-based ranging and localization it is important for a node to be able to distinguish between these two cases. Although TOA-based systems are more accurate compared to RSS or AOA systems, their implementation is usually more complex and they suffer severely in impaired indoor environments.

2.3.2. RSS-based Ranging

Ranging through RSS is accomplished by sensing the received signal and measuring the total received power, which can provide a distance estimate between the target object and the location sensor. The average RSS at a certain distance is given by

$$RSS_d = \sum_{i=1}^{L} \overline{|\alpha_i^d(t)|^2}, \tag{2.1}$$

where α is the amplitude of the arriving paths. Figure 2.6 shows a ranging example using the RSS-based technique. The measurement of the average RSS is independent of the bandwidth of the measurement device.

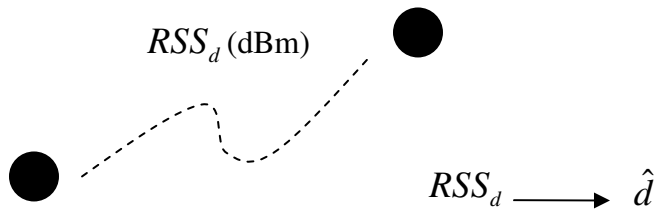

Figure 2.6: Ranging using RSS is implemented by estimating the distance from the signal power. A sensor node measures the received power from another node and translates that into an estimated distance. The distance estimates using this technique lack accuracy due to the method's reliance on pathloss models and the indirect relationship between power and distance.

In wideband measurements, the effect of multipath fading is averaged over the spectrum of the signal. This is done through measuring the strength of each arriving path and using Eq. (2.1) to compute the RSS. According to the multipath fading characteristics, only one arriving pulse with fluctuating amplitude is received. As a result, averaging the signal over a longer period can effectively eliminate multipath. In addition to the independence

of the ranging error in RSS to the system bandwidth, this technique is relatively simple and reliable. Nonetheless, the relationship between the measured RSS and the distance is complex and diversified. Therefore, the performance of these techniques depends on the accuracy of the model used for estimation of the RSS.

A number of statistical models relating the behavior of the RSS to the distance between a transmitter and a receiver in indoor areas have been developed for wireless communications [Pah02]. These models can be used for estimating the ranging distance between two nodes. The common principle behind all statistical models for calculation of the *RSS* in a distance *d* is given by

$$RSS_d = 10\log_{10} P_r = 10\log_{10} P_t - 10\gamma \log_{10} d + X \,, \tag{2.2}$$

where P_t is the transmitted power, d is the distance between the transmitter and the receiver, γ is the so-called distance-power gradient of the environment, and X is a lognormal random variable representing the shadow fading component. Since the location sensor using RSS does not know the exact value of γ and X, the distance calculated from these models is not as reliable as its TOA counterpart.

2.4. Wireless Localization Algorithms

2.4.1. Background

Using range estimates from multiple anchors, it is possible to employ simple geometrical triangulation techniques to estimate the location of a sensor. Due to estimation errors in the acquired TOA ranges, for example, the geometrical triangulation technique can only provide a region of uncertainty, instead of a single position fix for a

sensor node. To obtain an estimate of the location coordinates, a variety of direct and iterative statistical positioning algorithms have been developed to solve the problem by formulating it into a set of non-linear iterative equations. In some wireless geolocation applications, the purpose of the positioning systems is to provide a visualization of the possible mobile locations instead of an estimate of the location coordinates. In either case, the position accuracy is not constant across the area of coverage and poor geometry of relative position of the mobile terminal and RPs can lead to high geometric dilution of precision (GDOP). Further, geometric and statistical triangulation algorithms are used when both the region of uncertainty and the estimate of the location are required [Kap96]. Localization algorithms with well-defined properties, such as the least squares (LS) algorithm and maximum-likelihood algorithm, are available for satellite-based GPS systems. In addition, there are various types of sequential filters, including formulations, which adaptively estimate some unknown parameters of the noise processes [Mis02, Kap96]. In particular, GPS has focused a great deal of attention on positioning algorithms based on TOA with considerable success. GPS can provide positioning accuracy ranging from tens of meters to centimeters in real time depending upon a user's resources [Mis02]. In essence, these techniques are readily applicable to indoor location sensing systems. However, indoor location sensing involves quasi-stationary applications and a number of unreliable reference points for which the existing GPS algorithms, designed for mobile systems with a few reliable reference points, do not provide the optimum solution.

Geometrical techniques are based on iterative algorithms that estimate the node position by formulating and solving a set of non-linear equations. When the statistics of

the ranging error, be it TOA or RSS, are not available *a priori*, the LS algorithms can provide the best solution. However, if the statistics of the ranging error are available, a WLS algorithm can be implemented, which weighs the range measurements with the variance of the respective error distributions. Thus the availability of the range error information can substantially improve the accuracy of the localization process. Again, it is important to realize that the distribution of the ranging error is directly related to the RF wireless propagation channel.

2.4.2. Least Squares (LS) Algorithm

Estimating a node's position in 2(3) dimensions requires range information to at least 3(4) anchors/RPs. For the sake of simplicity, we will provide an analysis for 2-dimensional localization and an extension to higher dimensions can be easily obtained. Let $\boldsymbol{\theta} = [x, y]$ be the sensor node's x- and y-coordinates and let $\boldsymbol{\varphi}_i = \left[x_i^a, y_i^a\right]$ denote the coordinates of the *ith* anchor, where $i \in \{1,\ldots,M\}$. The range estimate between the *ith* anchor and the sensor node is then given by

$$\hat{d}_i = \left\|\boldsymbol{\theta} - \boldsymbol{\varphi}_i^a\right\| + \varepsilon_i + \tilde{z}_i = \sqrt{\left(x - x_i^a\right)^2 + \left(y - y_i^a\right)^2} + \varepsilon_i + \tilde{z}_i, \tag{2.3}$$

where ε_i is the ranging error and $\tilde{z}_i$ is additive measurement noise. Note that the statistics of ε_i are not necessarily identically distributed. In indoor environments, the ranging error will experience different means and variances depending on the distances between the nodes and the blockage condition. Also for the sake of simplicity and noting that the errors induced by the channel are substantially more significant than synchronization errors, we assume that the nodes involved in localization are synchronized. Given *M* noisy measurements to respective anchors, it is possible to obtain

an estimate of the sensor node location $\hat{\boldsymbol{\theta}}$. Figure 2.2 shows an example of 2-dimensional localization with 3 noisy measurements from the respective anchors.

The problem of LS localization is essentially to obtain a solution from a set of nonlinear equations given by [Kay93]

$$\mathbf{F}(\boldsymbol{\theta}) = \begin{bmatrix} \sqrt{(x - x_1^a)^2 + (y - y_1^a)^2} \\ \vdots \\ \sqrt{(x - x_M^a)^2 + (y - y_M^a)^2} \end{bmatrix}, \tag{2.4}$$

where the nonlinear problem in (2.4) requires minimizing the cost function given by [Kay93]

$$E\left[\hat{\boldsymbol{\theta}}\right] = \left[\mathbf{d} - \mathbf{F}\left(\hat{\boldsymbol{\theta}}\right)\right]^T \left[\mathbf{d} - \mathbf{F}\left(\hat{\boldsymbol{\theta}}\right)\right], \tag{2.5}$$

where *T* denotes the transpose of a matrix. In order to obtain a LS solution, we first linearize the set of nonlinear equations around $\boldsymbol{\theta}_0$. Linearizing $\mathbf{F}(\boldsymbol{\theta})$ can be achieved by using first-order Taylor series expansion around $\boldsymbol{\theta}_0$ and retaining the first two terms, i.e.,

$$\mathbf{F}(\boldsymbol{\theta}) \approx \mathbf{F}(\boldsymbol{\theta}_0) + \mathbf{H}(\boldsymbol{\theta} - \boldsymbol{\theta}_0), \tag{2.6}$$

where **H** is the Jacobian of **F** given by

$$\mathbf{H} = \begin{bmatrix} \frac{\partial f_1}{\partial \theta_1} & \cdots & \frac{\partial f_1}{\partial \theta_M} \\ \cdots & \cdots & \cdots \\ \frac{\partial f_N}{\partial \theta_1} & \cdots & \frac{\partial f_N}{\partial \theta_M} \end{bmatrix}_{\boldsymbol{\theta} = \boldsymbol{\theta}_0}. \tag{2.7}$$

For the 3-anchor example in Figure 2.2, the Jacobian is evaluated by computing the partial derivatives in (2.7), i.e., [Kay93]

$$\mathbf{H} = \begin{bmatrix} \frac{\partial f_1}{\partial x} & \frac{\partial f_1}{\partial y} \\ \frac{\partial f_2}{\partial x} & \frac{\partial f_2}{\partial y} \\ \frac{\partial f_3}{\partial x} & \frac{\partial f_3}{\partial y} \end{bmatrix} = \begin{bmatrix} \frac{x - x_1^a}{\sqrt{\left(x - x_1^a\right)^2 + \left(y - y_1^a\right)^2}} & \frac{y - y_1^a}{\sqrt{\left(x - x_1^a\right)^2 + \left(y - y_1^a\right)^2}} \\ \frac{x - x_2^a}{\sqrt{\left(x - x_2^a\right)^2 + \left(y - y_2^a\right)^2}} & \frac{y - y_2^a}{\sqrt{\left(x - x_2^a\right)^2 + \left(y - y_2^a\right)^2}} \\ \frac{x - x_3^a}{\sqrt{\left(x - x_3^a\right)^2 + \left(y - y_3^a\right)^2}} & \frac{y - y_3^a}{\sqrt{\left(x - x_3^a\right)^2 + \left(y - y_3^a\right)^2}} \end{bmatrix}. \tag{2.8}$$

The linearized LS solution is then given by [Kay93]

$$\hat{\boldsymbol{\theta}} = \boldsymbol{\theta}_0 + (\mathbf{H}^T\mathbf{H})^{-1}\mathbf{H}^T[\mathbf{d} - \mathbf{F}(\boldsymbol{\theta}_0)]. \tag{2.9}$$

This algorithm introduces errors when the linearized function does not accurately approximate the original nonlinear function. Also, it requires an initial estimate of the unknown parameters, i.e., the initial estimate of the node location coordinates. With a random initial estimate of the unknown parameters, this algorithm may converge to a local optimum, instead of a global optimum. This problem can be somewhat alleviated by performing this algorithm iteratively with each successive estimate being closer to the optimum estimate, i.e., [Kay93]

$$\hat{\boldsymbol{\theta}}_{i+1} = \hat{\boldsymbol{\theta}}_i + (\mathbf{H}^T\mathbf{H})^{-1}\mathbf{H}^T[\mathbf{d} - \mathbf{F}(\hat{\boldsymbol{\theta}}_i)]. \tag{2.10}$$

The iteration can be stopped when some criterion is met. For example, for a given small tolerance σ, the iterative algorithm must stop if $| E(\hat{\boldsymbol{\theta}}_{i+1}) - E(\hat{\boldsymbol{\theta}}_i) | < \sigma$. Alternatively, the algorithm can terminate after a maximum number of iterations has been performed.

2.4.3. Weighted Least Squares (WLS) Algorithms

In the case that the statistics of the ranging error are available, localization performance can be improved by applying a WLS technique. The WLS algorithm solution is formed as the vector $\hat{\boldsymbol{\theta}}$ that minimizes the cost function [Kay93]

$$E_w(\hat{\boldsymbol{\theta}}) = [\mathbf{d} - \mathbf{F}(\hat{\boldsymbol{\theta}})]^T \mathbf{W}[\mathbf{d} - \mathbf{F}(\hat{\boldsymbol{\theta}})], \tag{2.11}$$

where $\mathbf{W} = \text{diag}\{w_1 \quad ... \quad w_N\}$ is a diagonal weighting matrix with positive elements. Usually we choose small weights, where errors are expected to be large, and vice versa. Minimization of E_w yields the WLS estimator given by [Kay93]

$$\hat{\boldsymbol{\theta}} = \boldsymbol{\theta}_0 + (\mathbf{H}^T \mathbf{W} \mathbf{H})^{-1} \mathbf{H}^T \mathbf{W}[\mathbf{d} - \mathbf{F}(\boldsymbol{\theta}_0)], \tag{2.12}$$

where it is assumed that the inverse of the matrix $\mathbf{H}^T\mathbf{W}\mathbf{H}$ exists. If the distance estimation error vector has a zero mean, i.e., $E\{\mathbf{e}\} = \mathbf{0}$, we can obtain the minimum variance (MV) or Markov estimator, which is the best linear unbiased estimator (BLUE) by choosing $\mathbf{W} = \mathbf{R}_e^{-1}$, where $\mathbf{R}_e$ is the correlation matrix of the distance estimation error vector [Kay93].

2.5. Practical Performance Considerations

If the range measurements are corrupted by zero-mean normally-distributed random noise, the unbiased CRLB can be achieved through the use of WLS algorithms for identically and non-identically distributed errors, respectively. However, in the case that those measurements are biased, e.g., in indoor TOA estimation, applying WLS techniques can provide a sub-optimal solution. In order to implement these algorithms in

the indoor environments, the statistics of the bias must be incorporated. Obtaining the statistics of the bias in indoor environments requires extensive TOA-based ranging measurements and modeling campaigns [Als07b]. In addition, identification of NLOS on specific range measurements must be integrated with mitigation techniques that adjust the weights in WLS to improve the localization accuracy [Che99].

Another factor affecting the quality of location estimation is the geometry of the anchors relative to the sensor node. GDOP is commonly used in localization applications to quantify the geometrical impact on precision. The GDOP expression has many different forms [Kap96], but a simple expression in terms of the angles between the anchors and the sensor node is given by [Spi01]

$$GDOP(M,\phi) = \sqrt{\frac{M}{\sum_i \sum_{jj>i} \left|\sin(\phi_{ij})\right|^2}}, \tag{2.11}$$

where M is the number of anchors involved in the localization process and ϕ is the angle between each pair of anchors. An example illustrating the impact of geometry on the precision of localization is given in Figure 2.7. In this simulation example, the statistics of the ranging error between the node and the anchors are identical.

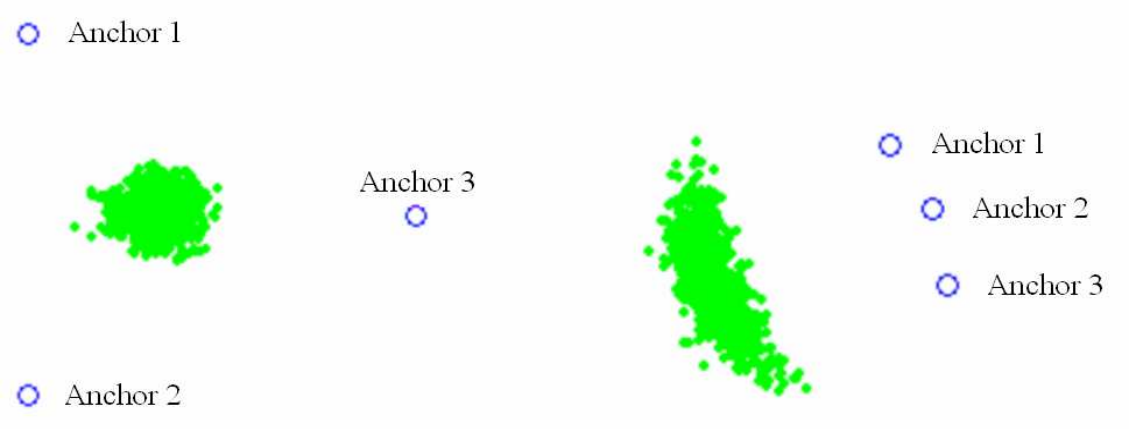

(a) (b)

Figure 2.7: Effect of geometry on sensor node position estimation: (a) Good geometry – the anchors evenly surround the sensor node. As a result, the location accuracy is high since the GDOP is minimized according to eq (2.11) (b) Bad geometry – when the anchors are very close to each other GDOP is high and that results in lower location accuracy characterized by the "smearing" of the location estimates.

In Figure 2.7 (a), the anchors are at 120^{o} relative to each other. While in Figure 2.7 (b), they are 20^{o} apart. The figure highlights the impact of geometry on the precision, where the effect of sensor node and anchor geometry can be clearly seen. The spreading of the ranging error in the 20^{o} case results in higher uncertainty.

2.6. Cooperative Localization in WSNs

2.6.1. Background

The previous sections provided an understanding of the different traditional approaches to the localization problem. It is evident that the localization accuracy

depends on the ranging technique employed, deployment environment (which affects the ranging error statistics), and the relative geometry of the sensor node to the anchors. The major difference between traditional localization and WSN localization is cooperative localization. Cooperative localization refers to the collaboration between sensor nodes to estimate their location information. In traditional wireless networks, nodes can only range to anchors, as shown in Figure 2.8 (a). As a result, nodes that are beyond the coverage of sufficient anchors fail to obtain a location estimate. However in a cooperative WSN nodes do not need to have a single-hop connection to anchors in order to localize. Cooperative localization makes propagating range information throughout the network possible. Note that due to random deployment in a WSN some parts of the network may still be isolated or ill-connected, which further introduces limitations in position estimation, e.g., node (x_1, y_1) in Figure 2.8 (b). Obviously, increasing the sensor node density can reduce the probability of isolated sub-networks, but this approach has its own limitations. Note that with increased ranging information cooperative localization has the following advantages. The first is that the *coverage* of the anchor nodes to the sensor nodes increases substantially relative to the traditional counterpart. This is because in addition to node-anchor measurement, node-node measurements further propagate information across the network and makes localization possible. Second, the increased range information exchange between the nodes allows for improvements in localization accuracy. For example in situations where TOA-based ranging suffers in indoor environments, WSN introduce redundancy in range information and as a result the channel impairments can be effectively mitigated.

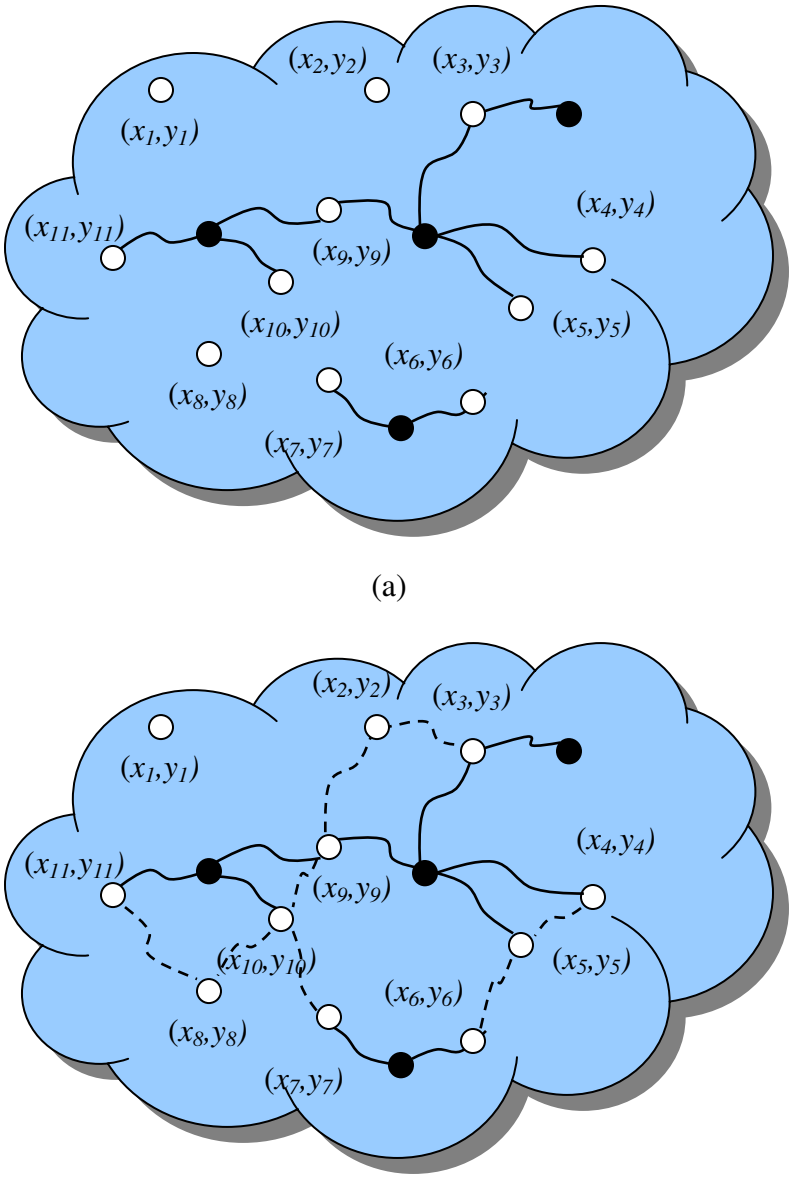

Figure 2.8: Cooperative localization concept in WSN. (a) Traditional wireless networks. (b) WSNs. Black circles are anchor nodes and white circles are "blind" sensor nodes. In WSNs the cooperation between the sensor nodes allows for increased information sharing. This specifically provides enhanced coverage and improvement in localization accuracy.

2.6.2. Cooperative Localization Techniques

In general, there are two main approaches to node localization in WSNs. The first is centralized and the second is distributed. In both approaches absolute and relative localization is possible. Unlike relative localization, in absolute localization anchor nodes are needed in order to provide a global frame of reference. Anchors or beacons are sensor nodes that are aware of their locations (usually through GPS or pre-programmed during setup) and they are necessary for WSN applications that require localization with respect to an absolute global frame of reference, e.g., GPS. Depending on the desired application, either relative or absolute cooperative localization is possible. In this section we briefly provide an overview and highlight the differences between centralized and cooperative localization techniques.

In centralized localization, information of each node in the network is determined centrally through a computer usually at one edge of the network. The range estimates between all node pairs in the network are forwarded to the processing unit, where a complex centralized algorithm estimates the location of each node in the network. Figure 2.9 (a) illustrates the centralized approach. The advantage of this technique is that all ranging information between node pairs is available to the central processor. As a result, the processor has a top-level view of the connectivity of the network. The amount of information allows the centralized algorithm to generate more accurate localization results. The drawbacks, on the other hand, include traffic congestion and computational complexities, especially for larger sensor networks. In the former, the possibility of congestion that occurs close to the central processing unit due to information going back and forth can reduce the effectiveness of this approach. Similarly, the latter drawback

imposes constraints on the computation time needed to handle estimating the node positions in a large WSN.

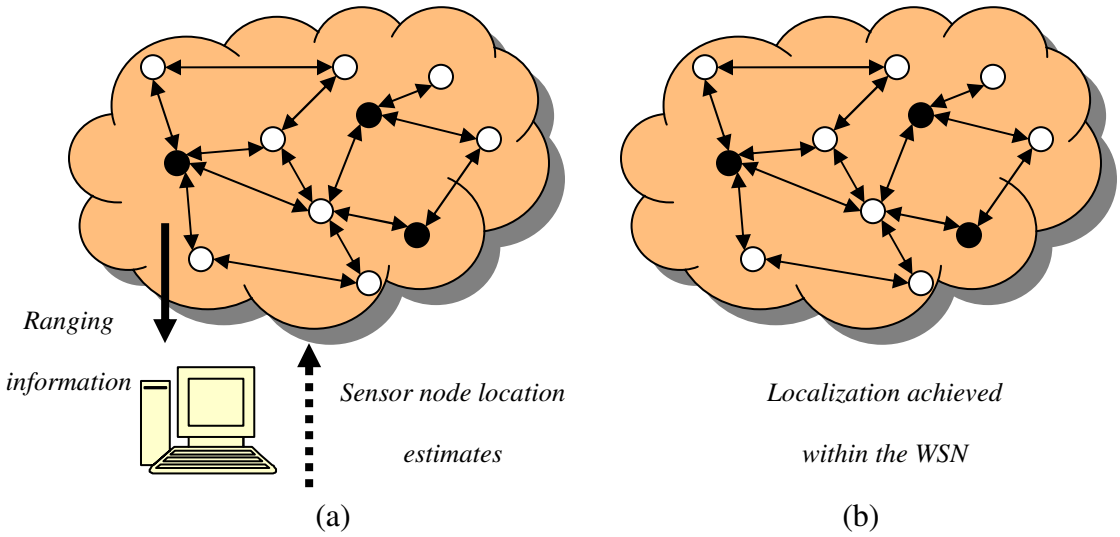

Figure 2.9: WSN localization: (a) centralized, (b) distributed.

The second approach used in WSN localization is distributed in nature (see Figure 2.9 (b)). The process is usually iterative, where sensor nodes attempt to localize themselves first and then aid the reminder of the nodes in the localization process. Distributed positioning algorithms provide the best alternatives so far in their approach. The algorithms are self-organizing and energy efficient.

2.6.3. Challenges Facing Distributed Localization Algorithms

In this dissertation, we will focus on distributed localization algorithms, mainly due to their simplicity in implementation and to their robustness to TOA-based ranging errors. In this subsection we briefly overview the major challenges facing WSN localization. These challenges can be categorized into network and channel parameters.

When considering network parameters, localization is mainly constrained by the size (i.e., the number of nodes and anchors), the topology, and the connectivity of the network. Network connectivity is determined by node density, which is usually defined as the number of nodes per square meter (nodes/m^2). A network with a high node density exhibits improved localization performance compared to a sparse networks. Further, in sparse WSNs there is a high probability of ill-connected or isolated nodes and in such cases localization accuracy can be degraded substantially. Therefore, it is always desirable to increase the node density (higher connectivity information means a lower probability of ill-connected networks) to improve the accuracy of localization. However, with increased sensor nodes, the error can substantially propagate from one hop to the next, which can be a serious problem in WSN distributed localization algorithms. This phenomenon is known as *error propagation* and it is caused by the iterative nature of these distributed algorithms. When a node transforms into an anchor, the error in the range estimates used in the localization process impacts its position estimate. When other nodes in the network use this *newly* transformed anchor, the position error will propagate to the new node's position estimate. Therefore, in several iterative steps, error propagation can substantially degrade the localization performance.

The second and most limiting factor affecting WSN localization is the wireless RF channel. Effective cooperative localization hinges on the RF ranging technology and its behavior in the deployed environment. The TOA techniques have been widely accepted as the most accurate but their behavior varies significantly in different deployment environments. For example, deploying hundreds of nodes in outdoor environments presents different challenges relative to trying to locate sensors inside a building. In

particular, WSNs in indoor areas face severe multipath fading and harsh radio propagation, causing large ranging estimation errors that impact localization performance directly. To develop practical and accurate cooperative localization algorithms, the behavior of the wireless channel must be first investigated and then integrated into the algorithm. Specifically, the localization algorithms must assess the quality of the ranging estimates and integrate that information into the localization process to further provide robust iterative performance.

Chapter 3 UWB TOA-based Ranging: Concepts, Measurements & Modeling

3.1. Background

Recently, UWB technology has been one of the major developments in the wireless industry with potential for high data-rate communication and precise TOA based ranging [Por03, Ghav04, Opp04]. Large bandwidth offers high resolution and signaling which allows for centimeter accuracies, low-power and low-cost implementation [Gez05]. Numerous potential applications have been identified for indoor localization in general and for UWB localization in particular [Gez05, Pah02, Fon02]. Depending on the nature of the application different ranging scenarios will be necessary for both traditional and WSNs. This means that scenarios will not be limited to indoor-to-indoor (ITI) ranging. Indeed for a variety of applications (e.g. firefighters, soldiers in hostile buildings) rapid deployment of beacon infrastructure surrounding and on top of buildings will be necessary. In these situations outdoor-to-indoor (OTI) and roof-to-indoor (RTI) will impose different challenges to UWB ranging (see Figure 3.1).

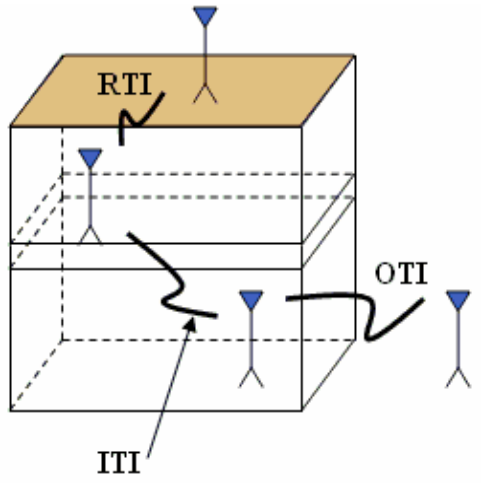

Figure 3.1: Indoor Ranging Scenarios. In many of the potential indoor geolocation applications sensor nodes will be deployed inside, outside and on top of buildings. As a result understanding the impact of those scenarios on TOA-based ranging is very important for accurate and reliable localization.

The performance of TOA-based UWB ranging systems depends on the availability of the DP signal [Lee02, Pah98]. In indoor environments the DP can be detected in both LOS and NLOS. Similar to wireless communications terminology, NLOS refers to the absence of a physical LOS between the transmitter and receiver and *not* the absence of the DP. This means that in these situations the DP can be detected, albeit attenuated. In short distance LOS, the DP is always detectible and accurate UWB TOA estimates in the range of centimeters are feasible due to the high time-domain resolution [Chu03], [Ala03a]. The challenge is UWB ranging in indoor NLOS conditions, which can be characterized as dense multipath environments [Lee02, Pah98]. In these conditions, depending on the presence or absence of the DP, the ranging errors can vary significantly. Specifically in the presence of the DP, the dominant sources of error are multipath and propagation delay. Multipath error corrupts the TOA estimates due to the multipath components (MPC), which are delayed and attenuated replicas of the original signal,

arriving and combining at the receiver shifting the estimate. Propagation delay, caused by the signal traveling through obstacles, can further add a positive bias to the TOA estimates. Although UWB can mitigate multipath with the availability of excess bandwidth [Ala03a, Tar06] its ability to perform in the absence of the DP needs to be further investigated. In the absence of the DP, also referred to as Undetected Direct Path (UDP) in [Pah98, Pah06], Type 1 and Type 2 NLOS in [Den04] and late errors in [Lee06], range estimates are corrupted by larger positive biases which have a significant probability of occurrence due to cabinets, elevator shafts, or doors that are usually cluttering the indoor environment. Furthermore, mitigation of this problem through increasing the system bandwidth alone has its limitation [Pah06].

Characterization of the UWB channels for ranging applications is different from communications [Pah02]. For the latter, the focus is on data rate and communication coverage through characterization of the delay spread and the pathloss of the total signal energy. However, the former requires special attention on the ranging accuracy, i.e. statistics of the ranging error, and ranging coverage. Characterizing the probability of DP blockage and the statistics of the error in the presence and absence of the DP provides an understanding of the challenges and limitations imposed by the multipath environment. For the ranging coverage, characterizing the pathloss-distance dependence of the DP in a given scenario and environment can provide practical indications of the maximum possible ranging distance [Als07a].

UWB indoor propagation experiments have been carried out extensively [Mol05, Gha04, Muq06, Cho05], but these efforts focus mainly on the communication aspects of UWB. Several indoor propagation experiments with a focus on indoor ranging, be it

UWB or otherwise, have been reported in [Fon02, Lee02, Pah98, Ala03a, Tar06, Den04, Fal06, Ala06, Pat03, Hat06, Ala05, Low05], where experiments are usually limited to a floor or several rooms but do not address modeling the spatial statistics of NLOS ranging or ranging coverage. The only available ranging error models were provided in [Den04, Ala06] but are based on limited measurement data sets, and only the latter focuses on characterization of errors according to the availability of the DP. As a result a comprehensive measurement and modeling of the UWB TOA-based ranging in different indoor environments and scenarios is not available in the literature. These models are needed to provide a realistic platform for algorithm performance analysis. More importantly, they are necessary for determining localization performance bounds in NLOS cluttered environments [Qi06], [Jou06a] which can provide insight into the fundamental limitations facing indoor UWB localization in both traditional wireless networks and sensor networks.

3.2. UWB TOA-based Ranging Concepts

UWB TOA-based ranging can be achieved through different technologies. There are, however, two promising solutions, namely, Multi-band Orthogonal Division Multiplexing (MBOFDM) and single pulse transmission. In the former, the OFDM modulated signal contains parallel transmissions of signals that are modulated at orthogonally spaced frequency carriers. Specifically in the 802.15.3a MB-OFDM standard, the UWB band is divided into 14-sub-bands. Each sub-band provides ranging with 528 MHz bandwidth capability [Bet04]. In the latter technique very narrow time-domain pulses have bandwidths in excess of 1 GHz provide even better time-domain

resolution [Lee02]. In this dissertation we will focus on the TOA-based ranging capabilities of these two promising systems. Specifically our results and analysis will be focused on two different system bandwidths 500MHz and 3 GHz resembling the MB-OFDM and pulse-based respectively.

One of the major factors determining the quality of TOA-based ranging in indoor geolocation is the ability to detect the DP between a RP and a MT in the presence of dense multipath. For the indoor multipath channel, the impulse response is usually modeled as,

$$h(\tau) = \sum_{k=1}^{L_p} \alpha_k e^{j\phi_k} \delta(\tau - \tau_k) \tag{3.1}$$

where L_p is the number of MPCs, and α_k, ϕ_k and τ_k are amplitude, phase and propagation delay of the k^{th} path, respectively [Pah05]. When the DP is detected $\alpha_1 = \alpha_{DP}$ and $\tau_1 = \tau_{DP}$ where α_{DP} and τ_{DP} denote the DP amplitude and propagation delay, respectively. Figures 2.4 and 2.5 provide sample measured channel profile and the relative amplitude and delay of the MPCs. The distance between the MT and the RP is $d_{DP} = v \times \tau_{DP}$, where v is the speed of signal propagation. In the absence of the DP, ranging can be achieved using the amplitude and propagation delay of the first Non-Direct Path (NDP) component given by α_{NDP} and τ_{NDP} respectively; resulting in a longer distance given by $d_{NDP} = v \times \tau_{NDP}$ where $d_{NDP} > d_{DP}$. For the receiver to identify the DP, the ratio of the strongest MPC to the DP given by

$$\rho_1 = \left(\frac{\max\left(|\alpha_i|_{i=1}^{L_p} \right)}{|\alpha_{DP}|} \right) \tag{3.2}$$

must be less than the receiver dynamic range ρ and the power of the DP must be greater than the receiver sensitivity φ [Kri99]. These constraints are given by,

$$\rho_1 \le \rho \tag{3.3a}$$

$$P_{DP} > \varphi \tag{3.3b}$$

where $P_{DP} = 20\log_{10}\left(\left|\alpha_{DP}\right|\right)$.

3.2.1. Ranging Coverage

The performance of UWB TOA-based ranging is then constrained by the maximum feasible distance where P_{DP} can satisfy (3.3a) and (3.3b). This is analogous to the dependence of a communication system's performance on the distance relationship of the total signal energy of all the detectable MPCs, or $P_T = 20\log_{10}\left(\sum_{k=1}^{L_p}\left|\alpha_k\right|\right)$. In indoor environments, the distance-dependence of P_T, which determines the limitations of communication coverage, is usually predicted from experimental pathloss models of the total signal energy in different environments and scenarios [Dur98, Mol05, Gha04]. Similarly, the distance-dependence behavior of P_{DP} is important in analyzing the physical limitations facing UWB TOA-based ranging. These indoor radio wave propagation measurements have focused mainly on determining the radio coverage in different environments. However, the reported results and models are not adequate for predicting the coverage of TOA-based UWB indoor geolocation systems because the performance in multipath rich indoor environments depends on the signal-to-noise (SNR) of the DP between the transmitter and the receiver. Unlike communication coverage which is related to the received power of all the MPCs in a given distance, ranging coverage is

related to the received power of the DP component. For a given system dynamic range, ρ, we define ranging coverage, R_c, as the distance in which the maximum tolerable average pathloss of the DP is within ρ [Als07a]. This is represented by

$$\max\left\{\overline{PL_{DP}}\right\} = 10\gamma\log_{10}(R_c) \le \rho \tag{3.4}$$

where $\overline{PL_{DP}}$ is the average pathloss of the DP and γ is the pathloss exponent. The pathloss behavior of the DP is distance-dependant but because of attenuation and energy removed by scattering its intensity decreases more rapidly with distance compared with the total signal energy [Siw03]. This means that for typical indoor multipath scattering environment communication coverage is greater than ranging coverage, $C_c > R_c$. Operating out of ranging coverage causes large TOA estimation errors and performance degradation.

In general, ranging coverage in indoor multipath environments depends on the channel condition between a pair of nodes. The channel condition is physically constrained by the environment and the scenario. The environment refers to the type of building such as residential, manufacturing or office. The scenario refers to the relative location of the node-node or anchor-node pair which can be grouped into the following: ITI, OTI, and RTI. In ITI ranging the pathloss behavior varies significantly between LOS and NLOS channel conditions. In the latter, ranging coverage is reduced due to penetration loss caused by the interior wall structures, which results in a higher DP pathloss exponent. Similarly OTI and RTI ranging imposes harsher constraints on the pathloss, due to the DP having to penetrate the outside walls and roof respectively, which

means that $R_c^{ITI} > R_c^{OTI} > R_c^{RTI}$ [Als07a]. This poses a challenge specifically for indoor localization in ad-hoc and WSN applications.

3.2.2. Ranging Error

Ranging and localization are further constrained by the statistics of the ranging error. Ranging error is defined as the difference between the estimated and the actual distance or

$$\varepsilon = \hat{d} - d_{DP}. \tag{3.5}$$

where $\hat{d}$ is the estimated distance and d_{DP} is the actual distance. In an indoor environment the MT experiences varying ranging error behavior depending on the relative location of the MT to that of the RP. More specifically it depends on the availability of the DP and in the case of its absence on the characteristics of the blockage. In this dissertation we categorize the error based on the following ranging states. In the presence of the DP, both (3.3a) and (3.3b) are met and the distance estimate is very accurate yielding

$$\hat{d}_{DP} = d_{DP} + \varepsilon_{DP} + n \tag{3.6a}$$

$$\varepsilon_{DP} = \begin{cases} b_m(\omega) & LOS \\ b_m(\omega) + b_{pd} & NLOS \end{cases} \tag{3.6b}$$

where $b_m(\omega)$ is the bias induced by the multipath that dominates when the DP is present and it is a function of the system's bandwidth, ω [Ala03a, Tar06]. b_{pd} is the propagation delay imposed by the NLOS condition. n is zero mean Gaussian measurement noise. Similar to wireless communications terminology, we will use the NLOS term to denote

the absence of a physical LOS between the transmitter and receiver and *not* the absence of the DP. This means that in these situations the DP can be detected, albeit attenuated.

When the MT is within ranging coverage but experiences sudden blockage of the DP, also known as UDP [Pah98], (3.3a) is not met and the DP is shadowed by some obstacle burying its power under the dynamic range of the receiver. In this situation, the ranging estimate experiences a larger bias error compared to (3.6). Emphasizing that ranging is achieved through NDP component, the estimate is then given by

$$\hat{d}_{NDP} = d_{DP} + \varepsilon_{NDP} + n \tag{3.7a}$$

$$\varepsilon_{NDP} = b_m(\omega) + b_{pd} + b_B(\omega) \tag{3.7b}$$

where $b_B(\omega)$ is positive, additive bias representing the nature of the blockage, and it dominates the error compared to measurement noise. Its dependence on bandwidth is through its impact on the energy per MPC. Higher bandwidth results in lower energy per MPC which increases the probability of DP blockage. Finally, when the user operates outside of the ranging coverage neither (3.3a) nor (3.3b) is met and large errors occur with high probability.

Formally, these ranging states can be defined as follows,

$$\zeta_1 = \left\{ \hat{d} = \hat{d}_{DP} \mid d \le R_c \right\} \tag{3.8a}$$

$$\zeta_2 = \left\{ \hat{d} = \hat{d}_{NDP} \mid d \le R_c \right\} \tag{3.8b}$$

$$\zeta_3 = \left\{ \hat{d} = \hat{d}_{NDP} \mid d > R_c \right\} \tag{3.8c}$$

$$\zeta_4 = \left\{ \hat{d} = \hat{d}_{DP} \mid d > R_c \right\} \tag{3.8d}$$

In this dissertation we will focus on modeling the error statistics within the ranging coverage. The performance in ζ_3 is dominated by large measurement noise variations which means the significance of (3.6b) and (3.7b) diminishes [Jou06a]. We further assume that $p(\zeta_4) \approx 0$ since from our definition in (3.4) the DP cannot be detected after the ranging coverage.

3.2.3. Factors Affecting Ranging Coverage and Accuracy

Both ranging coverage and accuracy are functions of system dynamic range, bandwidth, physical building environment and ranging scenario. Physical environment refers to the type of the building: residential, office or manufacturing floor. Ranging scenario refers to the location of the transmitter with respect to the receiver. Several scenarios are common in potential indoor geolocation applications. Figure 3.1 shows a typical multi-story building with three main ranging scenarios: ITI, OTI and RTI where the last two can be primarily used in firefighter or military applications where ad-hoc deployments are more practical. Ranging coverage is affected directly through the attenuation induced on the DP which is dependent on the environment and scenario. For example, residential environments, primarily composed of wooden structures, pose different attenuation characteristics compared to office buildings which are composed of concrete and metallic beam structures. In addition penetration loss due to exterior walls is higher than interior walls which mean that ITI, OTI and RTI must impose different physical constraints on the ranging performance. The impact of ranging environment and scenarios on the accuracy, however, can be attributed to multipath and probability of DP blockage. The harsher the indoor environment the higher the multipath error and the more likely the DP would be shadowed by obstacles. Changes in system bandwidth affect

multipath and probability of DP blockage but increasing the system bandwidth arbitrarily might reduce the former but emphasize the impact of the latter. Finally the impact of SNR or dynamic range is rather intuitive but in reality UWB systems, due to FCC regulations, face power constraints which make ranging under these conditions challenging.

3.3. UWB Measurement Campaign

3.3.1. Background

Frequency domain measurement techniques have been previously employed to characterize the channel impulse response [Gha04, Cho05, Pah05, How90]. The measurements provided characterization of communication parameters such as the RMS delay spread and power-distance relationship. In this dissertation we follow the same techniques but measure the large-scale, spatial characteristics of the DP, mainly $\hat{\alpha}_{DP}$ and $\hat{\tau}_{DP}$ which can be used to examine the ranging coverage (pathloss characterization) and accuracy, respectively. In the absence of the DP we measure the first detected path, $\hat{\tau}_{NDP}$ and analyze the probability of blockage and the error statistics in this condition.

3.3.2. Measurement System

The measurement system, similar to [Gha04, Cho05, How90], employs a 40GHz Agilent E8363B vector network analyzer (VNA) that is used to sweep the frequency spectrum of 3-8 GHz with 312.5 KHz sampling interval (16001 sampling points). The VNA measures the S21 S-parameter which is the transfer function of the channel. The transmitter and the receiver are a pair of disc-cone UWB antennas which are connected to

the VNA by low-loss, high quality doubly shielded cables. On the receiver side a low-noise amplifier (LNA) is connected between the antenna and the VNA. Figure 3.2 illustrates the measurement system. On the transmitter side a 30 dB power amplifier with the frequency range of 3-8GHz further improves the dynamic range.

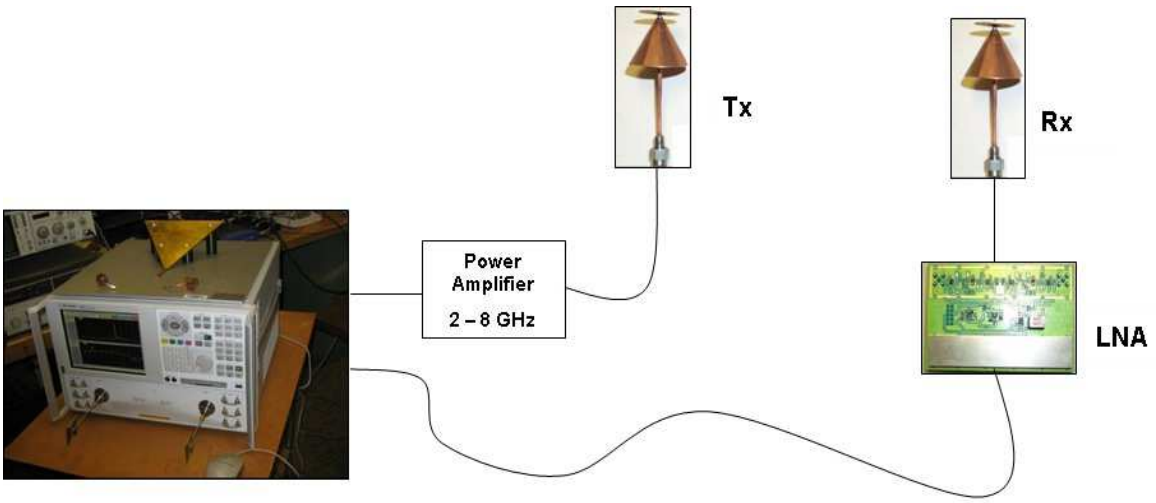

Figure 3.2: UWB frequency domain measurement system.

The transmitter and receiver heights were fixed to 1.5 meters. The overall measurement system has a dynamic range of 120 dB. The undesirable effects of the cables, LNA, and antennas are removed through system calibration.

3.3.3. Measurement Locations and Procedure

A comprehensive UWB propagation campaign was performed in 4 buildings: 17 Schussler Road - residential house, Fuller Laboratory - modern office, Norton Company - manufacturing floor and Atwater Kent (AK) - old office; all in Worcester, MA.

17 Schussler Road is a fairly big house with wooden exterior walls and sheetrock interior walls. Rooms have dimensions on the order of a few meters and contain furniture such as

couches, tables, chairs, etc. Fuller Laboratories is a modern building characterized by brick external walls with some aluminum siding on two sides, metallic window frames and doors.

Table 3.1: Summary of the measurement database

Environment	Scenario	TX or RX Location	Description of the scenarios	Max. meas. range (m)	Number of Meas.
Office (Fuller Laboratories)	OTI	Entrance I/II	Multi-floor – close to the door	45	336
		Arbitrary	Multi-floor – away from door		150
	ITI	LOS	Open area around entrance	24	120
		NLOS	Inter-floor – open area	23	72
			Inter-floor – close area		54
Residential (17 Schussler Rd.)	OTI	Entrance I	Multi-floor – front	15	186
		Entrance II	Multi-floor – side		186
	ITI	NLOS	Same-floor	10	108
			Inter-floor		66
Factory (Norton Company)	OTI	Entrance I	Same-floor – close to the door	38	120
		Entrance II	Same-floor – away from door		126
	ITI	LOS I	Open area with machinery	40	120
		LOS II	Straight walkway		126
Office (Atwater Kent Laboratories)	OTI	Entrance I /II	Same-floor – main& side	27	132
	ITI	NLOS	Rooms/corridors of 3rd floor	26	90
	RTI	AK3C	Corridors of 3rd floor	17	306
		offices	Small rooms		204
		labs	Large room		528
Total number of Measurements					3030

The dimension of the building is on the order of a few tens of meters and contains several computer labs, department offices and lecture halls. Norton Company is a manufacturer of welding equipment and abrasives for grinding machines with building dimensions on the order of a few hundred meters and the floor is cluttered with machines, equipment and metallic beams. The AK laboratory is a three floor building which has a traditional office structure consisting of rooms that have dimensions in the order of few

meters. This building particularly has been used for measurements from the roof due to ease of accessibility.

In the campaign, three ranging scenarios were measured: ITI, OTI and RTI. Table 3.1 describes the details of the measurement locations. ITI and OTI measurements were conducted in all buildings. While RTI measurements were only conducted in AK building. Figure 3.3 shows sample floor plans with the measurement locations. In each measurement the location of the transmitter was fixed while the receiver was moved along certain grid points.

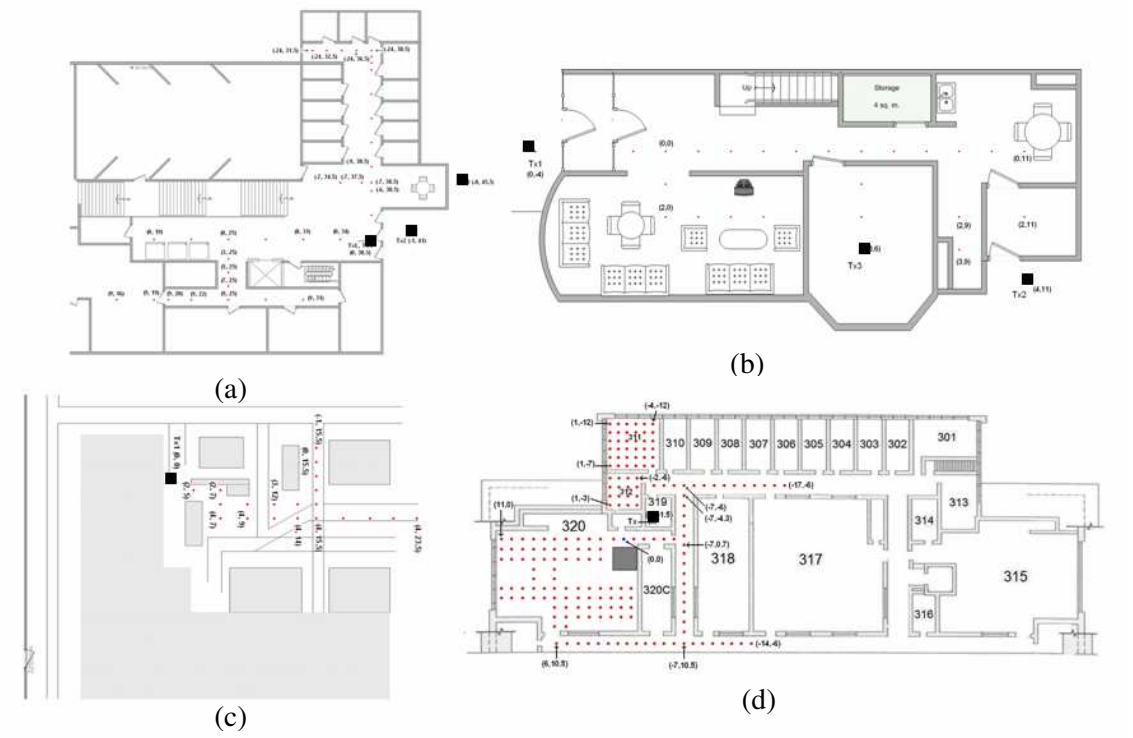

Figure 3.3: Sample measurement floor plans. (a) Fuller OTI/ITI (b) Schussler OTI/ITI (c) Norton ITI (d) AK RTI. Squares are Tx locations and dots are Rx locations

Care was taken to conduct the measurements in a variety of indoor NLOS conditions ranging from harsh obstacles such as elevator shafts, metallic doors and concrete walls to other lighter wall structures as this would provide a wide variety of performance conditions.

Measuring the behavior of the DP requires accurate *a priori* knowledge of the transmitter-receiver distances. In the variety of locations we measured, this proved to be a challenging task since there was no direct LOS. In order to cope with this problem we devised a practical method to grid the building floor with transmitter and receiver locations. We created a 3 dimensional Cartesian coordinate system with 1 meter as its unit. Then we placed grid points on the floor in the positions that we were interested to measure, and assigned x-, y-, and z-coordinates to each point. An extensive amount of time and effort was placed in planning and carrying out this procedure in order to minimize the error incurred from physically measuring the distance. For example, if the coordinates of the transmitter and the receiver are given by (x_A, y_A, z_A) and (x_B, y_B, z_B), respectively then the distance can be easily found using the Euclidian relation

$$d_{AB} = \sqrt{(x_A - x_B)^2 + (y_A - y_B)^2 + (z_A - z_B)^2} \,. \tag{3.9}$$

3.3.4. Post-Processing

In the post-processing of channel measurement data, the time-domain channel impulse response is obtained by first passing the frequency domain measurements through a Hanning window in order to reduce the noise side lobes. Even though some other window functions such as the Kaiser window provides higher dynamic range, the Hanning window is selected for its much faster decaying side-lobes which significantly

reduces the interfering effect of strong multipath components in peak detection. The windowed frequency response is then converted to time-domain through the inverse Fourier transform (IFT). For the analysis in this dissertation, 500 MHz and 3 GHz bandwidths were parsed out of the measured frequency domain data with a center frequency of 4.5 GHz. The channel transfer function was divided into these frequency bands in order to reflect different potential UWB systems, namely, MBOFDM and single pulse transmission. In addition, the impact of bandwidth on the pathloss exponent of the DP component and the ranging accuracy can be evaluated. Specifically, 500MHz of bandwidth provides time-domain resolution in the order of $\Delta t_{500MHz} = 2ns \approx 0.6m$, while 3 GHz provides $\Delta t_{3GHz} = 0.3ns \approx 0.1m$. The desired parameters $\hat{\alpha}_{DP}$ and $\hat{\tau}_{DP}$ are detected from the time-domain channel profile using a peak detection algorithm. The threshold for peak detection is set to -120 dB which is the system's noise threshold. Identifying the presence or absence of the DP required analyzing the power in the bin of the expected TOA of the DP which is related to the time-domain resolution, Δt, for that bandwidth. If a peak is detected within the bin, DP is declared present. Otherwise, DP is declared absent.

3.4. Modeling the Pathloss

Using the same established pathloss modeling approach used in the literature, [Gha04, How90, Pah05], we attempt to characterize the distance-power dependance of the measured DP which we believe is important in assessing the ranging coverage and the performance of UWB indoor geolocation systems [Als07a]. The distance-power gradient

is determined from measurement data through least-square (LS) linear regression [Pah05]. The pathloss expression in decibels at some distance d is given by,

$$PL(d) = PL_0 + 10\gamma \log_{10}\left(\frac{d}{d_0}\right) + \chi, \quad d \geq d_0 \tag{3.10}$$

where PL_0 is the pathloss at $d_0 = 1$ m, $10\gamma \log_{10}(d/d_0)$ is the average pathloss with reference to d_0 and γ is the pathloss exponent which is a function of the measured scenario, building environment and bandwidth; χ is the log-normal shadow fading.

We present our results by grouping different ranging scenarios and environments. For both ITI and OTI we provide models for Norton, Fuller, Schussler and AK buildings. For RTI we have only modeled AK building. Figures 3.4 to 3.6 show sample measured scatter plots of the pathloss as a function of TX-RX separation for different buildings and ranging scenarios.

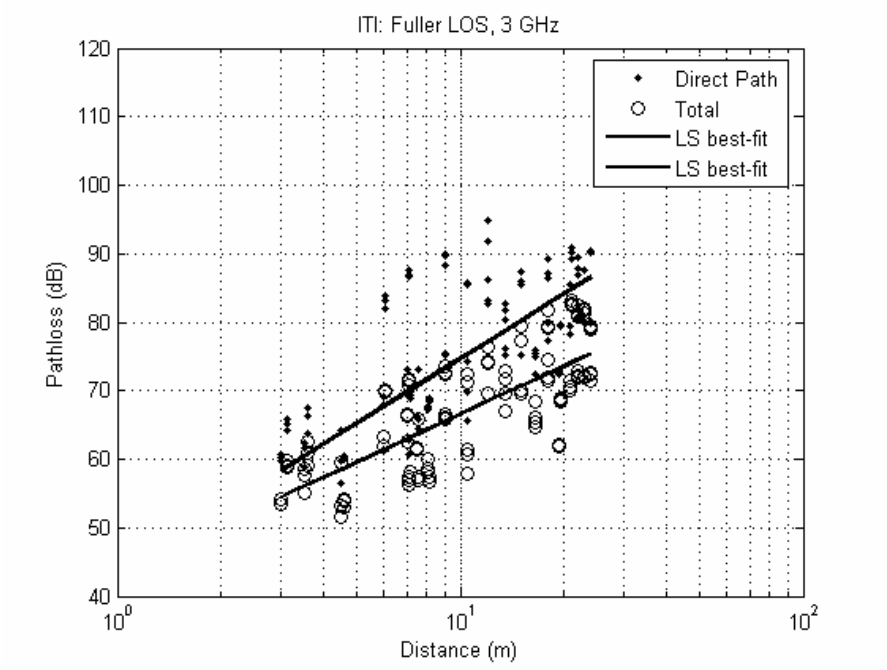

Figure 3.4: Pathloss scatter plots in Fuller ITI at 3 GHz bandwidth

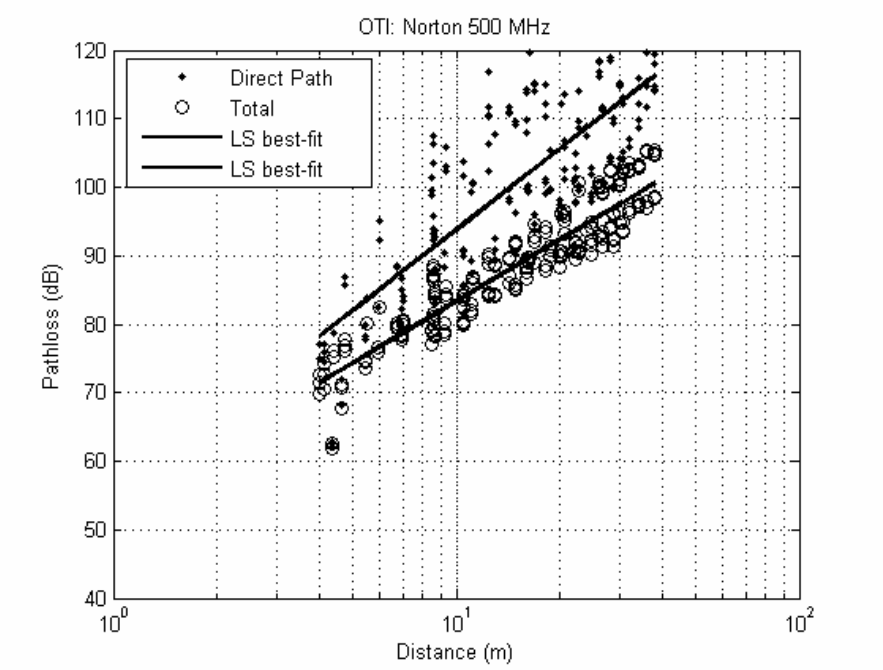

Figure 3.5: Pathloss scatter plots in Norton OTI at 500 MHz bandwidth.

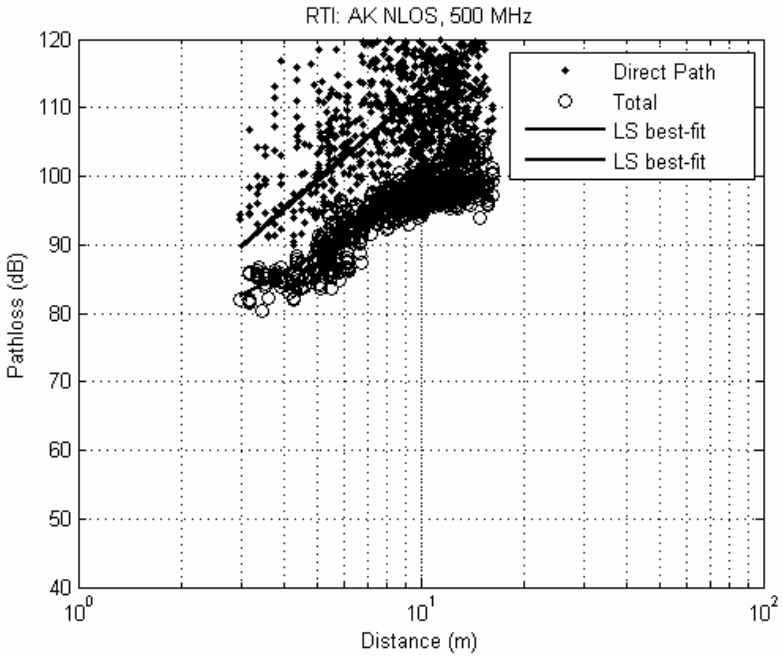

Figure 3.6: Pathloss scatter plots in AK RTI at 500 MHz

For each figure, the straight line is the best-fit LS linear regression. Like many other models in the literature, the value of PL_0 is found through fitting the data to (3.10). We observed that the intercept value changed according to the ranging scenarios and building environments. Therefore, we measured PL_0 at 1 m in free space to be around 42 dB and added another parameter to compensate for the penetration loss. Therefore the modification to the model in (3.10) is given by,

$$PL(d) = PL_0 + PL_p + 10\gamma \log_{10}\left(\frac{d}{d_0}\right) + \chi, \qquad d \geq d_0 \tag{3.11}$$

where PL_p is the penetration loss and it varies according to the measurement condition. Table 3.2 provides summary of the pathloss results. Several observations can be made from the table and the figures.

Table 3.2: Pathloss parameters

Scenario	Environment	PL_p(dB)	Direct Path				Total Signal	
			500 MHz		3 GHz			
			γ	χ (dB)	γ	χ (dB)	γ	χ (dB)
ITI	**Fuller (LOS)**	0	3.2	8.9	3.3	7.1	2.4	5.5
	Norton (Mixed)	0	3.5	8.5	4.5	9.1	2.6	3.4
	Schussler (NLOS)	6	3.4	7.9	4.0	8.4	3.0	4.6
	AK (NLOS)	7.5	5.4	6.2	5.6	8.5	3.6	6.2
OTI	**Fuller**	14.3	3.4	13.7	3.7	14.1	2.2	7.7
	Norton	8.7	3.9	7.8	5.0	10.1	3.3	4.4
	Schussler	7.6	4.1	10.5	4.2	11.1	3.2	6.1
	AK	10	4.6	8.7	5.1	8.9	3.1	3.2
RTI	**AK**	24.5	4.3	7.6	5.3	8.8	2.9	1.7

The first is that for all the measurement data the pathloss exponent is higher for the DP relative to the total signal power, which justifies our modeling approach. Second, the DP power experiences greater fluctuations around the mean pathloss as compared with

the total signal counterpart. This observation makes sense because small variations on the transmitter location affect the DP power more than the total power. Third, PL_p changes for the different penetration scenarios. In ITI scenarios Schussler NLOS suffers 6 dB penetration loss due to the walls compared to 7.5 in AK. Norton ITI measurements are a mixture of LOS/NLOS because the manufacturing floor contained scattered machines and the impact can be clearly seen on the pathloss exponent when the bandwidth increases, hence higher attenuation. Results of OTI measurements show that Fuller and AK exhibit the largest penetration loss mainly because the signal had to penetrate a heavier building construction when compared with Norton and Schussler. In addition the pathloss exponents in AK are large mainly because the measurement locations were conducted inside a metal shop on the edge of the building and between concrete corridors and rooms. AK in general imposes a very challenging environment for ranging because of the building material and dense cluttering. RTI measurements experienced the largest penetration loss and high pathloss exponent. Finally, note that the harsher the indoor environment the higher the pathloss exponent difference when moving to a higher system bandwidth. This is mainly due to the fact that larger system bandwidths provide better time domain resolution at the cost of reduced power per multipath component. This implies that the advantage of higher time-domain resolution comes at a cost of shorter ranging coverage.

3.5. Modeling the Ranging Error

3.5.1. Spatial Characterization

The goal of our modeling efforts is to provide tools to simulate the spatial ranging error behavior in indoor environments for two popular UWB system bandwidths. Ranging errors have been modeled using different approaches. In [Ala03b] and [Den04] they were modeled as a combination of Gaussian and exponential distributions using Ray-Tracing (RT) simulation software and through measurements, respectively. The latter refined the technique of the former and added an additional classification of extreme NLOS. The main problem with this approach is that it is not based on any system model, thereby lacking physical significance. Alternatively, our modeling approach will focus on the behavior of errors in presence and absence of DP similar to [Ala06].

The spatial characteristics of the ranging errors are determined by the behavior of the biases which are random due to the unknown structure of the indoor environment and the relative location of the user to them. Since the errors are highly dependent on the absence or the presence of the DP, we will model it according to the error classification in Section 3.2. Further, in order to model and compare the behavior in different building environments and scenarios, the normalized ranging error will be modeled instead, this is given by

$$\psi = \frac{\varepsilon}{d} = \frac{\left(\hat{d} - d\right)}{d}. \tag{3.12}$$

The range error experienced in an indoor environment can then be modeled by combining the conditions in (3.6) and (3.7) through the following expression

$$\psi = \psi_m + G\left(\psi_{pd} + X\psi_B\right), \tag{3.13}$$

where ψ_m is the normalized multipath error that exists in both the presence and absence of the DP. ψ_{pd} is the normalized propagation delay induced error. ψ_B is the normalized error due to DP blockage. In order to distinguish between the error behavior in LOS and NLOS we use a Bernoulli random variable, G. That is,

$$G = \begin{cases} 0, & LOS \\ 1, & NLOS \end{cases}, \tag{3.14}$$

where $p\left(G=0\right) = p\left(LOS\right)$ is the probability of being in LOS and $p\left(G=1\right) = p\left(NLOS\right)$ is the probability of being in NLOS. Similarly X is a Bernoulli random variable that models the occurrence of DP blockage given by

$$X = \begin{cases} 0, & \zeta_1 \\ 1, & \zeta_2 \end{cases} \tag{3.15}$$

where $p\left(X=1\right) = p(\zeta_2)$ denotes the probability of the occurrence of blockage, while $p\left(X=0\right) = p(\zeta_1)$ denote the probability of detecting a DP. Again we clarify that our modeling approach specifically focuses on the DP and not the traditional definition of NLOS used for communications. This means that a MT and a RP separated by a wall, for instance, is considered NLOS, but does not necessarily mean absence of the DP. In the remainder of the dissertation, ranging error, bias and normalized error will be used interchangeably and it will refer to (3.13).

3.5.2. Probability of DP Blockage

The probability of a MT within the ranging coverage of a RP to experience DP blockage depends on the system SNR, bandwidth, building environment, ranging

scenario and the relative location and density of scattering objects. Table 3.3 shows the measured blockage probabilities, $p(\zeta_2)$.

Table 3.3 Probabilities of the presence and absence of the DP

Scenario	Environment	500 MHz		3 GHz	
		% ζ_1	% ζ_2	% ζ_1	% ζ_2
ITI	Fuller	10	90	2	98
	Norton	96	4	83	17
	Schussler	89	11	87	13
	AK	39	61	32	68
OTI	Fuller	42	58	39	61
	Norton	57	43	24	76
	Schussler	77	23	60	40
	AK	40	60	22	78
RTI	AK	58	42	37	63

Several observations can be concluded. First, a positive correlation between the system bandwidth and the blockage probability $p(\zeta_2)$ exists due to lower energy per MPCs in higher system bandwidth. Secondly, as expected, DP blockage increases from ITI, to OTI and RTI. Attenuation due to penetration from exterior walls and ceiling results in higher $p(\zeta_2)$. Third, blockage is highly correlated with the building type. In residential environments blockage probability is low since the interior is composed of wooden structures with few metallic objects (e.g. a fridge, laundry room, etc.). Office buildings, however, pose harsher conditions with thicker walls, metallic beams, vending machines, metallic cabinets, shelves and elevator shafts resulting in a substantial blockage up to 90%, see Fuller and AK (ITI/OTI). Also ITI measurements in the manufacturing floor highlight the impact of occasional clutter of machineries. Finally it is worth mentioning that these results were measured using a 120 dB dynamic range provided by the external amplifiers and LNA extending the measured range. In realistic

UWB systems, unfortunately, this is truly not the case, which means that the results in here can be seen as a lower bound.

3.5.3. Behavior in the Presence of DP

Ranging in the presence of the DP occurs in LOS and NLOS environments. In the former the experienced errors are small and mainly due to the multipath. In the latter however, the impact of multipath is further emphasize through scattering (diffractions) and DP attenuation. Furthermore propagation delays, albeit a nuisance parameter in some instances can in some situations cause further degradation on the ranging estimate. The measurement results of the ranging error in LOS scenarios revealed that the impact of the multipath can be modeled through a normal distribution since the DP is available and the error deviates in both directions relative to the actual distance. In addition normality of the ranging error in this condition has been reported in [Ala03b, Ala06]. The error distribution can then be explicitly given by,

$$f\left(\psi \mid G=0\right)=\frac{1}{\sqrt{2\pi\sigma_m^2}}\exp\left[-\frac{\left(\psi-\mu_m\right)^2}{2\sigma_m^2}\right], \tag{3.16}$$

with mean μ_m and standard deviation σ_m specific to the LOS multipath induced errors. Figure 3.7 further confirms the normality of errors in this condition.

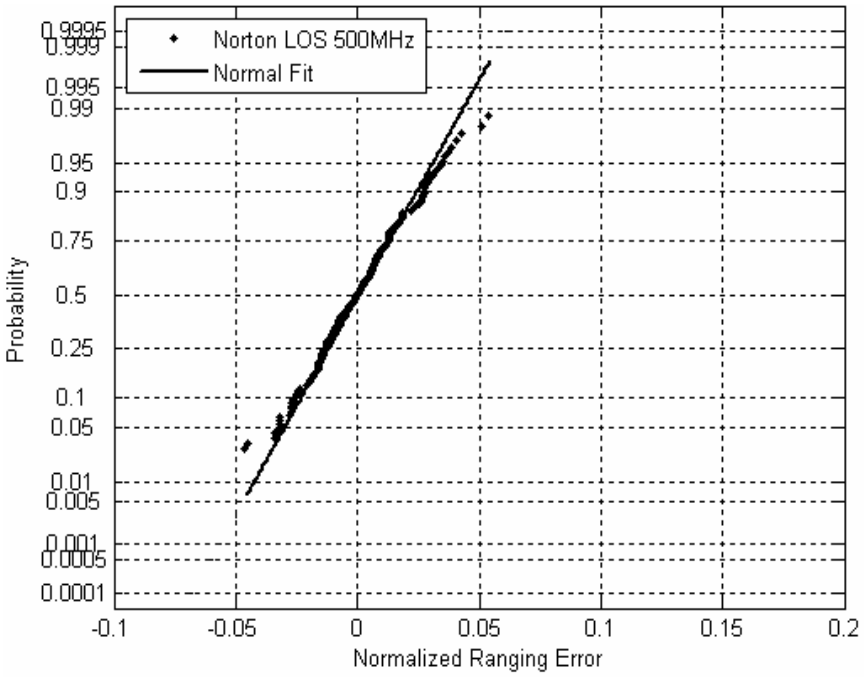

Figure 3.7: Norton ITI at 500 MHz bandwidth: confirming the normality of the biases in LOS conditions

A similar observation of the multipath effect in indoor LOS environments has been reported through measurements [Ala06]. In NLOS scenarios, when the DP is present, the amount of propagation delay and multipath due to obstructing objects such as wooden walls causes the biases to be more positive. The results show, see Figure 3.8, that the spatial characteristics retain the statistics of the LOS counterpart but with a higher mean and standard deviation.

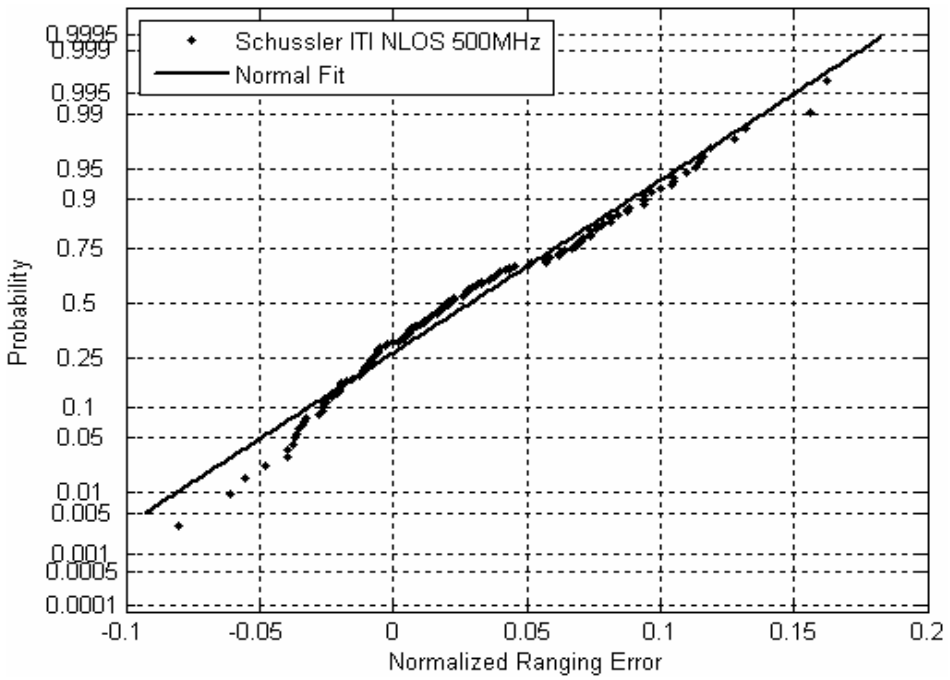

Figure 3.8: Schussler ITI NLOS: mean of biases is larger than LOS

According to these results we model the normalized ranging error similar to (3.16) but with emphasis on the condition. This is given by,

$$f\left(\psi \mid G=1, X=0\right)=\frac{1}{\sqrt{2\pi\sigma_{m,pd}^{2}}}\exp\left[-\frac{\left(\psi-\mu_{m,pd}\right)^{2}}{2\sigma_{m,pd}^{2}}\right]. \tag{3.17}$$

The subscripts in (3.17) specify the contributing error factors. Table 3.4 provides the modeling parameters of all the scenarios and environments in the presence of the DP.

Table 3.4: DP normal distribution modeling parameters for normalized ranging error

Scenario	Environment	500 MHz		3 GHz	
		μ_m	σ_m	μ_m	σ_m
ITI	Fuller (LOS)	0	0.028	0	0.006
	Norton (LOS)	0	0.022	0	0.007
		$\mu_{m,pd}$	$\sigma_{m,pd}$	$\mu_{m,pd}$	$\sigma_{m,pd}$
	Fuller (NLOS)	0.058	0.028	0.003	0.01
	Schussler (NLOS)	0.029	0.047	0.014	0.016
	AK (NLOS)	0.023	0.020	0.009	0.004
OTI	Fuller	0.015	0.017	0.002	0.011
	Norton	0.019	0.029	0.002	0.015
	Schussler	0.041	0.045	0.011	0.013
	AK	0.034	0.023	0.012	0.004
RTI	AK	0.029	0.041	0.012	0.012

The results show a positive correlation between the statistics of the normal distribution with the complexity of environment and/or ranging scenario. Negative correlation can be seen between the statistics and the system bandwidth due to reduction of multipath error in higher bandwidths.

3.5.4. Behavior in the Absence of DP

The shadowing of the DP impacts the error behavior in several ways. First, only positive errors occur, since the blockage induces a higher positive bias that dominates compared to the multipath counterpart. Second, there are occasionally large positive range errors that occur due to heavier indoor constructions such as elevator shafts, clustering of cabinets or even metallic doors. Third, the diversity of blocking material in indoor environments means that the spatial distribution of errors will in general exhibit a heavier positive tail. By examining the PDF of the errors in this condition, we observed that different subsets of the data showed varying tail behavior. The "heaviness" of the tail depended on the ranging environment and scenario. Thus harsher blockage conditions,

i.e. higher number of blocked MPCs, exhibited heavier tails. This critical observation led us to consider distributions with different tail characteristics.

In order to model the measurement data accurately we select distributions that are known to have the ability to fit data with different tail behavior. Among them are exponential, lognormal, Weibull and Generalized Extreme Value (GEV). The class of GEV distributions is very flexible with a specific tail parameter that controls the shape and size of the tail in addition to the location and scale parameters. It has been applied to model extreme events in hydrology, climatology, finance and insurance industries [Mar05], [Ber04].

In order to determine the goodness-of-fit of these different distributions to the data we apply the Kolmogorov-Smirnov (K-S) hypothesis test at 5% significance level. In addition we fit the data to the normal distribution to verify its lack of suitability in characterizing the spatial distribution of the ranging error in this condition. This is specifically important since normality is usually assumed as a model for the ranging error in localization performance analysis. Table 3.5 compares the passing rates of the K-S test for the mentioned distributions.

Table 3.5: Passing rate of K-S hypothesis test at 5% significance level

Scenario	Normal		Exponential		GEV		Lognormal		Weibull	
	500 MHz	3 GHz	500 MHz	3 GHz	500 MHz	3 GHz	500 MHz	3 GHz	500 MHz	3 GHz
ITI Fuller	70.8	68.8	85.1	83.3	91.7	86.4	90.7	88.1	85.1	85.3
ITI Norton	76.3	75.9	70.7	62.7	88.1	86.3	87.3	82.4	83.2	79.8
ITI Schussler	83.2	72.3	67.8	66.5	85.7	82.8	84.7	78.7	85.1	74.8
ITI AK	84.4	75.5	67.7	74.6	91.6	84.7	91.7	76.2	92.8	76.9
OTI Fuller	80.8	79.2	85.2	88.5	92.9	90.8	94.0	92.7	89.8	91.4
OTI Norton	80.2	83.1	75.9	71.4	92.1	93.9	91.6	90.5	86.5	88.1
OTI Schussler	77.3	86.9	68.7	71.2	91.9	94.5	89.0	93.4	82.7	89.7
OTI AK	80.1	78.1	69.1	76.2	89.1	84.5	88.3	89.4	83.1	85.5
RTI AK	85.4	87.6	72.3	76.3	96.9	94.0	93.9	95.4	89.8	91.6

The results show that both the normal and exponential distributions are not valid models for the ranging error in the absence of the DP because they are consistently poor in passing the K-S test, below 80% for most data sets. Similarly for the Weibull distribution most of the passing rate is below 90%. Comparing these results to GEV and lognormal, it is possible to see that their passing rate is above 90% for most of the data sets. Only in ITI Schussler is their performance similar to the Weibull and normal distributions; which is mainly due to the lightness of the tail. In addition, GEV distribution passing rates are close to the lognormal. For some data sets, the difference between their passing rates is less than 2%. As a result these two distributions are the best candidates for modeling the tail behavior of errors in the absence of the DP. The GEV distribution models the tail behavior with three degrees of freedom, compared with two in the lognormal distribution, providing enhanced flexibility in capturing the error statistics in a variety of circumstances. It is defined as

$$f(x;\xi,\mu,\sigma) = \frac{1}{\sigma}\exp\left(-\left(1+\xi\left(\frac{x-\mu}{\sigma}\right)\right)^{-1/\xi}\right)\left(1+\xi\left(\frac{x-\mu}{\sigma}\right)\right)^{-1-\frac{1}{\xi}} \qquad (3.18)$$

for $1+\xi(x-\mu)/\sigma > 0$; where μ, σ and ξ are the location, scale and shape parameters, respectively. GEV combines three simpler distributions in the form given in (3.18). The value of the shape parameter specifies the type of the distribution. Type I, also known as Gumbel, corresponds to $\xi = 0$. Type II, Frechet, corresponds to $\xi > 0$. Type III, Weibull, corresponds to $\xi < 0$. The Gumbel and Weibull in the GEV sense correspond to the mirror images of the usual distributions [Cas88]. The normalized error data in all the measurement sets in the absence of the DP fit the Frechet type of the GEV. Although this is a candidate fit to our data we choose lognormal instead for the following reasons. First

the K-S test performance of the lognormal distribution is close to the GEV, which attests to the ability of the former in modeling the data with two degrees of freedom compared to three in the latter. Second the simplicity of the lognormal model compared to the GEV makes its application in performance bounds analysis, e.g. Generalized-CRLB, analytically more feasible, see [Qi06].

The lognormal model is then given by,

$$f\left(\psi \mid G=1, X=1\right)=\frac{1}{\psi\sqrt{2\pi\sigma_{m,pd,B}^{2}}}\exp\left[-\frac{\left(\ln\psi-\mu_{m,pd,B}\right)^{2}}{2\sigma_{m,pd,B}^{2}}\right] \tag{3.19}$$

where $\mu_{m,pd,B}$ and $\sigma_{m,pd,B}$ are the mean and standard deviation of the ranging error's logarithm. The subscripts emphasize the contributing factors. Figure 3.9-3.11 provides sample measurement results confirming the lognormal behavior of the error.

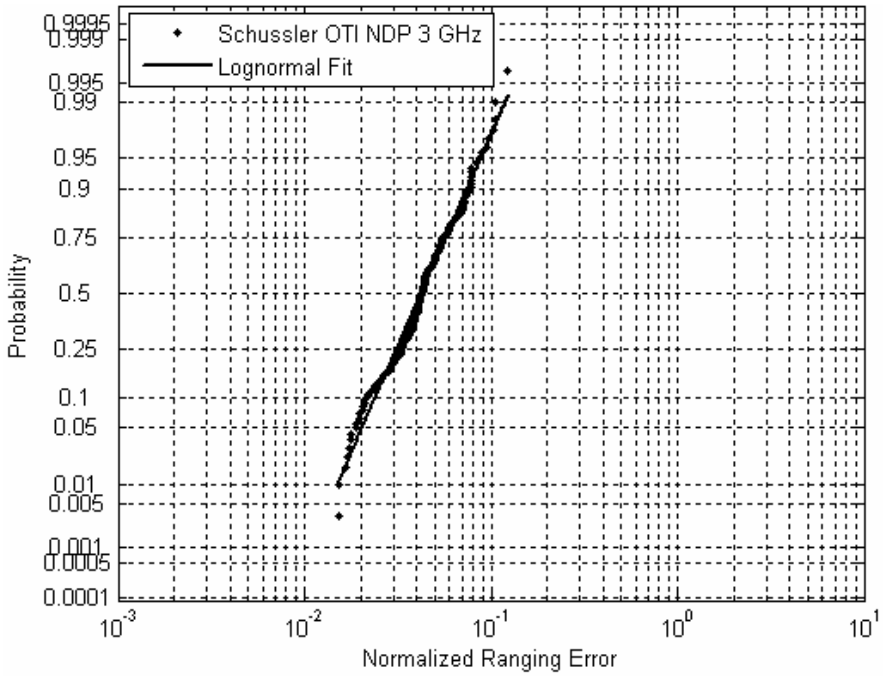

Figure 3.9: Schussler OTI at 3 GHz bandwidth: confirming the lognormality of the measured normalized ranging error

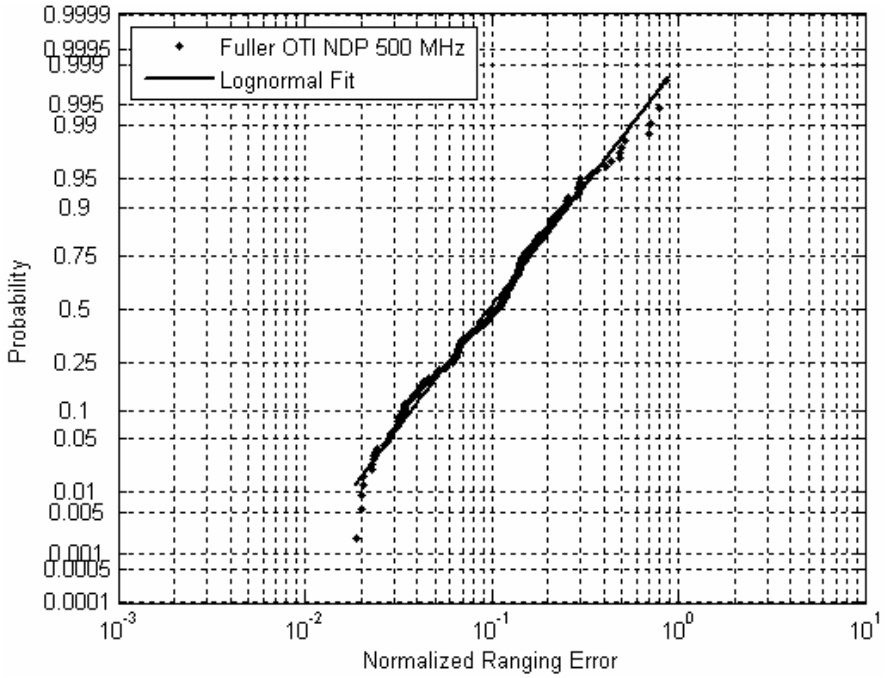

Figure 3.10: Fuller OTI at 500 MHz bandwidth: confirming the lognormality of the measured normalized ranging error

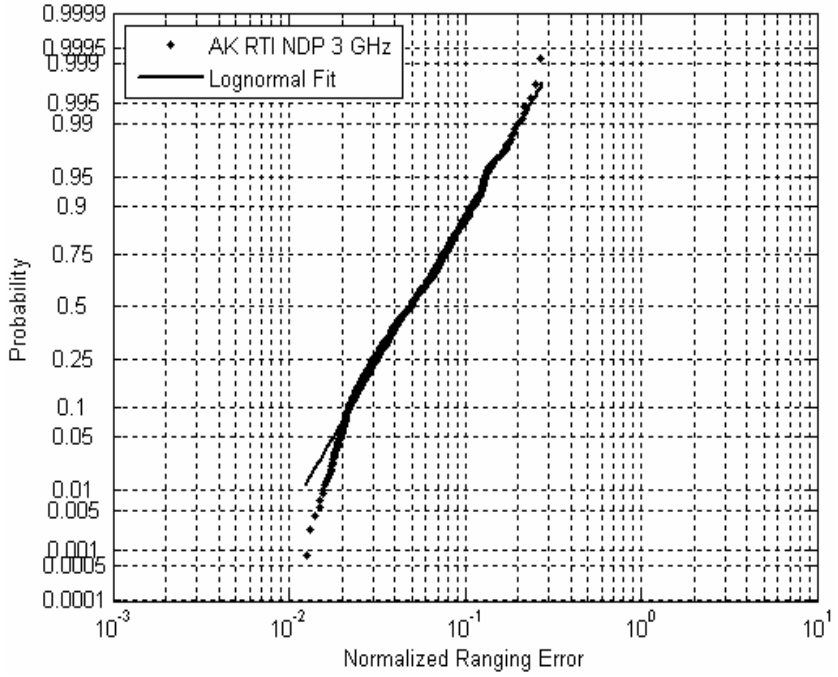

Figure 3.11: AK RTI at 3 GHz bandwidth: confirming the lognormality of the measured normalized ranging error

The estimated parameters of the lognormal distribution, obtained using Maximum Likelihood (ML) estimation techniques, for different ranging scenarios and environments are given in Table 3.6. Similar observations compared with earlier models can be observed for the correlation between the error statistics with bandwidth and ranging conditions.

Table 3.6: Lognormal distribution modeling parameters of the normalized ranging error in the absence of the direct path

Scenario	Environment	500 MHz		3 GHz	
		$\mu_{m,pd,B}$	$\sigma_{m,pd,B}$	$\mu_{m,pd,B}$	$\sigma_{m,pd,B}$
ITI	**Norton (NLOS)**	-3.13	0.62	-4.29	0.45
	Fuller (NLOS)	-1.68	0.88	-1.90	1.13
	Schussler	-1.59	0.49	-2.72	0.53
	AK (NLOS)	-2.17	0.45	-2.89	0.81
OTI	**Fuller**	-2.33	0.75	-2.99	1.17
	Norton	-2.78	0.65	-3.82	0.52
	Schussler	-2.03	0.58	-3.16	0.45
	AK	-2.32	0.51	-3.11	0.77
RTI	**AK**	-1.99	0.54	-3.01	0.61

However there are several scenarios where the extent of the correlation diminishes. For example Fuller OTI and ITI contain measurements in dense cluttered environments and increase in system bandwidth has limited impact on the parameters of the model. This is mainly due to ranging conditions that induce large blockage errors that are effectively insensitive to bandwidth changes, e.g. elevator shafts.

3.6. Simulation Results

3.6.1. Predicting Ranging Coverage

In order to predict the ranging coverage for different environments and scenarios we simulated the average DP pathloss using (3.11) according the model parameters in Table 3.2 and calculated R_c according to the definition in (3.4) for different values of system dynamic range, ρ. Figure 3.12 provides results of ranging coverage simulations against different system dynamic ranges for 500 MHz and 3 GHz system bandwidths.

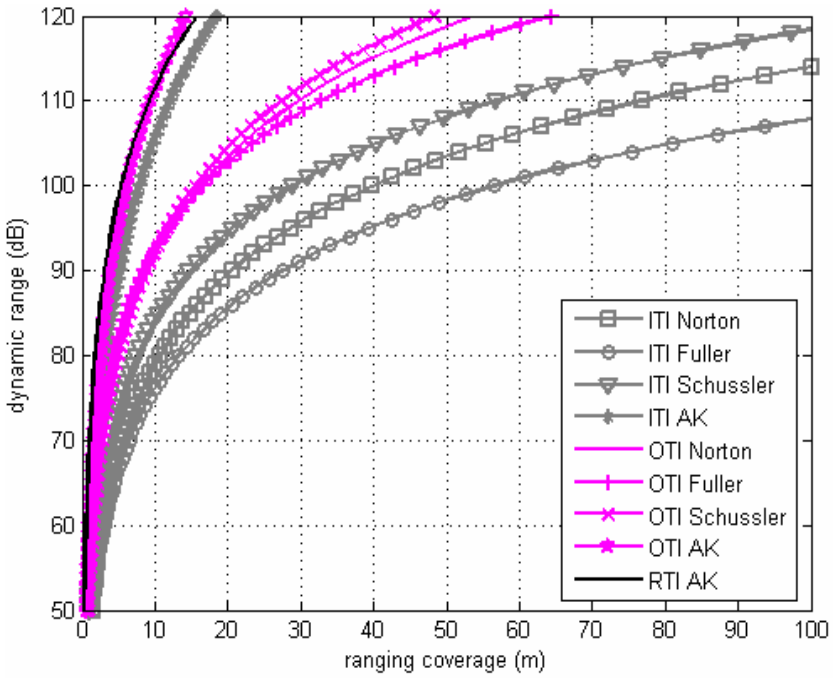

(a)

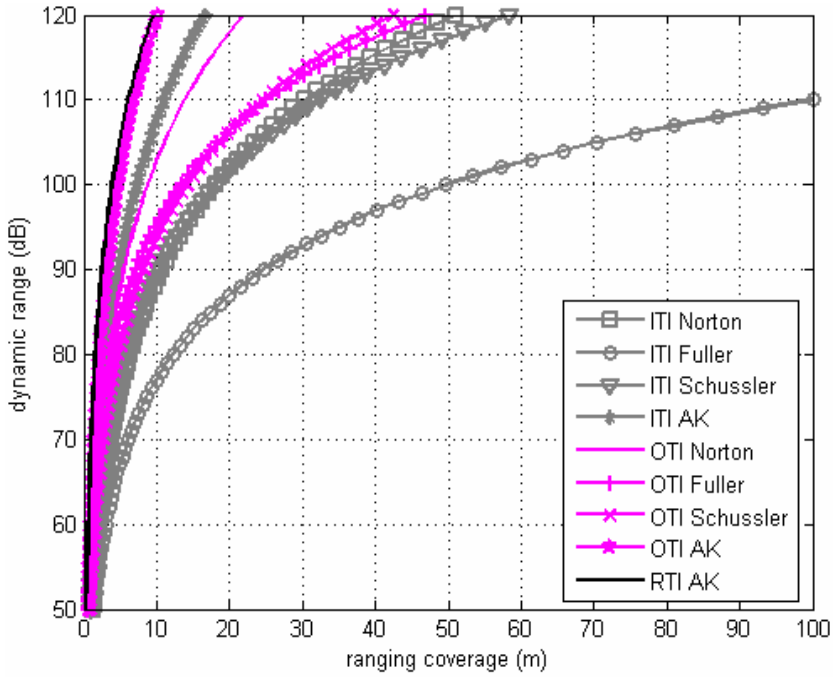

(b)

Figure 3.12: Simulating ranging coverage for system bandwidths (a) 500 MHz (b) 3 GHz.

The increase in bandwidth decreases ranging coverage due to lower energy per MPC.

As reflected in the measurement results, RTI faces the toughest constraint for ranging. The simulation reveals that for a dynamic range of around 100 dB and 500 MHz bandwidth, ranging coverage for AK RTI and OTI is less than 10 meters. For other OTI environments it is around 15 m; while ITI varies between 25-60 m depending on the LOS or NLOS conditions. Another observation from the simulation results is that the change in system bandwidth reduces the coverage substantially. This is less the case for pure LOS scenarios where the coverage is almost the same for both bandwidths, see ITI Fuller. The other ITI environments, however, are mixed LOS/NLOS for Norton and pure NLOS for Schussler and AK and that can be clearly observed in the change of their coverage between the bandwidths.

3.6.2. Ranging Error Simulation

The models presented in section 3.5, provide a very simple, yet realistic and flexible approach to statistically characterizing ranging errors experienced in typical indoor environments. The model parameters G and X provide control over the LOS/NLOS and the presence/absence of the DP conditions, respectively. The model distribution parameters then provide control over the error experienced in each condition. In order to further validate our modeling approach we simulate the normalized ranging error according to the models in section 3.5 and compare them with the measurements. For each ranging condition and scenario we run Monte Carlo simulations with 10,000 normalized range error samples. We focus on NLOS conditions since performance in LOS is intuitive and has been addressed sufficiently in the literature. Therefore we set $p(G=1)=1$ and for each sample, we run a Bernoulli trial with $p(X=1)=p(\zeta_2)$, from Table 3.3, where the outcome determines the distribution, (3.17) or (3.19). The simulated

samples are stacked in a vector and their CDF is compared to the measurement data set in that specific scenario and environment. Figure 3.13 and 3.14 provide several examples comparing the results of simulation to the measurements.

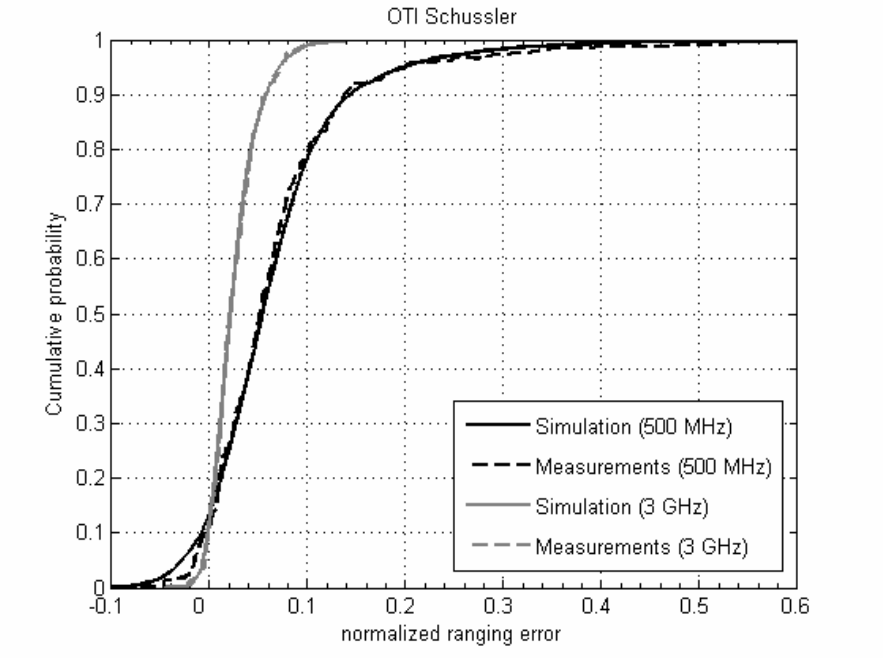

(a)

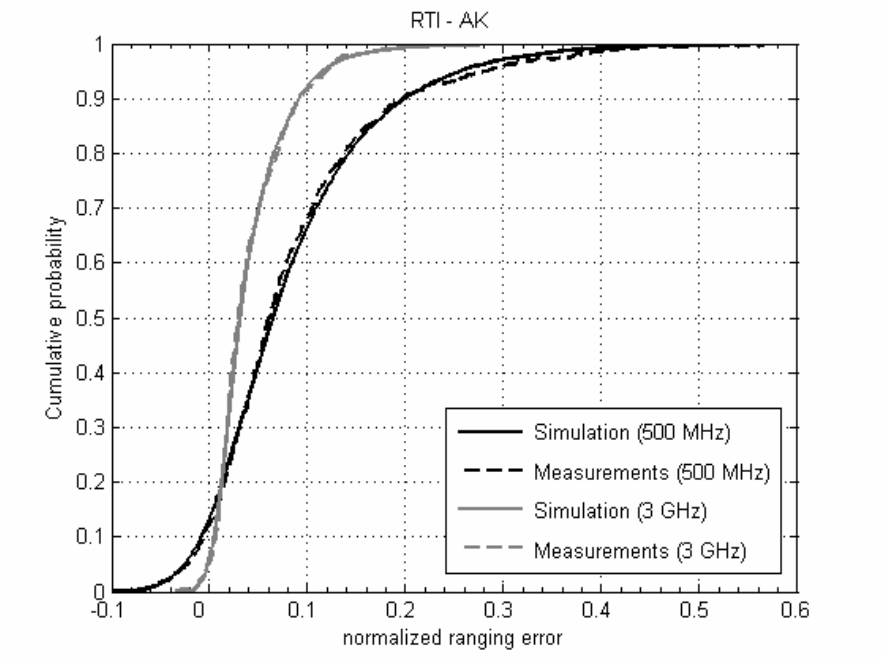

(b)

Figure 3.13: CDF of normalized ranging error: simulation vs. measurements. (a) Schussler OTI (b) AK RTI

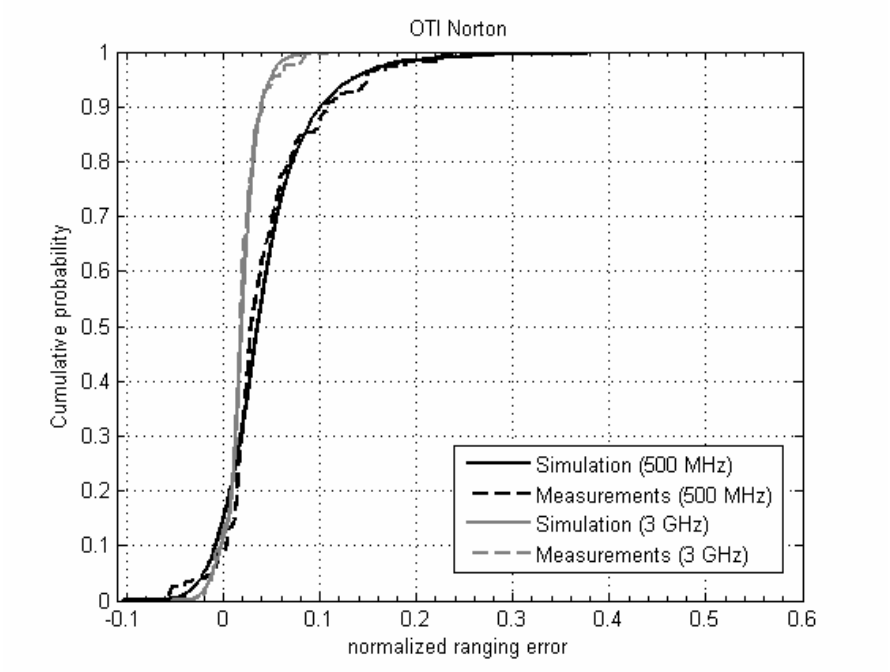

(a)

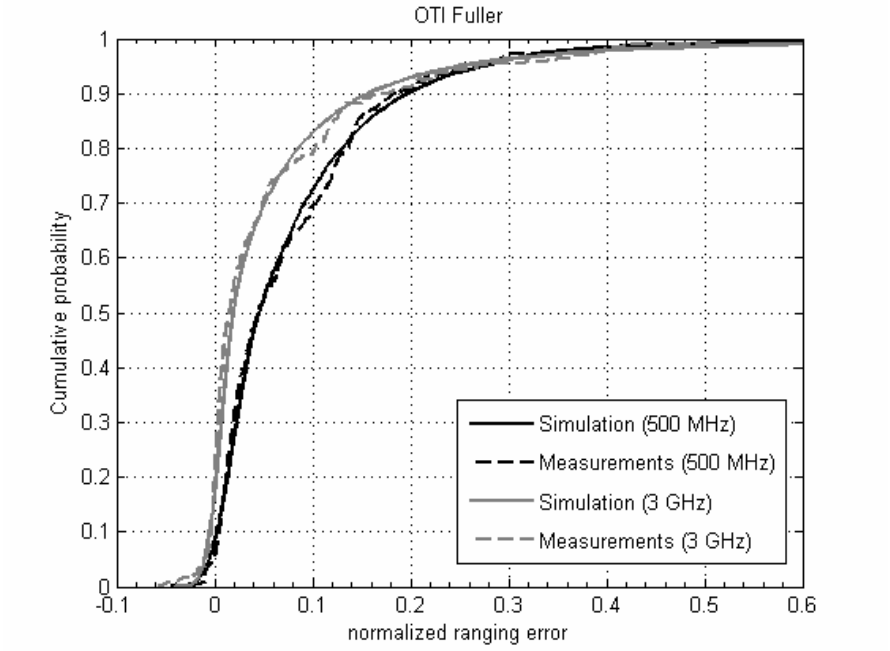

(b)

Figure 3.14: CDF of normalized ranging error: simulation vs. measurements. (a) Norton OTI (b) Fuller OTI

The models show close agreement with the measurements. This is mainly because the model has the ability to statistically describe the error in ζ_1 and ζ_2 independently. This approach provides flexibility in modeling the factors contributing to the error, which will be different depending on the ranging situation. For instance, if several MTs are scattered in an indoor environment and RPs are fixed in different locations in and surrounding the building then the ranging error PDF of all the ranging estimates can be described according to these models. The distribution will vary from heavy-tailed to normally distributed as the range conditions change from extreme NLOS to LOS.

3.7. Conclusion

In this chapter we have described a comprehensive UWB measurement and modeling campaign that was aimed at characterizing the spatial behavior of indoor TOA-based ranging. Spatial characterization involved analyzing and modeling the coverage and accuracy of ranging in indoor environments. The measurement involved four different building environments: residential, traditional office, modern office and manufacturing floor and three different ranging scenarios ITI, OTI and RTI. We showed that ranging coverage is inversely related to the bandwidth of the system and the harshness of the ranging scenario and environment. In addition, ranging error can be modeled as normal or lognormal in the presence or the absence of the DP, respectively. Furthermore, the modeling parameters are affected by the ranging scenario, environment and system bandwidth.

The modeling results in this dissertation provide an experimental analysis of the physical constraints imposed by the dense cluttered indoor environments on TOA-based

UWB ranging. In addition the models should help researchers obtain localization bounds specific to indoor environments, which are important in assessing and evaluating the limitations facing different localization algorithms.

Chapter 4 Cooperative Localization Bounds for Indoor UWB WSNs

4.1. Introduction

As we have seen from chapter 3, TOA-based ranging in indoor environments is constrained by ranging coverage and error. In addition the indoor boiling environment can cause limitation to OTI and RTI ranging due to signal penetration through the wall and roof, respectively. This can be a major challenge for firefighter or military applications. In these indoor cooperative localization applications, a small number (M) of sensors called anchors are deployed outside surrounding a building where they obtain their location information via GPS or are pre-programmed during setup. The N un-localized sensor nodes are then deployed inside the building, e.g. fire fighters or soldiers entering a hostile building, who with the help of the M anchors attempt to obtain their own location information. In traditional approaches, such as geometrical triangulation techniques, the exterior anchor nodes usually fail to cover a large building which makes localization ineffective. In addition, the problems of indoor multipath and NLOS channel conditions further degrade the range estimates yielding unreliable localization performance [Pah02]. Implementation of the cooperative localization approach, as seen in Figure 4.1, extends the coverage of the outside anchors to the inside nodes and has the ability to enhance localization accuracy through the availability of more range measurements between the sensor nodes.

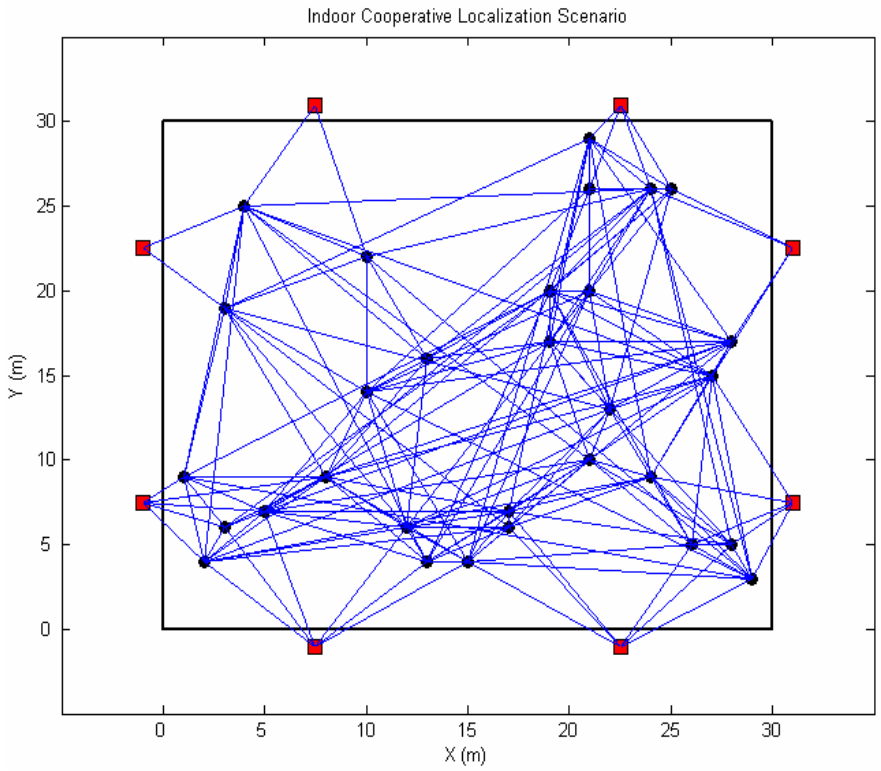

Figure 4.1: Indoor cooperative localization application. Squares are anchor nodes and circles are sensor nodes. Connectivity based on Fuller models at 500 MHz.

Effective cooperative localization in indoor WSNs does however hinge on the ranging technology. Among the emerging techniques, UWB TOA-based ranging has recently received considerable attention [Gez05, Gha04, Opp04]. In addition to its high data rate communications, it has been selected as a viable candidate for precise ranging and localization. This is mainly due to its large system bandwidth which offers high resolution and signaling that allows for centimeter accuracies, low-power and low-cost implementation [Por03, Gez05, Gha04, Opp04]. As highlight earlier in the dissertation, the performance of this technique depends on the availability of the DP signal between a pair of sensor nodes [Pah08, Lee02]. In the presence of the DP, i.e. short distance LOS conditions, accurate UWB TOA estimates in the range of centimeters are feasible due to

the high time-domain resolution [Fon02, Chu03, Ala06, Tar06]. The challenge, however, is UWB ranging in indoor NLOS conditions which can be characterized as dense multipath environments [Lee02, Pah98]. In these conditions the DP between a pair of nodes can be blocked with high probability, substantially degrading the range and localization accuracy. Therefore, there is a need to analyze the impact of these channel limitations on the performance of cooperative localization in indoor WSNs.

Evaluation of localization bounds in multi-hop WSNs have been examined extensively [Lar04, Sav05, Cha06], where the focus has been on analyzing the impact of network parameters such as the number of anchors, node density and deployment topology affecting localization accuracy. These localization bounds, however, have been analyzed with unbiased ranging assumptions between sensor nodes. In [Koo98, Bot04] the impact of biased TOA range measurements on the accuracy of location estimates is investigated for cellular network applications. Their approach assumes NLOS induced errors as small perturbations, which clearly is not the case in indoor environments. A comprehensive treatment of the impact of biases on the wireless geolocation accuracy in NLOS environments is reported in [Qi06]. Recently, position error bounds for dense cluttered indoor environments have been reported in [Jou06a, Jou06b] where the impact of the channel condition on the localization error is further verified in traditional localization.

In this chapter, based on empirical UWB TOA-based OTI and ITI ranging models in different indoor building environments reported in [Als07a, Als07b, Als08a] and presented in chapter 3, we extend the analysis of localization bounds in NLOS environments [Qi06] to cooperative localization in indoor multi-hop WSNs. We focus on

firefighter or military operation applications where we analyze the fundamental limitations imposed by the indoor dense cluttered environment. Specifically we analyze the impact of the channel modeling parameters such as ranging coverage, statistics of the ranging error, probability of NLOS and probability of DP blockage on localization accuracy. This modeling framework is necessary since OTI channel behavior affects anchor-node range estimation while ITI affects the node-node ranges. We first show that for the aforementioned indoor localization application, where traditional multi-lateration fails, cooperative localization, besides providing localization for the entire network, has the potential to further enhance the accuracy. We then evaluate the factors affecting localization accuracy, namely network and channel modeling parameters in different indoor environments: residential, manufacturing floor, traditional and modern office buildings. Indoor channel ranging model-specific cooperative localization bounds in WSNs are novel and provide comprehensive insight into the fundamental limitations facing indoor UWB TOA-based localization in both traditional and sensor networks.

The organization of this chapter is as follows. In section 4.2 we review the classification of UWB TOA-based ranging in indoor environments. In section 4.3, we present the problem formulation. In section 4.4 we derive the Generalized Cramer-Rao Lower Bound (G-CRLB) for cooperative localization in indoor multi-hop WSNs. In section 4.5 we provide results of simulation which highlight the network and ranging channel modeling parameters that affect the localization accuracy. Finally, we conclude the chapter in section 4.6.

4.2. UWB TOA-based Ranging Overview

Before proceeding with derivation of the theoretic limits of cooperative localization in indoor environments, it is necessary to review the behavior of UWB TOA-based ranging coverage and errors for the purpose of clarity. In addition to ranging coverage, localization bounds in indoor multipath channels are further constrained by the statistics of ranging error. The behavior of ranging error between a pair of nodes depends on the availability of the DP and in the case of its absence, on the statistics of the blockage. As seen in the earlier chapter the ranging error experienced in an indoor environment can then be modeled by combining the conditions in (3.6) and (3.7) through the following expression,

$$\varepsilon = b_m(\omega) + G \cdot \left(b_{pd} + X \cdot b_B(\omega) \right), \tag{4.1}$$

In order to facilitate the notations for the G-CRLB derivations we assign specific variables for each of the channel conditions in (4.1) that is,

$$\varepsilon = \begin{cases} \lambda, & G = 0, X = 0 \\ \eta, & G = 1, X = 0 \\ \beta, & G = 1, X = 1 \end{cases}. \tag{4.2}$$

The probability density functions (PDFs) of these conditions, $f_{\lambda}(\lambda)$, $f_{\eta}(\eta)$ and $f_{\beta}(\beta)$, have been experimentally obtained through comprehensive UWB channel measurements for the different ranging environments and scenarios [Als07b, Als08a] and their distance normalized distribution were introduced in chapter 3. Figure 4.2 further illustrates the different ranging conditions that are possible in a given indoor WSN.

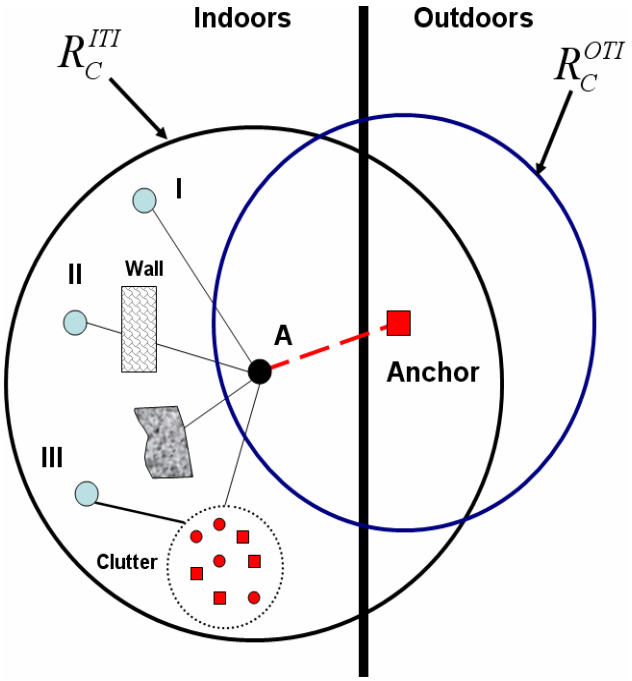

Figure 4.2: OTI/ITI ranging coverage and the associated ranging error conditions. I: λ (LOS), II: η (NLOS – DP), III: β (NLOS – NDP).

For the LOS channel, the ranging error was modeled as a normal distribution,

$$f_{\lambda}(\lambda) = \frac{1}{\sqrt{2\pi\sigma_{\lambda}^{2}}} \exp\left[-\frac{(\lambda-\mu_{\lambda})^{2}}{2\sigma_{\lambda}^{2}}\right], \tag{4.3}$$

with mean μ_{λ} and standard deviation σ_{λ} specific to the LOS multipath induced errors. In NLOS scenarios when the DP is present the amount of propagation delay and multipath due to obstructing objects, such as wooden walls, causes the biases to be more positive. Accordingly, the ranging error in this condition was modeled with a normal distribution similar to (4.3) but with higher mean and variance,

$$f_{\eta}(\eta) = \frac{1}{\sqrt{2\pi\sigma_{\eta}^{2}}} \exp\left[-\frac{(\eta-\mu_{\eta})^{2}}{2\sigma_{\eta}^{2}}\right]. \tag{4.4}$$

Finally in the absence of the DP the error was best modeled by the lognormal distribution since only positive errors are possible in this condition as seen from chapter 3. The PDF in this condition is given by,

$$f_{\beta}(\beta) = \frac{1}{\beta\sqrt{2\pi\sigma_{\beta}^{2}}} \exp\left[-\frac{\left(\ln\beta - \mu_{\beta}\right)^{2}}{2\sigma_{\beta}^{2}} \right] \tag{4.5}$$

where μ_{β} and σ_{β} are the mean and standard deviation of the ranging error's logarithm. The probability of DP blockage, $p(X=1)$, and the parameters of the normalized ranging error PDFs were reported in [Als07b, Als08a] and are reproduced in Tables 3.3, 3.4 and 3.6. The UWB ranging coverage and error models will provide a realistic platform in which to analyze the G-CRLB and the localization accuracy in different indoor multipath environments.

4.3. Problem Formulation

Based on the ranging models of chapter 3 we derive the G-CRLB for cooperative localization in indoor WSNs. The scenario we consider is as follows. *M* anchor nodes are placed outside surrounding the building with coordinates given by $\boldsymbol{\theta}_A = (x_m, y_m)^T$, where $m \in [-M, 0]$ and T is the transpose operation. These anchors are GPS-equipped where they have knowledge of their position. We assume that they are synchronized and that their position errors are negligible (or even calibrated). The problem then is to localize *N* sensor nodes with unknown coordinates that are randomly scattered in the indoor environment, see Figure 4.1. The coordinates of the nodes to be estimated are given by $\boldsymbol{\theta} = (x_n, y_n)^T$ where $n \in [1, N]$. A 2-dimensional analysis will be provided, as extension

to 3-dimensions is rather straight-forward. Furthermore, connectivity between node-node and anchor-node is assumed if the range measurements are within ITI and OTI ranging coverage, R_c^{ITI} and R_c^{OTI} respectively. Estimates beyond the ranging coverage will not be considered connected.

The range estimate between the *i*th and *j*th sensor node can then be given by

$$\hat{d}_{ij} = d'_{ij} + z_{ij} \tag{4.6}$$

where d'_{ij} is biased by one of the ranging conditions given in (4.2) or

$$d'_{ij} = d_{ij} + \begin{cases} \lambda_{ij}, & LOS \\ \eta_{ij}, & NLOS/DP \\ \beta_{ij}, & NLOS/NDP \end{cases} \qquad d_{ij} \le R_c \tag{4.7}$$

and z_{ij} is the zero mean measurement noise between the sensors. d_{ij} is the actual distance between the sensor nodes and it is given by,

$$d_{ij} = \sqrt{\left(x_i - x_j\right)^2 + \left(y_i - y_j\right)^2}\,, \tag{4.8}$$

where x and y are the x- and y-coordinates respectively. In the general case, an indoor WSN will be connected through R biased range measurements. Each $r \in [1, R]$ range measurement from node i to node j can be represented by $r \leftrightarrow (i, j)$. The range measurements are then stacked into a vector $\hat{\mathbf{d}} = \left(\hat{d}_1, \ldots, \hat{d}_R\right)^T$ where $\hat{\mathbf{d}} = \mathbf{d} + \boldsymbol{\varepsilon} + \mathbf{z}$ and the corresponding bias vector is $\boldsymbol{\varepsilon} = \left(\varepsilon_1, \ldots, \varepsilon_R\right)^T$. $\boldsymbol{\varepsilon}$ can be further decomposed into three subsets: L LOS, P NLOS/DP and Q NLOS/NDP or

$$\boldsymbol{\lambda} = \left(\lambda_1, \ldots, \lambda_L\right)^T \tag{4.9a}$$

$$\boldsymbol{\eta} = \left(\eta_1, \ldots, \eta_P\right)^T \tag{4.9b}$$

$$\boldsymbol{\beta} = \left(\beta_1, \ldots, \beta_Q\right)^T \tag{4.9c}$$

where $R = L + P + Q$. We further assume that it is possible to distinguish between these different ranging conditions through NLOS and DP blockage identification algorithms [Hei07, Guv07]. Note that even in LOS our modeling assumption maintains the existence of bias due to multipath. This is usually neglected in LOS analysis, since single-path propagation is assumed [Qi06]. The statistics of the multipath biases, obtained from measurements, are incorporated into the analysis to provide a realistic evaluation of the problem.

4.4. The Generalized Cramer-Rao Lower Bound

The unknown vector of parameters to be estimated is then obtained by combining the coordinates of the unknown nodes' positions with the bias vector, or

$$\boldsymbol{\theta} = \left(x_1, y_1, \ldots, x_N, y_N, \lambda_1, \ldots, \lambda_L, \eta_1 \ldots, \eta_P, \beta_1, \ldots \beta_Q\right)^T. \tag{4.10}$$

The CRLB provides a lower bound on the variance of any unbiased estimate of the unknown parameters [Van68]. In the case the estimates are biased it is possible to obtain the G-CRLB given that the statistics of the biases are available a priori [Qi06, Van68]. The empirical PDFs of $\boldsymbol{\lambda}$, $\boldsymbol{\eta}$ and $\boldsymbol{\beta}$ or $f_{\boldsymbol{\lambda}}(\lambda)$, $f_{\boldsymbol{\eta}}(\eta)$ and $f_{\boldsymbol{\beta}}(\beta)$ respectively were introduced in chapter 3 and their distance-normalized parameters are presented in Tables 3.4 and 3.6.

The G-CRLB is then given by [Van68],

$$E\left[\left(\hat{\boldsymbol{\theta}}-\boldsymbol{\theta}\right)\left(\hat{\boldsymbol{\theta}}-\boldsymbol{\theta}\right)^{T}\right]\geq \mathbf{J}^{-1}, \tag{4.11}$$

where $E[\cdot]$ is the expectation operation and $\mathbf{J}$ is the information matrix that consists of two parts,

$$\mathbf{J}=\mathbf{J}_{\boldsymbol{\theta}}+\mathbf{J}_{P}. \tag{4.12}$$

$\mathbf{J}_{\boldsymbol{\theta}}$ is the Fisher information matrix (FIM) which represents the data and $\mathbf{J}_{P}$ represents the a priori information that reflects the statistics of the biases. Specifically, the data FIM can be obtained by evaluating,

$$\mathbf{J}_{\boldsymbol{\theta}}=E_{\boldsymbol{\theta}}\left[\frac{\partial}{\partial\boldsymbol{\theta}}\ln f\left(\hat{\boldsymbol{d}}\,|\,\boldsymbol{\theta}\right)\cdot\left(\frac{\partial}{\partial\boldsymbol{\theta}}\ln f\left(\hat{\boldsymbol{d}}\,|\,\boldsymbol{\theta}\right)\right)^{T}\right] \tag{4.13}$$

where $f\left(\hat{\boldsymbol{d}}\,|\,\boldsymbol{\theta}\right)$ is the joint PDF of the range measurement vector $\hat{\boldsymbol{d}}=\left(\hat{d}_{1},\ldots,\hat{d}_{R}\right)^{T}$ conditioned on $\boldsymbol{\theta}$. Since the measurement noise is usually assumed zero mean Gaussian, the joint PDF can be given by,

$$f\left(\hat{\boldsymbol{d}}\,|\,\boldsymbol{\theta}\right)\propto\exp\left\{-\frac{1}{2}\left(\hat{\boldsymbol{d}}-\boldsymbol{d}'\right)\boldsymbol{\Lambda}\left(\hat{\boldsymbol{d}}-\boldsymbol{d}'\right)^{T}\right\} \tag{4.14}$$

where $\boldsymbol{\Lambda}$ is the inverse of the measurements' covariance matrix or $\boldsymbol{\Lambda}^{-1}=E\left[\left(\hat{\boldsymbol{d}}-\boldsymbol{d}'\right)\left(\hat{\boldsymbol{d}}-\boldsymbol{d}'\right)^{T}\right]$ and $\boldsymbol{d}'$ is the biased vector of the range measurements. Assuming that the measurements are uncorrelated, $\boldsymbol{\Lambda}$ is then diagonal with the elements given by $\boldsymbol{\Lambda}=diag\left(\sigma_{z_1}^{-2},\ldots,\sigma_{z_R}^{-2}\right)$. Since $f\left(\hat{\boldsymbol{d}}\,|\,\boldsymbol{\theta}\right)$ is a function of $\boldsymbol{d}'$ which is in turn a function of $\boldsymbol{\theta}$, $\mathbf{J}_{\boldsymbol{\theta}}$ can be obtained by application of the chain rule or,

$$\mathbf{J}_{\boldsymbol{\theta}} = \left(\frac{\partial \boldsymbol{d}'}{\partial \boldsymbol{\theta}}\right) \cdot E_{\boldsymbol{d}'}\left[\left(\frac{\partial}{\partial \boldsymbol{d}'} \ln f\left(\hat{\boldsymbol{d}} \mid \boldsymbol{d}'\right)\right)\left(\frac{\partial}{\partial \boldsymbol{d}'} \ln f\left(\hat{\boldsymbol{d}} \mid \boldsymbol{d}'\right)\right)^T\right] \cdot \left(\frac{\partial \boldsymbol{d}'}{\partial \boldsymbol{\theta}}\right)^T \tag{4.15a}$$

$$\mathbf{J}_{\boldsymbol{\theta}} = \mathbf{H} \cdot \mathbf{J}_{\boldsymbol{d}'} \cdot \mathbf{H}^T \tag{4.15b}$$

where $\mathbf{J}_{\boldsymbol{d}'}$ is the FIM but conditioned on $\boldsymbol{d}'$ and it is given by

$$\mathbf{J}_{\boldsymbol{d}'} = E_{\boldsymbol{d}'}\left[\frac{\partial}{\partial \boldsymbol{d}'} \ln f\left(\hat{\boldsymbol{d}} \mid \boldsymbol{d}'\right) \cdot \left(\frac{\partial}{\partial \boldsymbol{d}'} \ln f\left(\hat{\boldsymbol{d}} \mid \boldsymbol{d}'\right)\right)^T\right]. \tag{4.16}$$

The $\mathbf{H}$ matrix contains information regarding the geometry of the WSN connectivity and the condition of the biased range measurements. As a result, it can be decomposed into the three ranging conditions λ, η, and β given by

$$\mathbf{H} = \begin{pmatrix} \mathbf{H}_{\lambda}^{1} & \mathbf{H}_{\eta}^{1} & \mathbf{H}_{\beta}^{1} \\ \vdots & \vdots & \vdots \\ \mathbf{H}_{\lambda}^{N} & \mathbf{H}_{\eta}^{N} & \mathbf{H}_{\beta}^{N} \\ \mathbf{I}_{\lambda} & \mathbf{0} & \mathbf{0} \\ \mathbf{0} & \mathbf{I}_{\eta} & \mathbf{0} \\ \mathbf{0} & \mathbf{0} & \mathbf{I}_{\beta} \end{pmatrix}, \tag{4.17}$$

and it is a $(2\times N + R)\times R$ matrix. The sub-matrix components are then given by

$$\mathbf{H}_{\lambda}^{n} = \begin{pmatrix} \partial d'_{\lambda_1} / \partial x_n & \cdots & \partial d'_{\lambda_L} / \partial x_n \\ \partial d'_{\lambda_1} / \partial y_n & \cdots & \partial d'_{\lambda_L} / \partial y_n \end{pmatrix} \tag{4.18a}$$

$$\mathbf{H}_{\eta}^{n} = \begin{pmatrix} \partial d'_{\eta_1} / \partial x_n & \cdots & \partial d'_{\eta_P} / \partial x_n \\ \partial d'_{\eta_1} / \partial y_n & \cdots & \partial d'_{\eta_P} / \partial y_n \end{pmatrix} \tag{4.18b}$$

$$\mathbf{H}_{\beta}^{n} = \begin{pmatrix} \partial d'_{\beta_1} / \partial x_n & \cdots & \partial d'_{\beta_Q} / \partial x_n \\ \partial d'_{\beta_1} / \partial y_n & \cdots & \partial d'_{\beta_Q} / \partial y_n \end{pmatrix} \tag{4.18c}$$

for $n \in [1, N]$ and their respective dimensions are $(2\times L)$, $(2\times P)$ and $(2\times Q)$. $\mathbf{I}_\lambda$, $\mathbf{I}_\eta$, and $\mathbf{I}_\beta$ are the identity matrices of order L, P and Q, respectively. Elements of (4.18) will be non-zero when a range measurement is connected to node $(x_n, y_n)^T$ and zero otherwise. For example if node 1 with coordinates $(x_1, y_1)^T$ is connected to node 2 with coordinates $(x_2, y_2)^T$ by the LOS range $d'_{\lambda_1} = \sqrt{(x_1 - x_2)^2 + (y_1 - y_2)^2} + \lambda_1$ then the respective element in (4.18a) is

$$\begin{pmatrix} \partial d'_{\lambda_1} / \partial x_1 \\ \partial d'_{\lambda_1} / \partial y_1 \end{pmatrix} = \begin{pmatrix} (x_1 - x_2) \Big/ \sqrt{(x_1 - x_2)^2 + (y_1 - y_2)^2} \\ (y_1 - y_2) \Big/ \sqrt{(x_1 - x_2)^2 + (y_1 - y_2)^2} \end{pmatrix}. \tag{4.19}$$

Similarly, $\mathbf{J}_{d'}$ can be decomposed according to the ranging conditions where

$$\mathbf{J}_{d'} = \begin{pmatrix} \mathbf{\Lambda}_\lambda & \mathbf{0} & \mathbf{0} \\ \mathbf{0} & \mathbf{\Lambda}_\eta & \mathbf{0} \\ \mathbf{0} & \mathbf{0} & \mathbf{\Lambda}_\beta \end{pmatrix} \tag{4.20}$$

is an $R \times R$ matrix. Specifically, $\mathbf{\Lambda}_\lambda = diag\left(\sigma_{z_1}^{-2}, \ldots \sigma_{z_L}^{-2}\right)$, $\mathbf{\Lambda}_\eta = diag\left(\sigma_{z_1}^{-2}, \ldots \sigma_{z_P}^{-2}\right)$ and $\mathbf{\Lambda}_\beta = diag\left(\sigma_{z_1}^{-2}, \ldots \sigma_{z_Q}^{-2}\right)$. In this dissertation our focus is on analyzing the impact of the biases due to multipath and DP blockage and in reality, the measurement noise time variations in these different ranging conditions might not differ significantly for a high system dynamic range [Alj04]. As a result we will assume equal noise variance, that is $\mathbf{\Lambda}_\lambda = \mathbf{\Lambda}_\eta = \mathbf{\Lambda}_\beta$. $\mathbf{J}_{\boldsymbol{\theta}}$ can then be obtained by substituting (4.17) and (4.20) into (4.15b) or,

$$\mathbf{J}_{\boldsymbol{\theta}} = \begin{pmatrix} \mathbf{H}_{\lambda}^{1} & \mathbf{H}_{\eta}^{1} & \mathbf{H}_{\beta}^{1} \\ \vdots & \vdots & \vdots \\ \mathbf{H}_{\lambda}^{N} & \mathbf{H}_{\eta}^{N} & \mathbf{H}_{\beta}^{N} \\ \mathbf{I}_{\lambda} & \mathbf{0} & \mathbf{0} \\ \mathbf{0} & \mathbf{I}_{\eta} & \mathbf{0} \\ \mathbf{0} & \mathbf{0} & \mathbf{I}_{\beta} \end{pmatrix} \cdot \begin{pmatrix} \boldsymbol{\Lambda}_{\lambda} & \mathbf{0} & \mathbf{0} \\ \mathbf{0} & \boldsymbol{\Lambda}_{\eta} & \mathbf{0} \\ \mathbf{0} & \mathbf{0} & \boldsymbol{\Lambda}_{\beta} \end{pmatrix} \cdot \begin{pmatrix} \mathbf{H}_{\lambda}^{1} & \mathbf{H}_{\eta}^{1} & \mathbf{H}_{\beta}^{1} \\ \vdots & \vdots & \vdots \\ \mathbf{H}_{\lambda}^{N} & \mathbf{H}_{\eta}^{N} & \mathbf{H}_{\beta}^{N} \\ \mathbf{I}_{\lambda} & \mathbf{0} & \mathbf{0} \\ \mathbf{0} & \mathbf{I}_{\eta} & \mathbf{0} \\ \mathbf{0} & \mathbf{0} & \mathbf{I}_{\beta} \end{pmatrix}^{T} = \tag{4.21}$$

$$\begin{pmatrix} \mathbf{H}_{\lambda}^{1}\boldsymbol{\Lambda}_{\lambda}\left(\mathbf{H}_{\lambda}^{1}\right)^{T} + \mathbf{H}_{\eta}^{1}\boldsymbol{\Lambda}_{\eta}\left(\mathbf{H}_{\eta}^{1}\right)^{T} + \mathbf{H}_{\beta}^{1}\boldsymbol{\Lambda}_{\beta}\left(\mathbf{H}_{\beta}^{1}\right)^{T} & \cdots & \mathbf{H}_{\lambda}^{1}\boldsymbol{\Lambda}_{\lambda}\left(\mathbf{H}_{\lambda}^{N}\right)^{T} + \mathbf{H}_{\eta}^{1}\boldsymbol{\Lambda}_{\eta}\left(\mathbf{H}_{\eta}^{N}\right)^{T} + \mathbf{H}_{\beta}^{1}\boldsymbol{\Lambda}_{\beta}\left(\mathbf{H}_{\beta}^{N}\right)^{T} & \mathbf{H}_{\lambda}^{1}\boldsymbol{\Lambda}_{\lambda} & \mathbf{H}_{\eta}^{1}\boldsymbol{\Lambda}_{\eta} & \mathbf{H}_{\beta}^{1}\boldsymbol{\Lambda}_{\beta} \\ \vdots & \ddots & \vdots & \vdots & \vdots & \vdots \\ \mathbf{H}_{\lambda}^{N}\boldsymbol{\Lambda}_{\lambda}\left(\mathbf{H}_{\lambda}^{1}\right)^{T} + \mathbf{H}_{\eta}^{N}\boldsymbol{\Lambda}_{\eta}\left(\mathbf{H}_{\eta}^{1}\right)^{T} + \mathbf{H}_{\beta}^{N}\boldsymbol{\Lambda}_{\beta}\left(\mathbf{H}_{\beta}^{1}\right)^{T} & \cdots & \mathbf{H}_{\lambda}^{N}\boldsymbol{\Lambda}_{\lambda}\left(\mathbf{H}_{\lambda}^{N}\right)^{T} + \mathbf{H}_{\eta}^{N}\boldsymbol{\Lambda}_{\eta}\left(\mathbf{H}_{\eta}^{N}\right)^{T} + \mathbf{H}_{\beta}^{N}\boldsymbol{\Lambda}_{\beta}\left(\mathbf{H}_{\beta}^{N}\right)^{T} & \mathbf{H}_{\lambda}^{1}\boldsymbol{\Lambda}_{\lambda} & \mathbf{H}_{\eta}^{1}\boldsymbol{\Lambda}_{\eta} & \mathbf{H}_{\beta}^{1}\boldsymbol{\Lambda}_{\beta} \\ \boldsymbol{\Lambda}_{\lambda}\left(\mathbf{H}_{\lambda}^{1}\right)^{T} & \cdots & \boldsymbol{\Lambda}_{\lambda}\left(\mathbf{H}_{\lambda}^{N}\right)^{T} & \boldsymbol{\Lambda}_{\lambda} & \mathbf{0} & \mathbf{0} \\ \boldsymbol{\Lambda}_{\eta}\left(\mathbf{H}_{\eta}^{1}\right)^{T} & \cdots & \boldsymbol{\Lambda}_{\eta}\left(\mathbf{H}_{\eta}^{N}\right)^{T} & \mathbf{0} & \boldsymbol{\Lambda}_{\eta} & \mathbf{0} \\ \boldsymbol{\Lambda}_{\beta}\left(\mathbf{H}_{\beta}^{1}\right)^{T} & \cdots & \boldsymbol{\Lambda}_{\beta}\left(\mathbf{H}_{\beta}^{N}\right)^{T} & \mathbf{0} & \mathbf{0} & \boldsymbol{\Lambda}_{\beta} \end{pmatrix}$$

and it is a $\left(2\times N+R\right)\times\left(2\times N+R\right)$ matrix.

$\mathbf{J}_{\boldsymbol{P}}$, which contains the a priori statistics of the biases in (4.2), can be similarly obtained by

$$\mathbf{J}_{\boldsymbol{P}} = E\left[\frac{\partial}{\partial\boldsymbol{\theta}}\ln p_{\boldsymbol{\varepsilon}}\left(\boldsymbol{\varepsilon}\right)\cdot\left(\frac{\partial}{\partial\boldsymbol{\theta}}\ln p_{\boldsymbol{\varepsilon}}\left(\boldsymbol{\varepsilon}\right)\right)^{T}\right] \tag{4.22}$$

and can be decomposed into the respective ranging conditions,

$$\mathbf{J}_{\boldsymbol{P}} = \begin{pmatrix} \mathbf{0} & \mathbf{0} & \mathbf{0} & \mathbf{0} \\ \mathbf{0} & \boldsymbol{\Omega}_{\lambda} & \mathbf{0} & \mathbf{0} \\ \mathbf{0} & \mathbf{0} & \boldsymbol{\Omega}_{\eta} & \mathbf{0} \\ \mathbf{0} & \mathbf{0} & \mathbf{0} & \boldsymbol{\Omega}_{\beta} \end{pmatrix} \tag{4.23}$$

where $\mathbf{J}_{\boldsymbol{P}}$ has the same order as $\mathbf{J}_{\boldsymbol{\theta}}$. Since the biases caused by scattering and DP blockage are dependant on the indoor architecture and the range estimates between different node pairs, the elements of (4.23) can be assumed independent. With this

assumption the elements of (4.23) are $\mathbf{\Omega}_{\lambda} = diag\left(\vartheta_1^{-2},\ldots,\vartheta_L^{-2}\right)$, $\mathbf{\Omega}_{\eta} = diag\left(\vartheta_1^{-2},\ldots,\vartheta_P^{-2}\right)$, and $\mathbf{\Omega}_{\beta} = diag\left(\vartheta_1^{-2},\ldots,\vartheta_Q^{-2}\right)$, where ϑ_r^{-2} is given by,

$$\vartheta_r^{-2} = -E\left[\frac{d^2}{d\varepsilon_r^2}\ln p_{\varepsilon_r}\left(\varepsilon_r\right)\right], \qquad r \in [1, R]. \tag{4.24}$$

From chapter 3, λ and η were modeled with Gaussian distributions which means that ϑ_r^2 is the variance in the strict sense. However, β is lognormally distributed, see (4.5) and chapter 3, and evaluation of (4.24) is non-trivial but it can be shown to be,

$$\vartheta_q^{-2} = \exp\left[-2\mu_q + 2\sigma_q^2\right] \times \left(1 + \frac{1}{\sigma_q^2}\right), \quad q \in [1, Q] \tag{4.25}$$

where μ and σ are the mean and standard deviation of the ranging error's logarithm. The G-CRLB for the *N* sensor nodes can then be obtained by computing $\left[\mathbf{J}^{-1}\right]_{(2\times N)\times(2\times N)}$ from (4.12) which is the first $(2\times N)\times(2\times N)$ diagonal sub-matrix of $\left[\mathbf{J}^{-1}\right]$.

4.5. Simulation Results

4.5.1. Setup

The simulation setup is based on the application of fire-fighters or soldiers requiring localization in indoor environments. *M* anchors are distributed evenly around the building where they are placed 1 m away from the exterior wall, see Fig. 4.1. *N* sensor nodes are then uniformly distributed inside the building. Connectivity is assumed between node-node and anchor-node if the respective TOA range measurements are within ITI and OTI ranging coverage, R_c^{ITI} and R_c^{OTI}, respectively. The simulations were carried out for four

different building environments: Fuller-modern office, Schussler-residential, Norton-manufacturing floor and Atwater Kent (AK)-traditional office. All these buildings are in Worcester, MA. The UWB modeling parameters of these buildings were reported in [Als07a, Als07b, Als08a] for two system bandwidths 500 MHz and 3 GHz and they are reproduced in Tables 3.2, 3.3, 3.4, and 3.6. The dynamic range of the system, ρ, is set to 90 dB and this parameter controls the ranging coverage and the number of inter-node range measurements in the WSN. For example at 500 MHz bandwidth and 90 dB dynamic range, R_c^{ITI} will correspond roughly to 15-30 m depending on the LOS or NLOS condition and building environment. Similarly, R_c^{OTI} will be around 5-10 m depending on the building type. We set the measurement noise σ_z equal to 20 mm. For most simulations, unless otherwise stated, the probability of NLOS, $p(G=1)$, was set to 0.5. The probability of blockage, $p(X=1)=p(\zeta_2)$, however, was obtained from the measurement results in Table 3.3. The ranging conditions and the WSN inter-node connectivity are ultimately governed by the random variables G and X, see (4.1).

The models in Tables 3.4 and 3.6 are based on normalized ranging error $\psi=\varepsilon/d$. In order to compute $\mathbf{J}_P$, the de-normalized distributions, $f_\varepsilon(\varepsilon)$ must first be obtained, where $\varepsilon\in\{\lambda,\eta,\beta\}$. Thus for a given distance, d, the de-normalized distribution for one of the ranging conditions in (4.2) can be obtained by $f_\varepsilon(\varepsilon)=\left[f_\psi(\varepsilon/d)\right]/d$.

For the analysis of the simulations we compute the average RMS of the location error of each WSN topology. For a given WSN topology, the RMSE is computed by

$$RMSE = \frac{\sqrt{tr\left(\left[\mathbf{J}^{-1}\right]_{(2\times N)\times(2\times N)}\right)}}{N} = \frac{\sqrt{\sum_{i=1}^{N}\sigma_{x_i}^2 + \sigma_{y_i}^2}}{N}, \tag{4.26}$$

where $tr(\cdot)$ is the trace operation. $\sigma_{x_i}^2$ and $\sigma_{y_i}^2$ are the diagonal elements of the ith diagonal sub-matrix of $\left[\mathbf{J}^{-1}\right]_{(2\times N)\times(2\times N)}$. The average RMSE is obtained by averaging (4.26) over the total number of topologies and simulations.

4.5.2. Traditional VS Cooperative Localization

In traditional triangulation only node-anchor range measurements are used and reliable 2-dimensional location information can be obtained only if a node is covered by at least 3 anchors. In the outdoor-indoor application, for a fixed R_c^{OTI}, the dimension of the building will dictate the fraction of nodes that can be localized. Calculation of G-CRLB in traditional localization uses the same formulation in section 4.3 but only node-anchor range measurements are used. In order to verify the necessity and effectiveness of cooperative localization we carried out 5000 Monte Carlo simulations with 100 different topologies and 50 simulations per topology for different D/R_c^{OTI} values. 500 MHz Fuller models were used with 4 anchors and 40 sensor nodes. We also assumed a square building with dimensions $(D,D)^T$. Figure 4.3 provides the results of this simulation where the percentage of un-localized nodes is plotted as function of D/R_c^{OTI}. Figure 4.4 shows the average RMSE results.

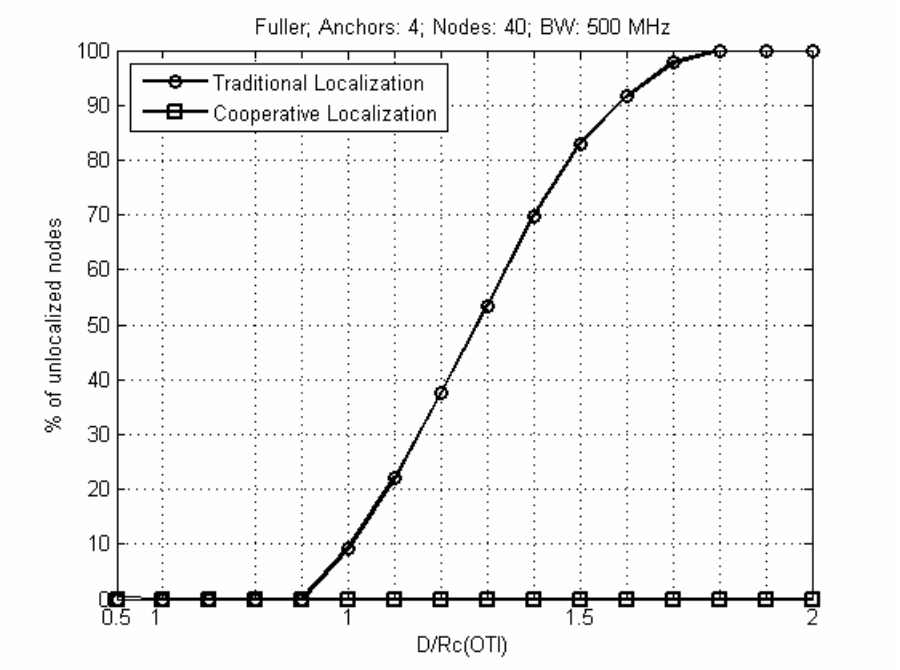

Figure 4.3: Percentage of un-localized sensor nodes as a function of D/R_c^{OTI} .

As expected, starting around $D/R_c^{OTI} = 1$, 10% of the nodes are un-localized in traditional localization. As the size of the building increases more nodes lose direct coverage to at least 3 of the outside anchors. By $D/R_c^{OTI} = 1.8$, triangulation is no longer possible. In comparison, cooperative localization is effective and provides position estimates for all the nodes.

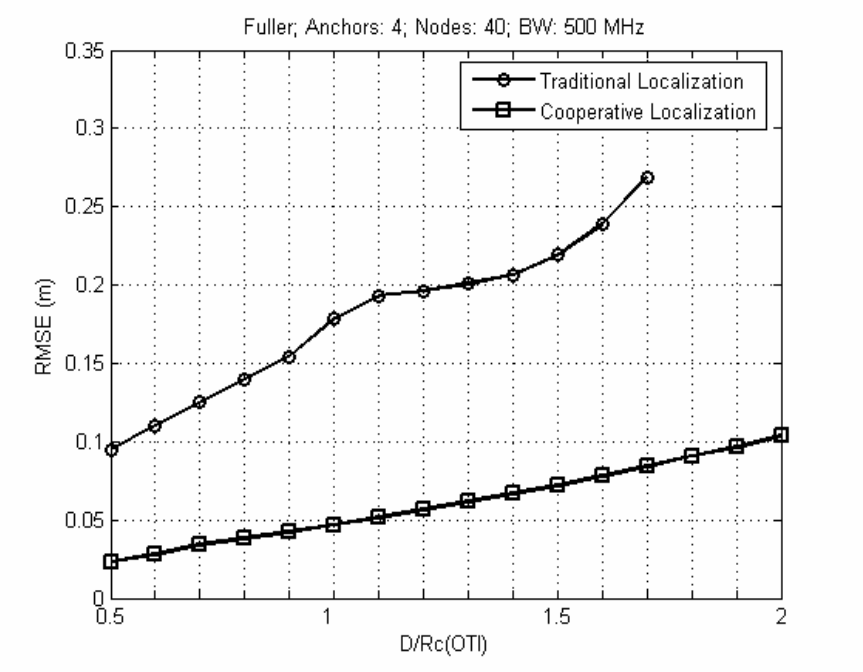

Figure 4.4: Traditional triangulation vs. cooperative localization performance.

Moreover, Figure 4.4 shows that cooperative localization substantially outperforms the traditional counterpart. This means that for firefighter/military applications, localization in indoor environments, especially in large buildings, cannot be achieved with triangulation alone. Cooperative localization will not only extend the coverage of the outside anchors to the inside nodes but enhance localization accuracy substantially. Further, for large building scenarios $D/R_c^{OTI} > 2$ more sensor nodes (i.e. greater node density) need to be deployed to maintain sufficient connectivity for effective cooperative localization.

4.5.3. Network Parameters

In this subsection we evaluate the impact of network parameters on localization accuracy. In the first experiment we investigate the impact of node density. For the

simulation we fixed the number of anchors to be 4 and the dimension of the building to be $D = 25$ m and increased the number of nodes, i.e. node density which is defined by $S = N/D^2$. 5000 Monte Carlo simulations were carried out (50 different topologies and 100 simulations per topology). The latter is needed, since the ranging conditions and WSN connectivity are governed by Bernoulli random variables G and X . Figure 4.5 shows the simulated results for 500 MHz modeling parameters.

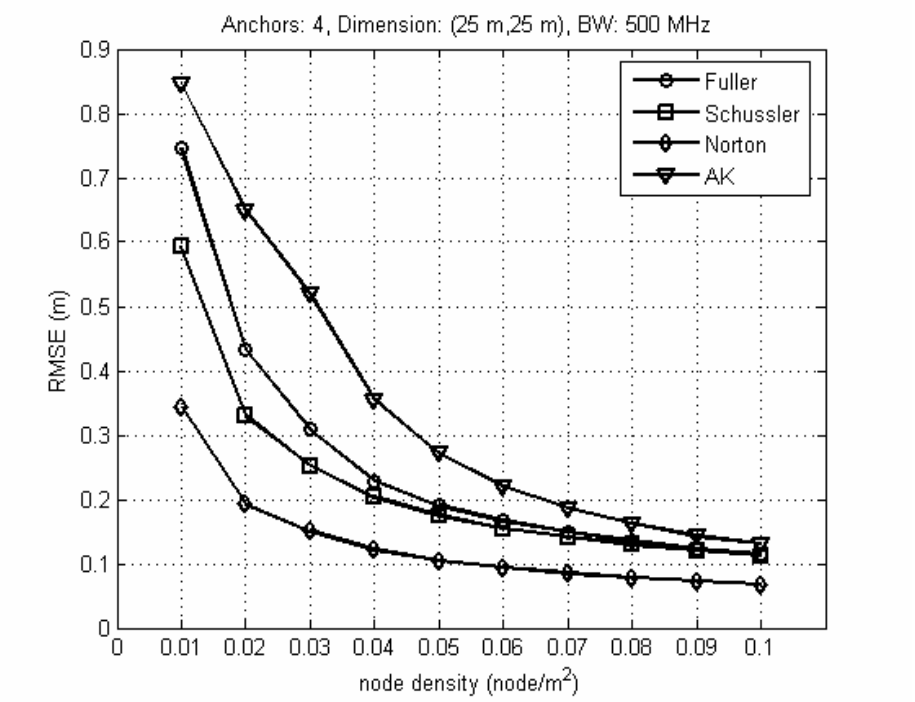

Figure 4.5: Localization performance as a function of node density in different indoor environments using 500 MHz models.

Office buildings, AK and Fuller, exhibit the worst performance especially in sparse densities. Norton, a manufacturing floor, shows the best localization accuracy among the different buildings. This is expected since the manufacturing building's interior is an open-space with cluttered machines and metallic beams which is reflected in the ranging

coverage and error models. Further, the localizaiton bounds clearly indicate that performance is dependant on ranging coverage, R_c^{ITI} and R_c^{OTI}, probability of DP blockage, $p(X=1)$ and the respective error distributions $f_\varepsilon(\varepsilon)$, see Tables 3.2, 3.3, 3.4 and 3.6. Although AK has a lower ITI $p(X=1)$ than Fuller, the performance in the former is worse due to shorter ITI ranging coverage. This can be seen by the difference in the pathloss exponents in Table 3.2. Shorter R_c^{ITI} means less inter-node range information and thus higher localization error. Another important observation that can be concluded from this simulation is that the disadvantages of the indoor channel condition, ranging coverage and error, can be minimized by increasing node density. For instance, at 0.1 node/m^2 the difference in localization performance between the buildings diminishes significantly.

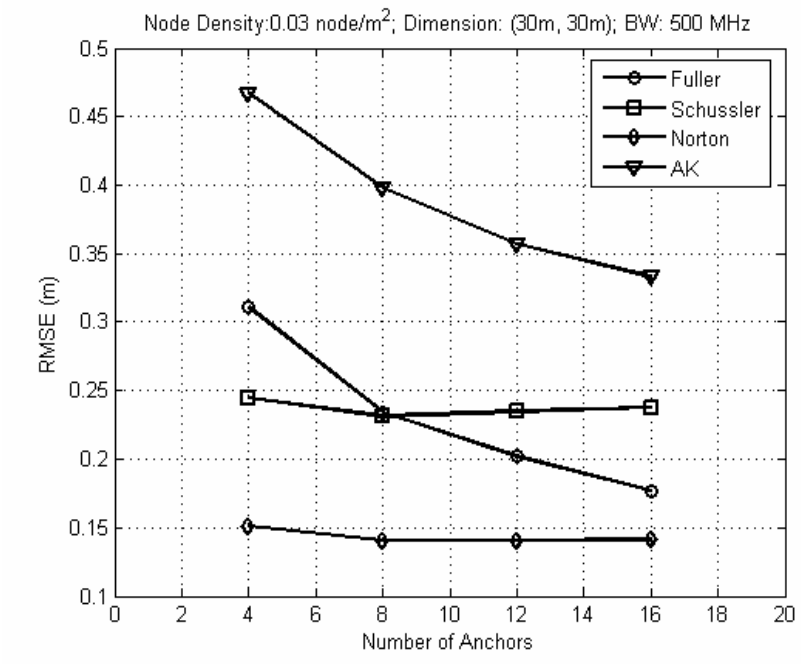

Figure 4.6: Localization performance as a function of number of anchors in different indoor environments using 500 MHz models.

The impact of anchors on the localization accuracy is investigated in Figure. 4.6. In this experiment, 5000 simulations were carried out with $D = 30$ m, $S = 0.03$ node/m^2 and the number of anchors were varied from 4 to 16 (anchors per side varies from 1 to 4). The results show that the effect of increasing the number of anchors is higher in the office buildings compared to the residential and manufacturing floor. This means that building environments with harsher indoor multipath channels (lower R_c^{ITI} and higher $p(G=1)$ and $p(X=1)$) require more anchors around the building for a fixed amount of sensor nodes to achieve similar localization performance as environments with "lighter" multipath channels. Finally, comparing both Figs. 4.5 and 4.6 it is apparent that node density has a higher impact on the localization accuracy compared with the number of anchors. A similar observation was reported in [Sav05] where localization error exhibited less sensitivity to the number of anchors.

4.5.4. Ranging Model Parameters

In this sub-section we investigate the impact of the ranging model parameters: system dynamic range, ρ, $p(G=1)$ and $p(X=1)$ for 500 MHz and 3 GHz system bandwidths. First we evaluate the localization bounds for different values of ρ which controls both the R_c^{ITI} and R_c^{OTI}. In this experiment, the number of anchors is 4, $S = 0.04$ node/m^2 and the building dimension is $D = 30$ m. We ran 5000 Monte Carlo simulations (100 topologies and 50 simulations per topology). Figure 4.7 shows the simulated localization results as a function of dynamic range for different building environments and ranging models.

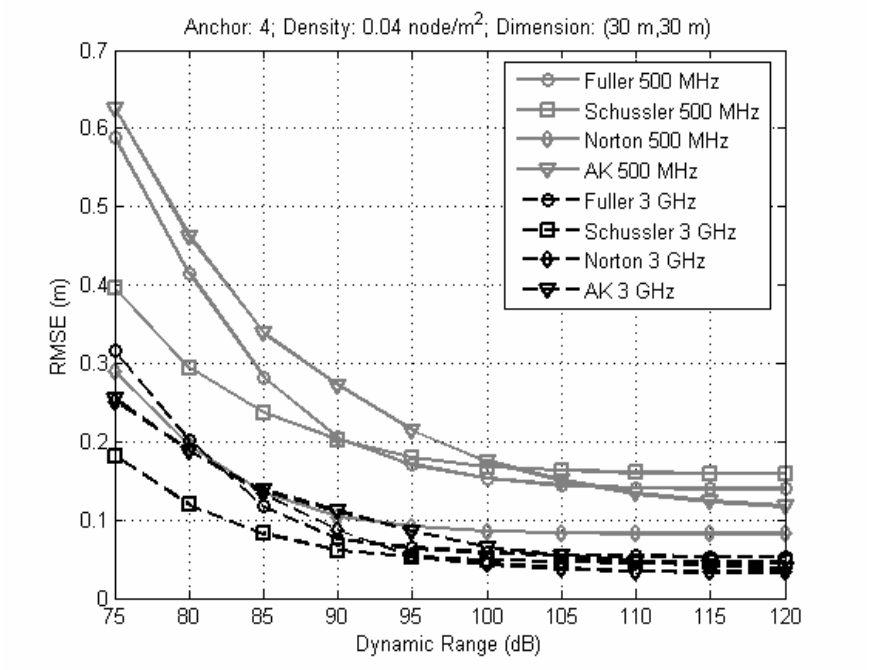

Figure 4.7: Localization Performance as a function of dynamic range, ρ for 500 MHz and 3 GHz models.

The localization performance in office buildings at 500 MHz is in general worse than in residential and manufacturing buildings. However, at 3GHz, the difference diminishes. Another interesting observation is that the impact of increasing the dynamic range eventually saturates. This means that after a certain dynamic range value all the nodes are connected to each other and no further gain can be achieved. The performance in buildings with higher ranging coverage tends to saturate earlier as seen when comparing AK with Norton or Schussler buildings.

The second experiment focuses on the impact of the probability of NLOS on the localization bounds where we varied $p(G=1)$ experienced by the ITI ranges from 0 to 1. This doesn't affect OTI since it is always considered NLOS. $p(X=1)$, however, was obtained from Table 3.3 and the respective ranging error distribution parameters from

Tables 3.4 and 3.6. We ran 5000 Monte Carlo simulations (50 topologies and 100 simulations per topology). The number of anchors is 4, $S = 0.03$ node/m^2 and $D = 30$ m which means N is around 34. The results are presented in Figure 4.8.

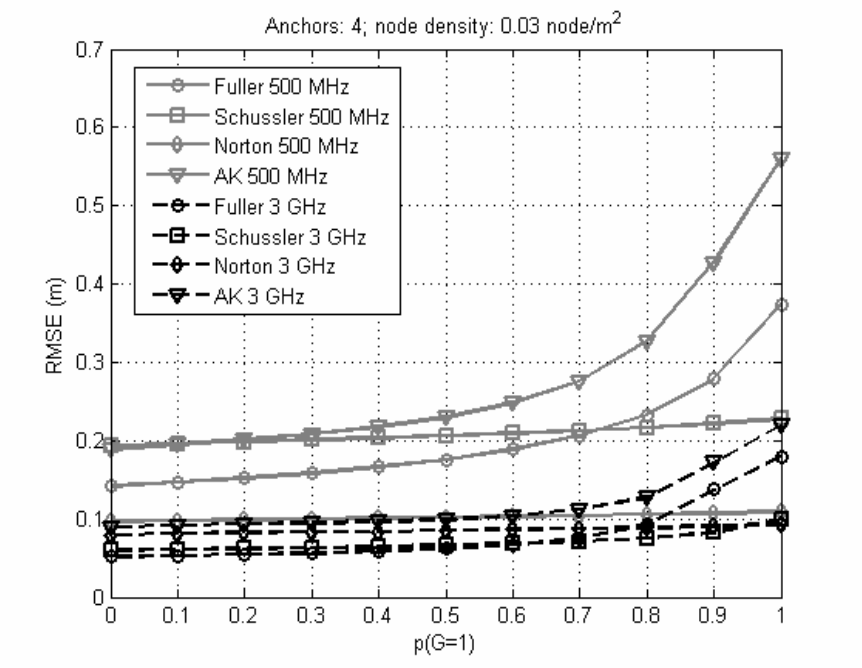

Figure 4.8: Localization performance as a function of $p(G=1)$ for 500 MHz and 3 GHz models.

The impact of multipath on localization error can be clearly seen for $p(G=1)=0$. Although the variance of the multipath bias models is dependant on the measurement campaign, it is important nonetheless to see that an average RMSE between 0.14-0.2 m can be caused by multipath alone for 500 MHz models. The effect of multipath however decreases substantially for the 3 GHz system bandwidth. As expected, increasing $p(G=1)$ further degrades the localization performance in an indoor environment. The effect will be greater in buildings where $p(X=1)$ is high. For example, both Fuller and

AK NLOS channel models, see Table 3.3, exhibit rather high probabilities of DP blockage and this is reflected in the localization performance. Finally Norton building is least impacted by NLOS because the blockage probability is low and the error statistics are significantly smaller than the other buildings.

Lastly, we investigate the impact of DP blockage probability. For the ranging error distributions given in Tables 3.4 and 3.6 we fix $p(G=1)=1$ and vary $p(X=1)$ between 0 and 1. We ran 5000 Monte Carlo simulations (50 topologies and 100 simulations per topology). The number of anchors is 4, $S=0.04$ node/m^2 and $D=30$ m. The results are presented in Figure 4.9.

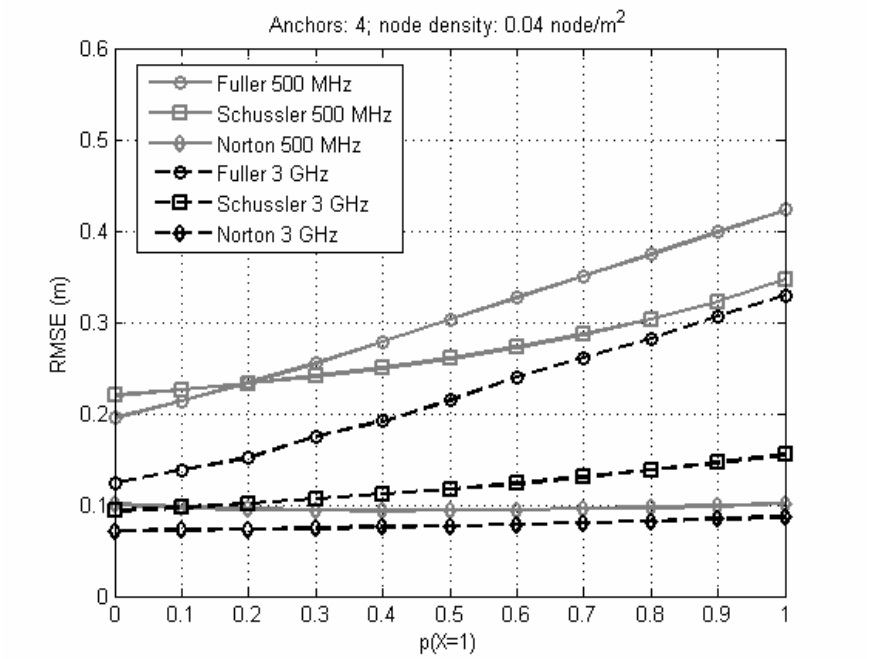

Figure 4.9: Localization performance as a function of DP blockage probability, $p(X=1)$ for 500 MHz and 3 GHz models.

For this specific experiment, results for AK were not available because $p(G=1)=1$, which means that the ITI ranges are always NLOS and thus shorter ranging coverage. In AK's case, the WSNs in all the simulations were ill-connected. Nonetheless, the results in the other buildings show that increasing $p(X=1)$ worsens the localization error. Norton is an exception, since the statistics of the ranging error in the presence and absence of the DP are close to each other (see Tables 3.4 & 3.6). The impact of blockage probability on office buildings is the highest, since the statistical distribution of the lognormal biases exhibits a higher "variance" compared to manufacturing or residential buildings. This can be seen in the Fuller model in Table 3.6 where such an environment exhibits a heavier tailed distribution of the spatial ranging errors [Als07b, Als08a]. For these conditions, when the DP blockage occurs, larger number of MPCs are lost causing higher ranging error. Finally it is interesting to note that the impact of system bandwidth has limitations in areas where heavier construction and obstacles separate sensor nodes. This can be seen by comparing the impact of bandwidth on the localization performance in Schussler and Fuller.

4.6. Conclusion

In this chapter we provided an analysis of cooperative localization bounds for WSNs based on empirical models of UWB TOA-based OTI and ITI ranging in indoor multipath environments. We verified the need for cooperative localization in applications where indoor sensor nodes lack sufficient coverage to outdoor anchor nodes. We also verified that in addition to extending coverage, cooperative localization has potential for improving accuracy. In addition we provided a comprehensive evaluation of the

limitations imposed by the indoor multipath environment on cooperative localization performance in multi-hop WSNs.

Simulation results showed that increasing node density improves localization accuracy and can improve performance on indoor multipath channels. Increasing the number of anchors however has greater impact on harsh indoor environments such as office buildings due to shorter ranging coverage, i.e. less inter-node connectivity. For the ranging model parameters, localization is constrained by the ranging coverage, statistics of ranging error, probability of NLOS, probability of DP blockage and bandwidth. In general, office building structures introduce higher probability of NLOS/DP blockage and shorter ranging coverage (higher DP penetration loss and pathloss exponent) which means higher localization error. Manufacturing floors and residential buildings on the other hand exhibit better performance due to "lighter" indoor channel conditions. Also, increasing the system bandwidth has the effect of improving accuracy although reduces ranging coverage. The localization performance in office buildings exhibited less sensitivity to changes in bandwidth because the range measurements faced harsher obstacles such as metallic doors, vending machines and elevators.

As for the cooperative localization application for firefighter or military operations, it is clear that in order to improve accuracy numerous nodes must be deployed in the indoor environment alongside those attached to the personnel. In addition to providing the necessary network density required for effective localization, these stationary nodes can constantly provide ranging/localization information which further improves performance in dense cluttered environments.

Future work in this area should aim to extend the analysis to 3-dimensions where RTI ranging can provide coverage extension to multi-floor buildings. Further measurements and modeling are needed to analyze the ranging error beyond ranging coverage. Specifically the behavior of the biases and measurement time variations with distance must be evaluated for different ranging scenarios and environments. Finally, research in localization algorithms for indoor-specific WSNs is needed to identify and mitigate NLOS biased range measurements in order to achieve acceptable localization performance.

Chapter 5 A Cooperative Localization Algorithm for Indoor WSNs

5.1. Background

Distributed localization algorithms iteratively achieve an estimate through the sharing of the range and location information. They can be further sub-divided into two branches: direct ranging (DR) based or extended ranging (ER) based. The DR-based algorithms are usually referred to as Recursive Position Estimation (RPE), while the ER-based algorithms are usually referred to as Multi-hop Network Localization (MNL). Most of the proposed algorithms in the literature are derivatives of these two and the distinction is based on the method by which a distance between a pair of nodes is obtained. In DR, a node only obtains range estimates to anchors. Once the node has range measurements to 3(4) anchors, it is possible to obtain the 2(3)-dimension position estimate. The node then joins the existing anchors and helps the remaining nodes in the localization process. Figure 5.1 illustrates the DR-RPE distributed algorithm.

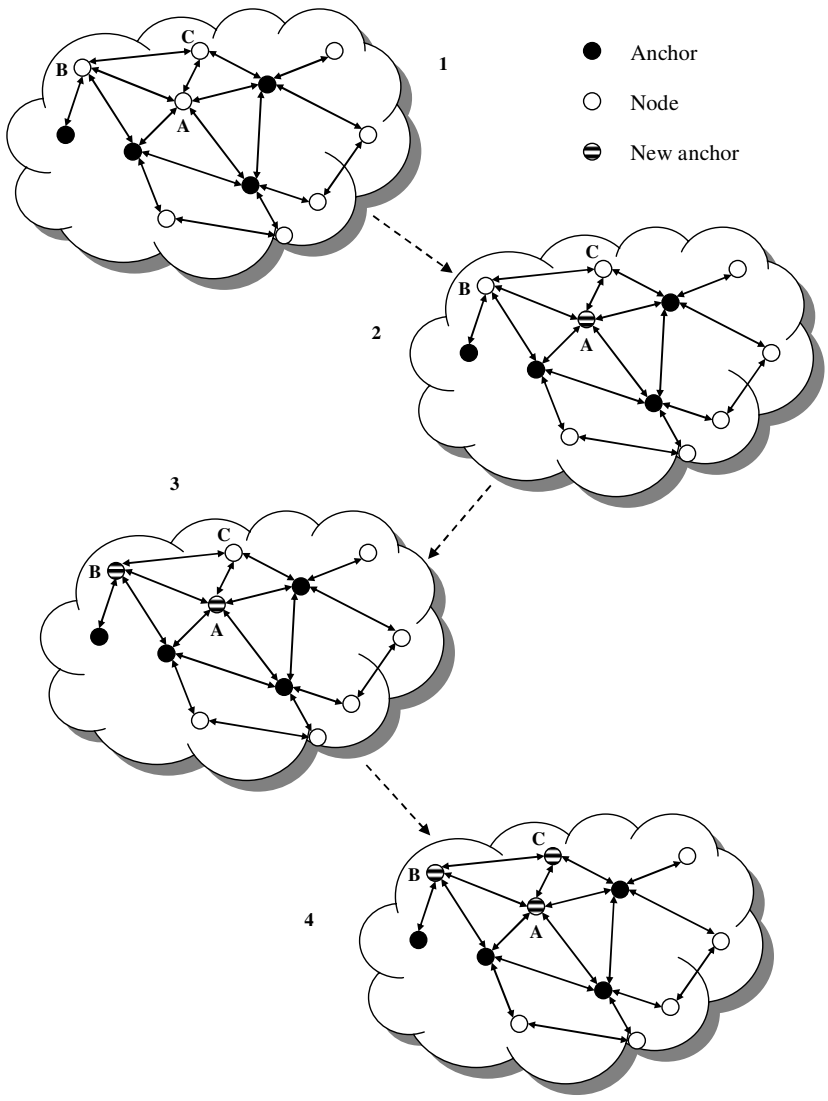

Figure 5.1: Direct Ranging - Recursive Position Estimation Distributed Localization

In this example, node A is the only node in the network that has DR measurements to three other anchors. As a result, it obtains a position estimate through the LS or WLS algorithm described earlier. In step 2, node B, with the help of newly transformed A, obtains a position estimate. Node B upgrades to an anchor in step 3. The process repeats and node C becomes an anchor in step 4. Note that one drawback of this algorithm is that

it is possible that some nodes on the *edge* of the network lack sufficient direct connectivity anchors and thus are unable to localize themselves.

In the case of ER, however, nodes attempt to estimate the distances between themselves and a fixed pool of anchors. The nodes will obtain the distance estimate through a variety of methods, including counting the number of hops to an anchor, measuring the distance to the anchor (adding all distances in the path) or more accurately trying to obtain a geometric estimate of the distance by relying on the relative location of nodes surrounding it. In other words, nodes *extend their range* to anchors by measuring and cooperating to provide an estimate of their distances to an anchor, which is beyond their coverage. Figure 5.2 provides an example of ER distributed localization.

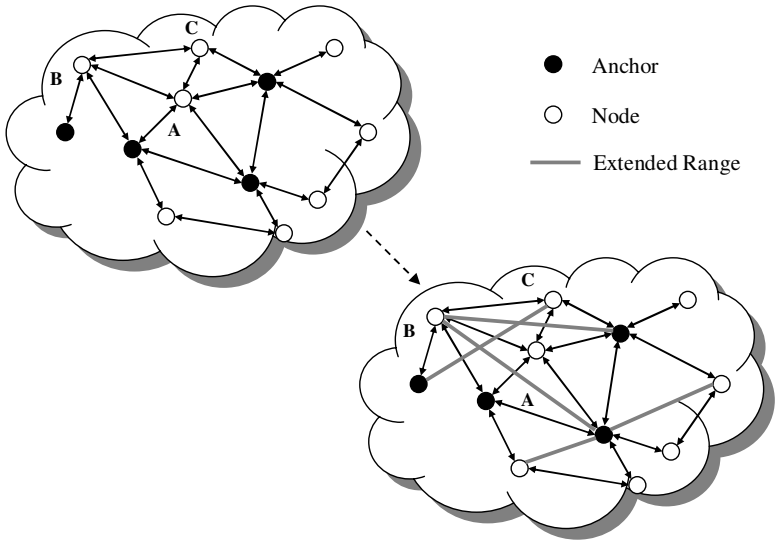

Figure 5.2: Extended Ranging - Multi-hop Distributed Localization

In this example, nodes A, B and C attempt to estimate their distances to the fixed anchors. Once they have that information, they localize themselves. In this fashion, nodes that are not in the direct range of the anchors get a best-effort estimate of the range. Intuitively, DR-based algorithms are more accurate because there is no error

accumulation in the range information. The major draw-back of DR-based algorithms, however, is the requirement for a certain node and anchor densities. The advantages include very accurate localization and substantially less error propagation. DR-based algorithms have been reported in [Alb01, Als06a, Als06b]. ER-based algorithms, on the other hand, have less reliable error characteristics because the distance to an anchor is not measured. Instead, it is estimated by either the number of hops or geometric estimation. Although ER-based algorithms have less stringent requirements on the densities of anchors and nodes, they exhibit substantial error propagation characteristics, which explain the divergence problems that some of the algorithms in the literature have reported. ER-based algorithms have been used in N-hop multilateration [Savr01], Robust Positioning Algorithm [Savr01, Savr02], and Ad-hoc Positioning Algorithm (APS) [Nic01].

The ER-MNL algorithm is easier to implement than the DR-RPE because the multi-hop positioning algorithm requires a minimum of three reference nodes within the whole operational field, assuming mobile nodes can communicate with all reference nodes through multi-hop communications, while the RPE algorithm has a stricter requirement on the deployment density of reference nodes and mobile nodes. For example, when the deployment density of reference nodes or mobile nodes is low, in some situations, the iterative process may not be able to continue due to the lack of nodes in the close neighborhood.

In this chapter we introduce a novel DR-RPE distributed algorithm that incorporates a mechanism for robust iterative node-anchor transformation. The algorithm named Cooperative LOcalization with Quality of Estimation (CLOQ) essentially relies on its

ability to estimates the quality of the channel condition between sensor nodes and incorporate that information in the localization process. In addition in order to mitigate the effects of error propagation, the algorithm also estimates the quality of anchor position estimates which can then be utilized in order to safely update the pool of available anchors. This algorithm is specifically needed in indoor environments in order to allow for effective cooperative localization. Simulation results have showed that CLOQ is capable of providing substantial localization performance improvements.

In this chapter we first introduce the details of CLOQ algorithm and show how the channel and position information can improve performance. Then in section 5.3 we provide simulation results highlighting the impact of node density, anchor density and network parameters on the performance of localization. Specifically we show that CLOQ algorithm can get closer to the G-CRLB when compared to traditional RPE algorithms. Finally we will conclude the chapter with section 5.4.

5.2. Cooperative LOcalization with Quality of estimation (CLOQ)

5.2.1. Overview

As evident from the earlier chapters, the most fundamental challenges to node localization in indoor WSNs are the effects of the RF propagation channel on TOA estimation. The problem becomes even more challenging for iterative algorithms such as RPE where the biased range errors affecting single node localization, directly impacts the localization performance in the entire WSN. As a result, in order to improve localization in WSNs, distributed algorithms must address the following:

- The quality of TOA-based range measurements must be assessed and integrated into the position estimation.
- The quality of the estimated node position must be assessed and integrated into the iterative node-anchor transformation procedure.

The incorporation of these two major points is necessary in order to mitigate the effects of the indoor channel, reduce the divergence in the solution and control error propagation. These will ultimately provide enhanced localization accuracy which can enable effective WSNs communication and localization in indoor environments.

In order to clarify these estimation criteria we refer to Figure 5.3 which provides an illustrative explanation of the concept of *quality*.

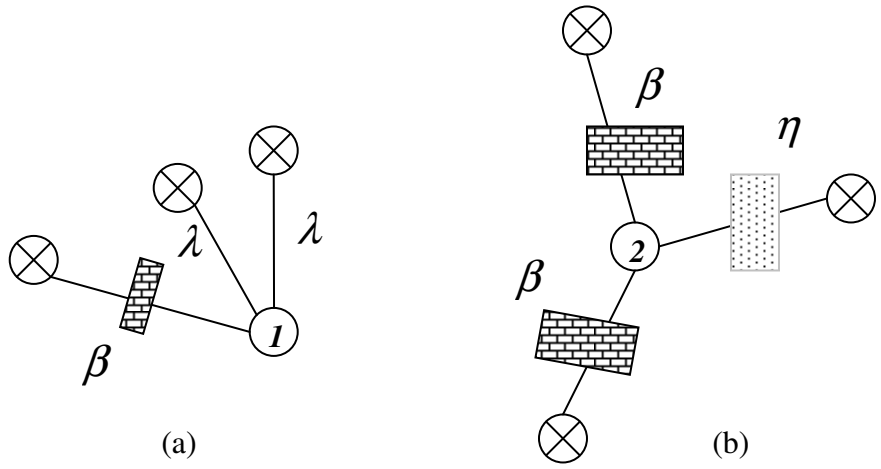

Figure 5.3: Quality of range measurements & position estimates. (a) Bad geometry but acceptable range measurements. (b) Good geometry but unreliable measurements.

In Figure 5.3 (a), node *1* has two LOS range measurements and one DP blocked range measurements but its geometrical configuration results in a *bad* GDOP. On the other hand, although node *2* in Figure 5.3 (b) has a better GDOP, its range measurements to the

anchors are not reliable. Specifically it has three NLOS ranges with two of them the DP is blocked. It would be therefore desirable from a performance point of view to be able to quantify the impact of these propagation and network constraints on the localization accuracy of nodes *1* and *2*.

CLOQ is an iterative distributed algorithm that addresses these two issues by incorporating the range measurement information and the confidence of the position estimates. The algorithm has 4 stages:

1. Channel Identification & Mitigation: sensor nodes perform TOA ranging to available anchor nodes and identify the channel conditions. The channel conditions can be either λ (LOS), η (NLOS – DP) or β (NLOS – NDP). Please refer to Figure 4.2 for further clarifications.
2. Position Estimation: Once a node receives range information from at least 3 anchors (for 2-dimensional localization) it performs localization using WLS algorithm described earlier. The weights in WLS algorithm are created by *combining* the ranging weights with the position confidence weights of the selected anchors. The node then computes its own position and confidence index and enters into *anchor nominee* phase.
3. Anchor Nomination: the potential anchor nominees then compare their position confidence by broadcasting their information to other direct-hop nominees and the node with highest variation from the norm withdraws from the process. The remaining nominees move on to the next stage.
4. New Anchor Incorporation: anchor nominees transform into anchor nodes and start transmitting anchor range packets to the remainder of the WSN.

5.2.2. Step I: Channel Identification

The statistical relationship between the RF channel and the TOA ranging error are essential in the identification process. In [Guv07] the kurtosis of the channel was used to distinguish between LOS and NLOS. In [Hei07], on the other hand, the statistics of the propagation channel such as RMS delay spread, mean excess delay, total signal power and their combination were used in order to identify between the presence and absence of the DP. In this dissertation we use the first path power (FPP) and the total signal power (TP) in order to identify between LOS, NLOS/DP and NLOS/NDP. As a result a sensor node would examine the measured FPP and TP and attempt to identify the channel condition. This is then used to *weigh* the TOA range measurements to the respective anchors in order to further improve the localization performance.

Using the measurement database introduced in chapter 3, we can analyze the statistical relationship between the power and the channel condition. Accordingly we divide the database into OTI and ITI and their respective ranging conditions such as illustrated in Figure 5.4. Instead of analyzing the FPP or TP individually we decide to examine their ratio. Therefore we define the following ratio

$$\delta = \frac{|\alpha_1|}{\sum_{k=1}^{L_p} |\alpha_k|} \tag{5.1}$$

where L_p is the number of MPCs, and α_k is the amplitude of the k^{th} path. In (5.1), α_1 refers to the first path power. In the case the first path power is the DP then $\alpha_{DP} = \alpha_1$.

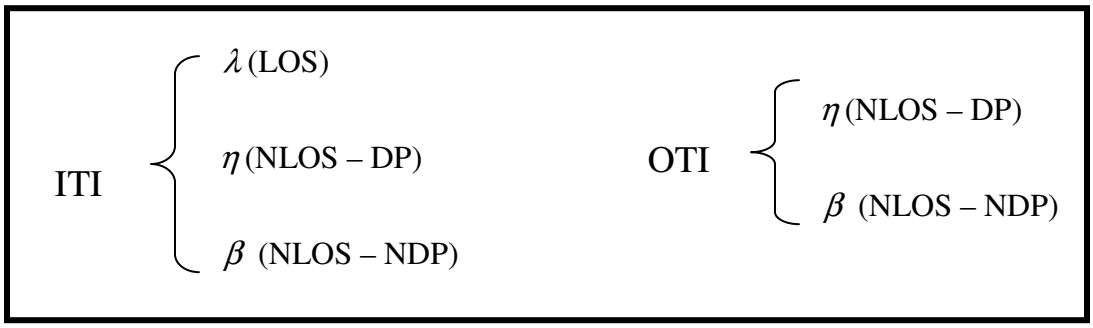

Figure 5.4: Database classification for channel identification

We are then interested in examining the conditional PDFs given by $f_\delta(\delta|\lambda)$, $f_\delta(\delta|\eta)$ and $f_\delta(\delta|\beta)$ in ITI; and $f_\delta(\delta|\eta)$ and $f_\delta(\delta|\beta)$ in OTI. This distinction is both physically sound and necessary since the characteristics of the signal propagating on an ITI range are different from those propagating on an OTI. Specifically for the latter, all the MPCs must penetrate the exterior of the building in order to reach the indoor sensor node. In practical implementation sensor nodes can identify ITI from OTI ranges by examining the node ID in the transmitted packet. We assume here that OTI anchors will have unique IDs that can be easily identified from the interior sensor nodes.

First we provide the statistical analysis of the ITI measurements. Figure 5.5 provides the results for ITI data at 500 MHz and 3 GHz.

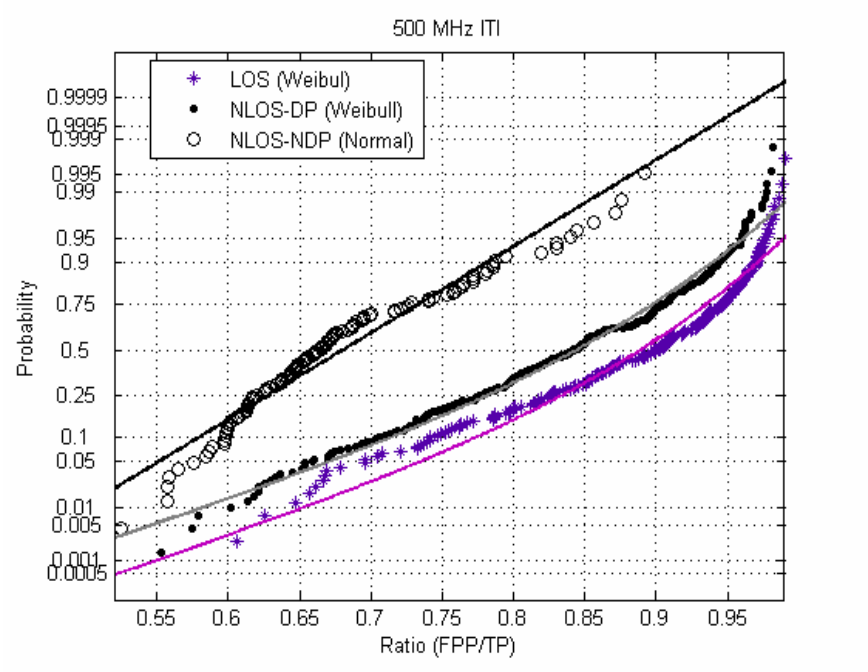

(a)

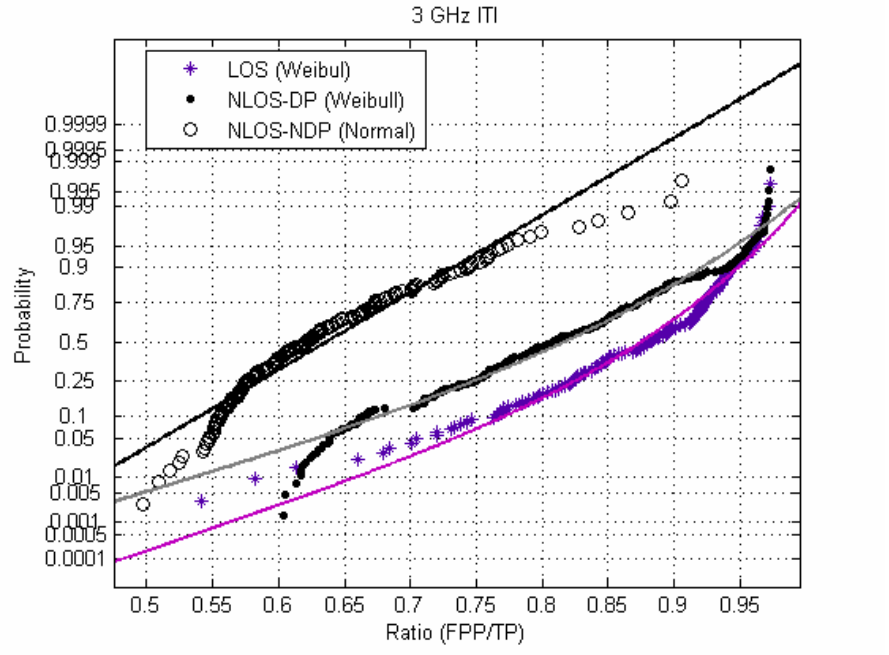

(b)

Figure 5.5: Probability plots of ITI data and their distribution fits at (a) 500 MHz and (b) 3 GHz.

The results of the distribution fitting showed that in the presence of the DP (LOS or NLOS) the ratio is best modeled by the Weibull distribution or

$$f_\delta(\delta \mid \lambda) = \frac{a_\lambda}{b_\lambda}\left(\frac{\delta}{b_\lambda}\right)^{a_\lambda - 1} \exp\left[-\left(\delta / b_\lambda\right)^{a_\lambda}\right] \tag{5.2a}$$

$$f_\delta(\delta \mid \eta) = \frac{a_\eta}{b_\eta}\left(\frac{\delta}{b_\eta}\right)^{a_\eta - 1} \exp\left[-\left(\delta / b_\eta\right)^{a_\eta}\right]. \tag{5.2b}$$

In the absence of the DP the ratio is best modeled by the normal distribution or

$$f_\delta(\delta \mid \beta) = \frac{1}{\sigma_\beta \sqrt{2\pi}} \exp\left[-\frac{\left(\delta - \mu_\beta\right)^2}{2\sigma_\beta^2}\right] \tag{5.3}$$

In order to identify the channel condition based on the ratio we implement a tertiary hypothesis testing with hard decision using the following hypotheses:

$$\begin{aligned} H_0 &: \lambda \\ H_1 &: \eta \\ H_2 &: \beta \end{aligned} \tag{5.4a}$$

$$\begin{aligned} H_0 &: \delta > th_1^{ITI} \\ H_1 &: th_2^{ITI} < \delta \le th_1^{ITI} \\ H_2 &: \delta \le th_2^{ITI} \end{aligned} \tag{5.4b}$$

In order to select the decision thresholds we refer to Figure 5.6 which illustrates the best fit distributions and the respective thresholds.

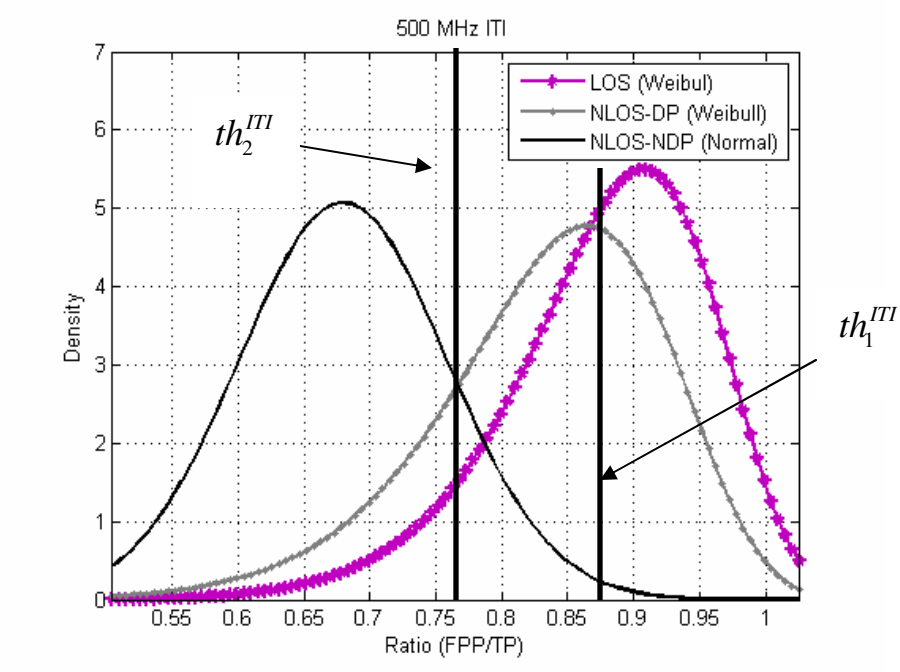

(a)

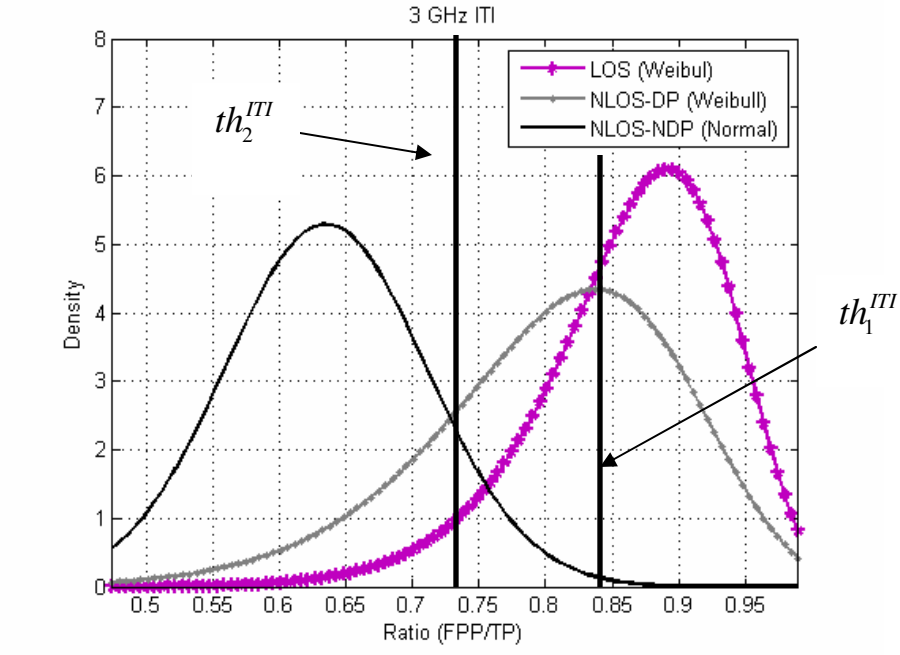

(b)

Figure 5.6: Distribution fits and the respective thresholds. (a) 500 MHz and (b) 3 GHz.

A similar analysis and decision framework can be followed for OTI ranges. The probability plots are provided in Figure 5.7. The data are best modeled by the Weibull distribution in the presence of the DP and normal in the absence and they can also be represented by (5.2b) and (5.3).

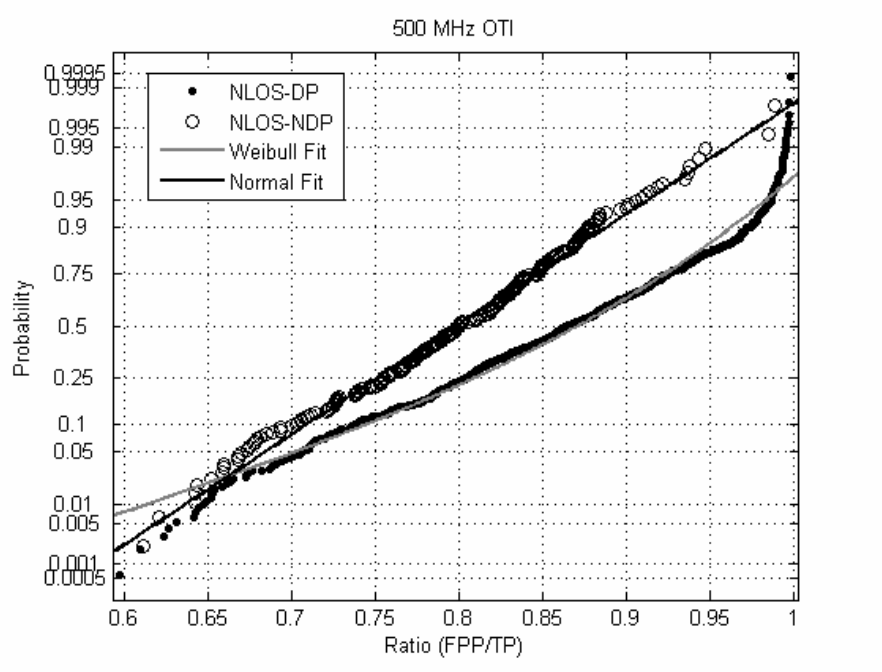

(a)

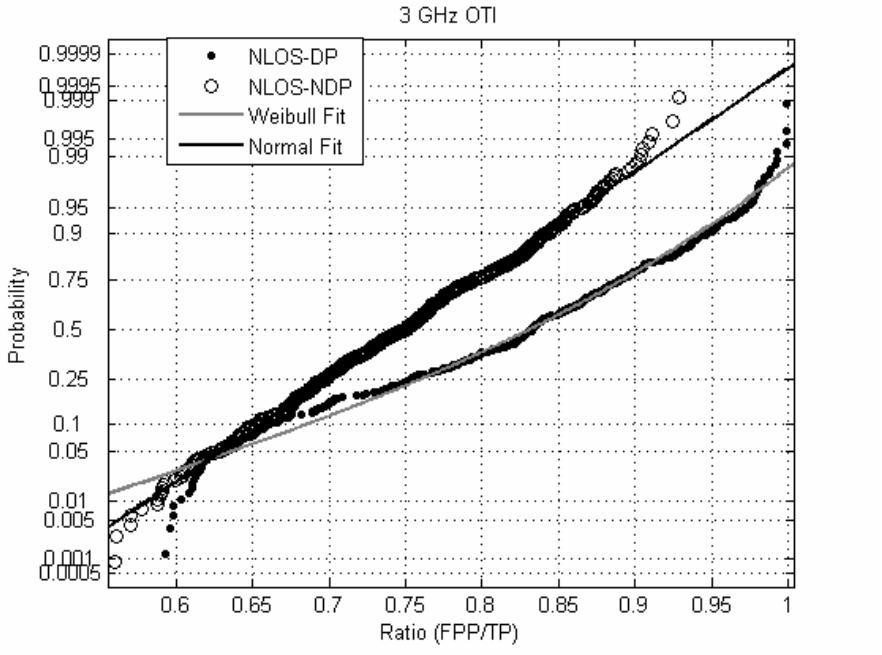

(b)

Figure 5.7: Probability plots of OTI data and their distribution fits at (a) 500 MHz and (b) 3 GHz.

In order to identify the OTI channel condition based on the ratio we implement a binary hypothesis testing with hard decision using the following hypotheses:

$$\begin{aligned} H_1 &: \eta \\ H_2 &: \beta \end{aligned} \tag{5.5a}$$

$$\begin{aligned} H_1 &: \delta > th^{OTI} \\ H_2 &: \delta \leq th^{OTI} \end{aligned} \tag{5.5b}$$

In order to select the decision thresholds we refer to Figure 5.8 which illustrates the best fit distributions and the respective thresholds.

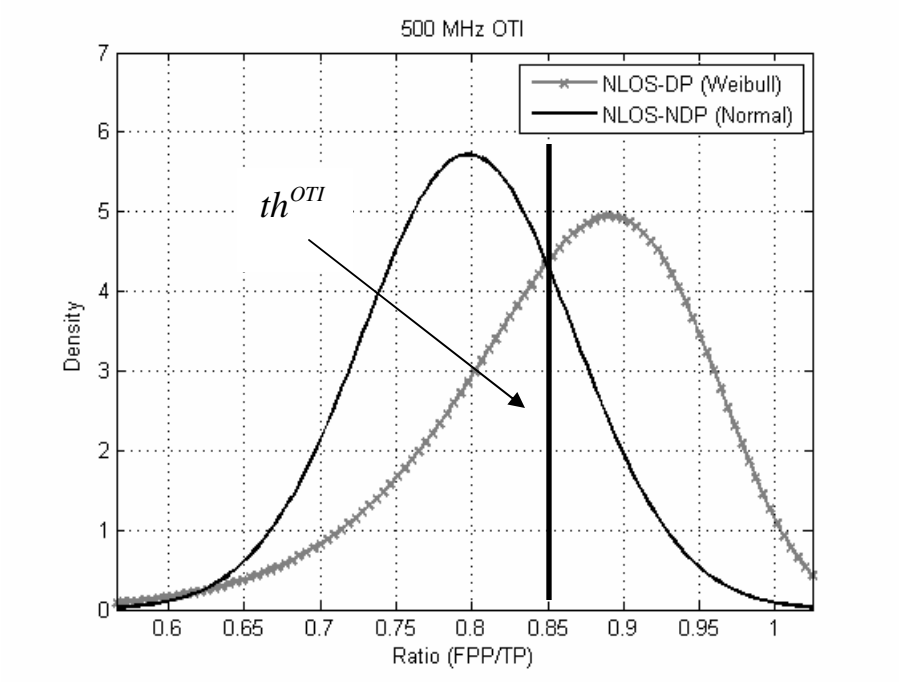

(a)

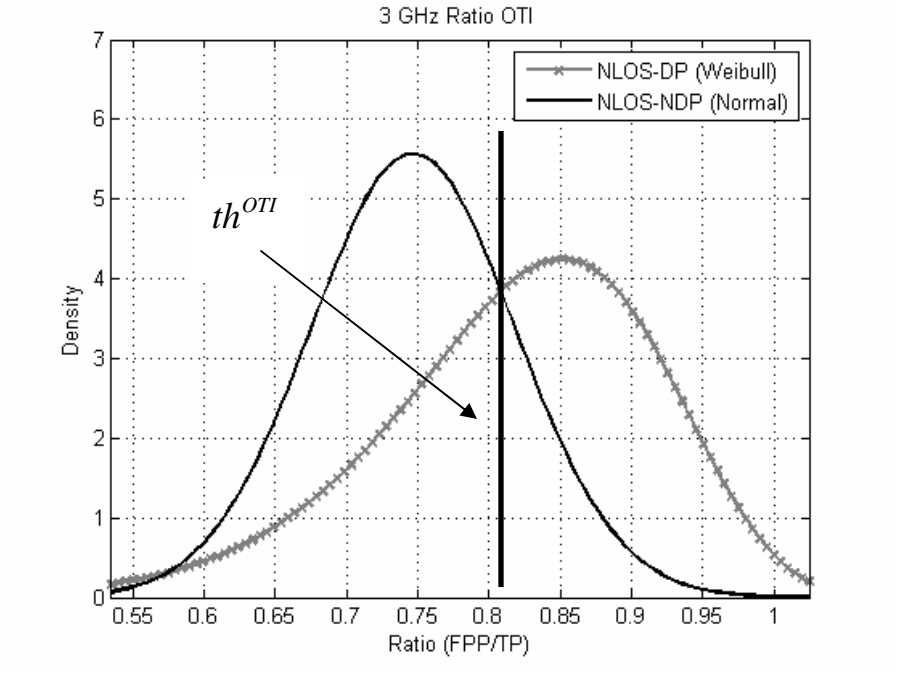

(b)

Figure 5.8: Distribution fits and the respective thresholds. (a) 500 MHz and (b) 3 GHz.

Tables 5.1 and 5.2 provide the parameters of the distributions and the respective threshold values.

Table 5.1: Distribution parameters for δ.

Scenario	Ranging Scenario	500 MHz		3 GHz	
		a	b	a	b
ITI	LOS - λ (Weibull)	0.9	13.6	0.9	14.8
	NLOS - η (Weibull)	0.87	11.3	0.85	9.94
		μ	σ	μ	σ
	NLOS - β (Normal)	0.68	0.078	0.64	0.075
		a	b	a	b
OTI	NLOS - η (Weibull)	0.019	0.029	0.002	0.015
		μ	σ	μ	σ
	NLOS - β (Normal)	0.79	0.07	0.75	0.07

Table 5.2: ITI and OTI decision thresholds

Scenario	Thresholds	500 MHz	3 GHz
ITI	th_1	0.87	0.83
	th_2	0.77	0.73
OTI	th	0.85	0.81

5.2.3. Step II: Position Estimation

Once a sensor node receives ranging measurements to at least 3 anchors (2-Dimensional positioning), the node extracts the channel parameters such as the first path power and the total signal power, distinguishes between ITI and OTI ranges, computes the ratio δ and identifies the channel conditions to each link. This information is essentially used to asses the quality of the range measurement to each anchor which is needed to adjust the *ranging weights* in the WLS which can mitigate these ranging errors associated to the ranging conditions. These ranging weights will then be combined with the anchors' *position weights* to create the final weights which get incorporated into the WLS algorithm.

In general, at a given instant in the distributed localization process, a sensor node with the coordinates $\boldsymbol{\theta}_n = (x_n, y_n)^T$ can be connected to M exterior anchors with coordinates $\boldsymbol{\theta}_m^{OTI} = (x_m, y_m)^T$ and U interior *newly* transformed anchors with coordinates $\boldsymbol{\theta}_u^{ITI} = (x_u, y_u)^T$, where $n \in [0, N]$ and $m \in [-M, 0]$ and $u \in [0, U]$, respectively. The node will receive range measurements from the respective anchors and form a range measurement vector given by $\hat{\mathbf{d}} = \left(\hat{d}_{n1}, \cdots, \hat{d}_{nM}, \hat{d}_{n1}, \cdots, \hat{d}_{nU}\right)^T$. Associated with this vector the node extracts the first path and total signal power from the ranging signals and forms the ratio vector $\boldsymbol{\delta} = (\delta_{n1}, \cdots, \delta_{nM}, \delta_{n1}, \cdots, \delta_{nU})^T$ according to (5.1). By comparing the ratio vector to the thresholds in Table 5.1 the sensor node identifies the condition of the channel be it λ (LOS), η (NLOS – DP) or β (NLOS – NDP). Once the channel is identified, the node uses the available ranging error models presented in chapter 3 to generate the de-normalized weights. In both λ (LOS) and η (NLOS – DP), the ranging error is normally distributed and as a result the weights can be obtained by the inverse of the de-normalized variance or,

$$w_{\lambda/\eta} = \frac{1}{\left(\sigma\hat{d}\right)^2}, \tag{5.6}$$

where σ is the standard deviation of the normalized ranging error and $\hat{d}$ is the biased range measurement. In the case the ranging condition is β (NLOS – NDP), the ranging error is lognormally distributed and the weight can then be obtained by the following,

$$w_\beta = \exp\left[-2\left(\mu + \log\hat{d}\right) + 2\sigma^2\right] \times \left(1 + \frac{1}{\sigma^2}\right) \tag{5.7}$$

where μ and σ are the mean and standard deviation of the normalized ranging error's logarithm and the values are presented in chapter 3.

The position weights on the other hand are obtained by the inverse of the position variance of the anchors. Original anchors (which are located outside) are assumed to have no position errors and thus zero variance. Newly transformed anchors on the other hand compute their position variance from the error covariance given by [Shi01],

$$\mathbf{C} = \left(\mathbf{H}^T \mathbf{W}^{-1} \mathbf{H}\right)^{-1} \tag{5.8}$$

and the position variance is then $\sigma_p^2 = trace\left(\mathbf{C}\right)$. In actual implementation (5.8) needs to be re-orientated and thus singular value decomposition (SVD) is usually performed before extracting σ_x^2 and σ_y^2 of the position error covariance.

The weighting matrix $\mathbf{W}$ that is used in the WLS algorithm and (5.8) is given by $\mathbf{W} = diag\left(w_1, \cdots, w_M, w_1, \cdots, w_U\right)$, where w_i is a combination of the range measurement weight w_g and the position weight w_p or formally given by

$$w_i = \frac{1}{\left(1/w_g\right) + \left(1/w_p\right)}. \tag{5.9}$$

This weighting method implies that the higher the error position variance the smaller the weight (less contribution in the overall weight and thus WLS localization). Similarly, the higher the ranging error variance the lower is the ranging weight w_g and thus the lower the weight in (5.9). This ensures that range or position incorporated into the WLS is weighed according to their respective *quality.*

In order to clarify the weighting procedure it is best to resort to a simple example. Figure 5.9 provides a localization example where node *6* is trying to obtain its localization information at the i^{th} iteration of the algorithm.

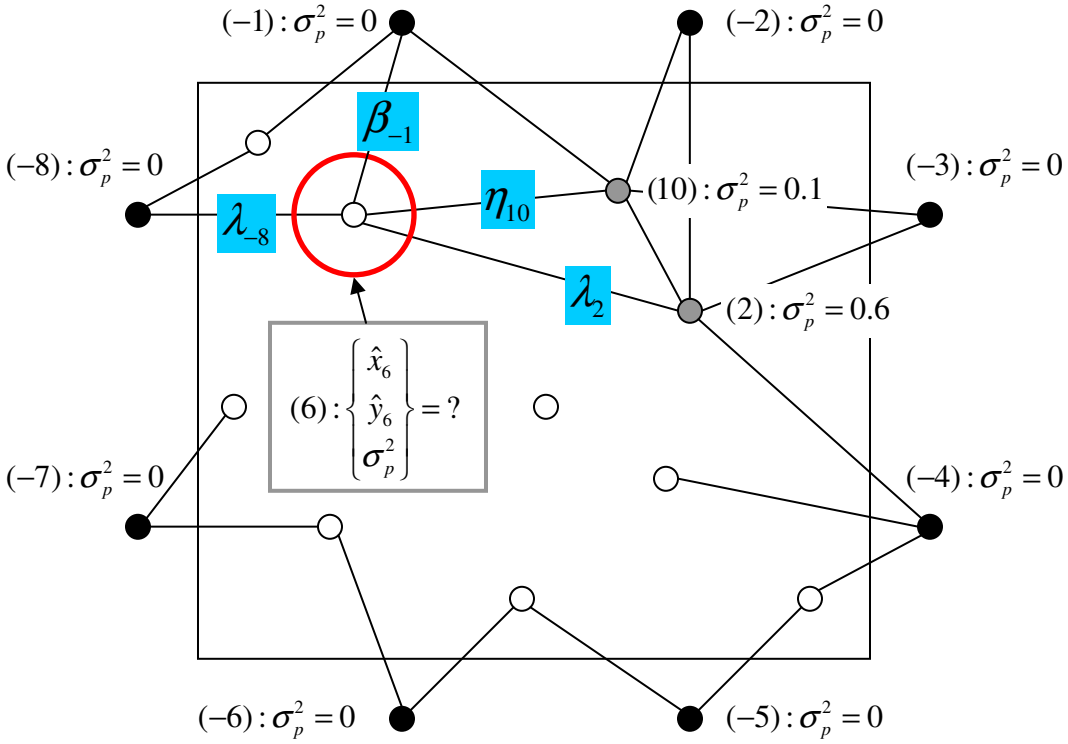

Figure 5.9: CLOQ Algorithm – Stage II position estimation. Black circles are anchors, grey circles are newly transformed anchors and white circles are un-localized sensor nodes.

In Figure 5.9, external anchors have identification numbers that are distinct from indoor nodes. Specifically, $\boldsymbol{\theta}^{OTI} = \left(x_{-1}, y_{-1}, \ldots, x_{-8}, y_{-8}\right)^T$ while the interior nodes have positive IDs. In addition note that due to initial setup we assume that the exterior anchors have a knowledge of their coordinates without any position errors, that is $\sigma_p^2(m) = 0$ where

$m \in [-8,-1]$. At any given instant during the localization process nodes can be connected to a combination of original and newly formed anchors. In the example provided in Figure 5.9, node 6 is connected to original anchors with IDs: -8 and -1; and to newly transformed anchors with IDs: 10 and 2. CLOQ algorithm provides a mechanism to estimate the location information by incorporating the statistical uncertainties of the range measurements and the anchors' position errors. According to the signal powers the node receives from the anchors (not shown here), an identification of the channel conditions leads to two LOS, one NLOS DP and one NLOS NDP. Node 6 then forms a table of this information in order to create the weights necessary for the WLS algorithm. Table 5.3 provides an overview of the connectivity information node 6 observes.

Table 5.3: Connectivity information that node 6 gathers about surrounding anchors.

Range	Channel	Range Weight	Anchor Position Weight	Final Weight
$\hat{d}_{6,-1}$	NLOS-NDP	w_β	$w_p = 1/\sigma_p^2 = \infty$	$w_{6,-1} = \frac{1}{(1/w_\beta)}$
$\hat{d}_{6,-8}$	LOS	w_λ	$w_p = 1/\sigma_p^2 = \infty$	$w_{6,-8} = \frac{1}{(1/w_\lambda)}$
$\hat{d}_{6,10}$	NLOS-DP	w_η	$w_p = 1/\sigma_p^2 = 10$	$w_{6,10} = \frac{1}{(1/w_\eta)+(1/w_p)}$
$\hat{d}_{6,2}$	LOS	w_λ	$w_p = 1/\sigma_p^2 = 1.67$	$w_{6,2} = \frac{1}{(1/w_\lambda)+(1/w_p)}$

The range weights in Table 5.3 can be obtained from (5.6) and (5.7). Also note that in this example, node 6 is connected to two original anchors (-1 and -8) and this is reflected in the final weights. Node 6 uses the weights $\mathbf{W} = diag\left(w_{6,-1}, w_{6,-8}, w_{6,10}, w_{6,2}\right)$ in the WLS to estimate its own position. For more details about the WLS algorithm please refer to chapter 2. Finally node 6 uses (5.9) to compute the covariance of the position error and

thus the position variance $\sigma_p^2(6)$. The estimated position $(\hat{x}_6, \hat{y}_6)$ and the position variance $\sigma_p^2(6)$ are then broadcast to entire WSN in order to aid the remaining sensor node in the localization process.

5.2.4. Step III: Anchor Nomination

Once a node has estimated its position coordinate and its position variance it enters into *anchor nominee* stage where it broadcasts and listens to nominee packets. The main purpose for this stage is to ensure that nominees with a very bad position estimate do not transform into anchors and thus reduce error propagation. In addition only anchor nominees broadcast, receive and forward nominee packets. Thus the other sensor nodes do not forward nominee packets. This ensures the prevention of excessive flooding of messages which can cause performance degradation. For further clarification we refer to Figure 5.10 where we assume the network is at a *j*th iteration where several anchor nominees are comparing their position variance.

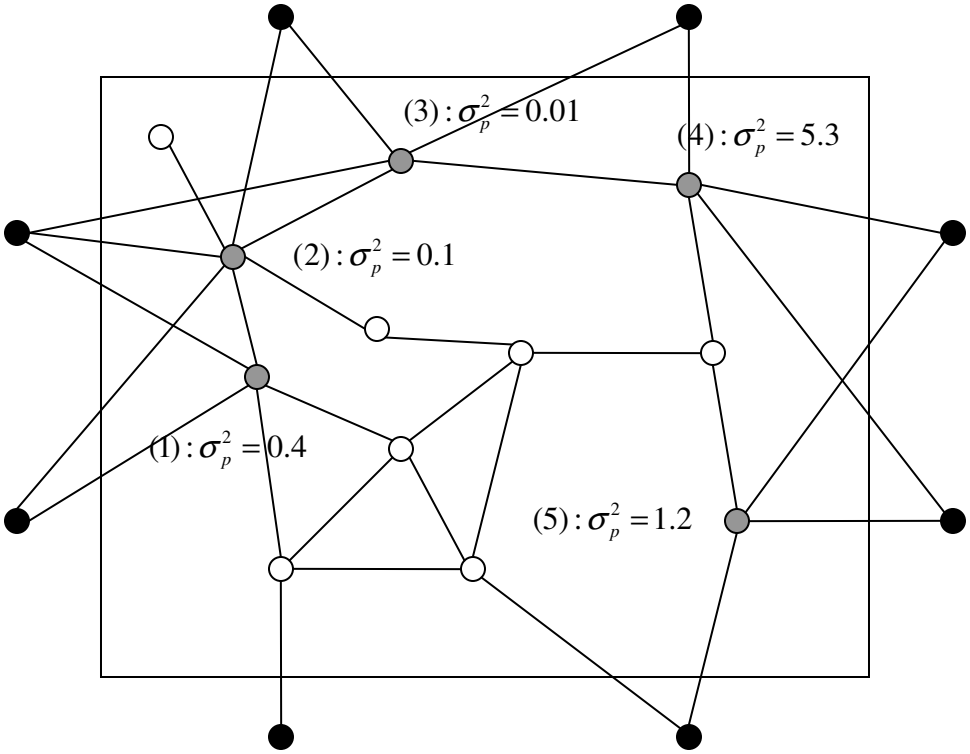

Figure 5.10: CLOQ Algorithm – Stage III Anchor Nomination. Black circles are anchor nodes, grey circles are anchor nominees and white circles are un-localized sensor nodes.

In this example, after broadcasting and forwarding, nominees 1, 2, 3 and 4 will be able to compare their quality of position estimate. Only anchor nominee 4 withdraws from the anchor transformation process, since its position variance is substantially higher than the rest. It thus has to wait for future iterations in order to transform. In addition, note that anchor nominee 5 is not connected to any other nominees. In this case it assumes it's the only one in the network and proceeds in the transformation. This approach ensures that isolated parts of the WSN will be able to localize effectively.

5.2.5. Step IV: New Anchor Incorporation

In the final stage of CLOQ algorithm all the nominees that passed stage 3 are now ready to transform into anchors. They modify the status flag into anchor flag in the transmitted packet and include their newly estimated node position and position variance information. The process then repeats until the entire network is localized. Figure 5.11 shows a diagram that summarizes the execution of CLOQ algorithm in each sensor node.

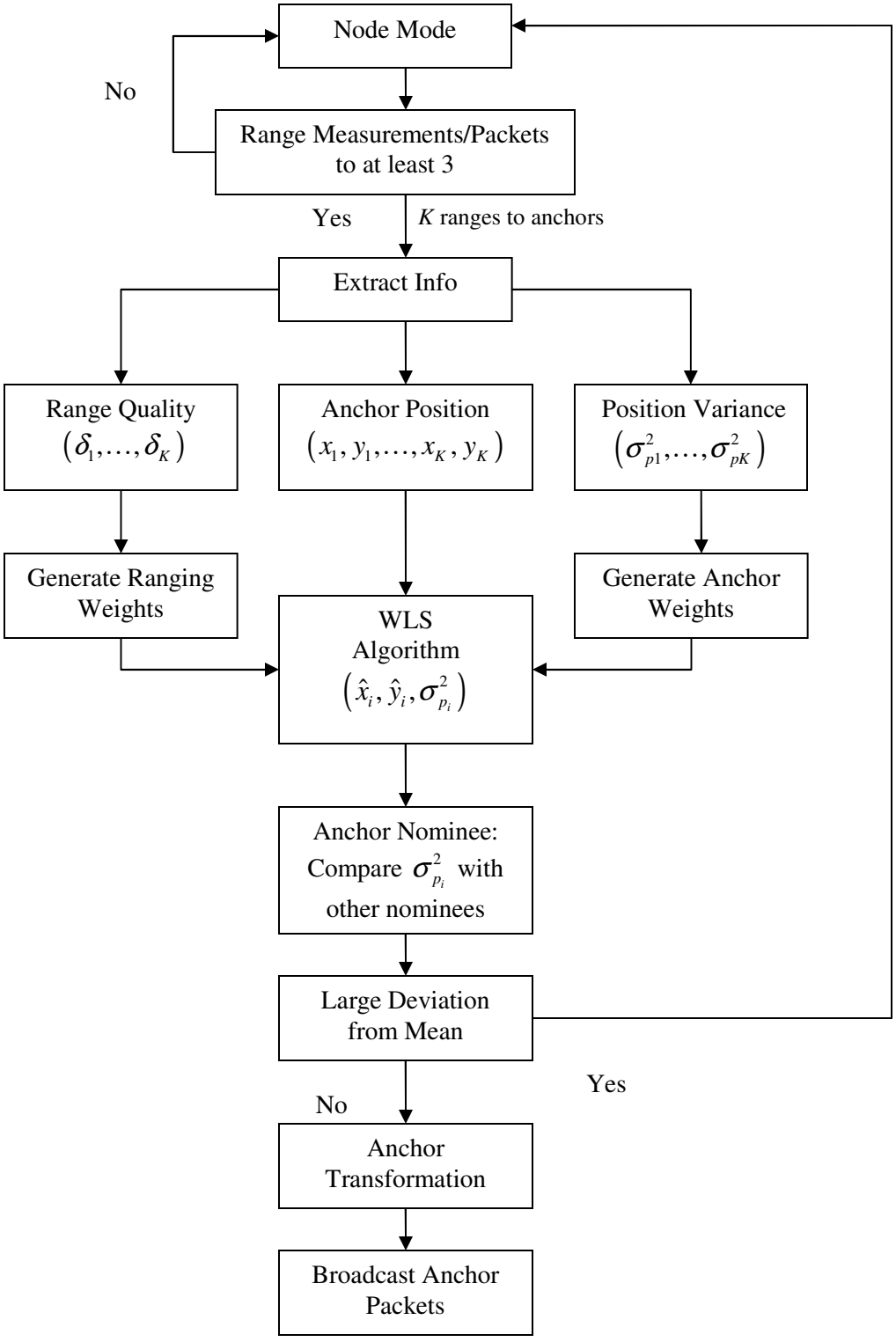

Figure 5.11: CLOQ Algorithm flow diagram

5.3. Performance Analysis

5.3.1. Simulation Setup

The simulation setup is based on the application of firefighters or soldiers requiring localization in indoor environments. *M* anchors are distributed evenly around the building where they are placed 1 m away from the exterior wall, see Fig. 4.1. *N* sensor nodes are then uniformly distributed inside the building. Connectivity is assumed between node-node and anchor-node if the respective TOA range measurements are within ITI and OTI ranging coverage, R_c^{ITI} and R_c^{OTI}, respectively. The simulations were carried out using the models from chapter 3. The dynamic range of the system, ρ, is set to 90 dB and this parameter controls the ranging coverage and the number of inter-node range measurements in the WSN. For example at 500 MHz bandwidth and 90 dB dynamic range, R_c^{ITI} will correspond roughly to 15-30 m depending on the LOS or NLOS condition and building environment. Similarly, R_c^{OTI} will be around 5-10 m depending on the building type. We set the measurement noise σ_z equal to 20 mm. For most simulations, unless otherwise stated, the probability of NLOS, $p(G=1)$, was set to 0.5. The probability of blockage, $p(X=1)=p(\zeta_2)$, however, was obtained from the measurement results in Table 3.3. The ranging conditions and the WSN inter-node connectivity are ultimately governed by the random variables G and X, see (4.1). The first path power and total signal power were simulated from the empirical pathloss models.

For the analysis of the simulations we compute the average RMS of the location error of each WSN topology. The RMSE is computed by

$$RMSE = \frac{\sqrt{tr\left(\left[\mathbf{J}^{-1}\right]_{(2\times N)\times(2\times N)}\right)}}{N} = \frac{\sqrt{\sum_{i=1}^{N}\sigma_{x_i}^2 + \sigma_{y_i}^2}}{N}, \tag{5.10}$$

where $tr(\cdot)$ is the trace operation. $\sigma_{x_i}^2$ and $\sigma_{y_i}^2$ are the diagonal elements of the ith diagonal sub-matrix of $\left[\mathbf{J}^{-1}\right]_{(2\times N)\times(2\times N)}$. The average RMSE is obtained by averaging (5.10) over the total number of topologies and simulations.

5.3.2. Node Density

In the first experiment we investigate the impact of node density. For the simulation we fixed the number of anchors to 8 and the dimension of the building to $D = 20$ m and increased the number of nodes, i.e. node density which is defined by $S = N/D^2$. 5000 Monte Carlo simulations were carried out (100 different topologies and 50 simulations per topology). The latter is needed, since the ranging conditions and WSN connectivity are governed by Bernoulli random variables G and X.

Figure 5.12 shows the results for fuller building using 3 GHz models. We have chosen one of the worst indoor building environments in order to test the ability of CLOQ in improving performance. The comparative performance of the buildings is provided in chapter 4. In addition to the CLOQ algorithm, we have simulated a typical LS distributed algorithm that doesn't have any channel or position quality incorporation. It is clear from the figure that the CLOQ algorithm mitigates ranging errors in indoor environments, improves the performance and approaches the lower bound.

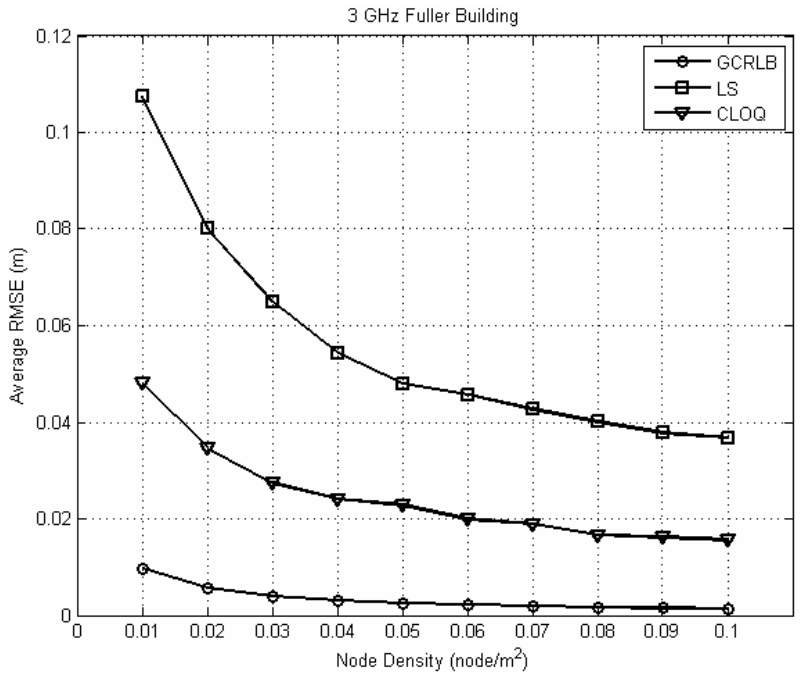

Figure 5.12: Localization Performance in Fuller Building at 3 GHz.

5.3.3. Anchor Density

In this experiment, 5000 simulations were carried out with $D = 20\,\text{m}$ and 20 nodes. The number of anchors were varied from 4 to 16 (anchors per side varies from 1 to 4). The results are presented in Figure 5.13.

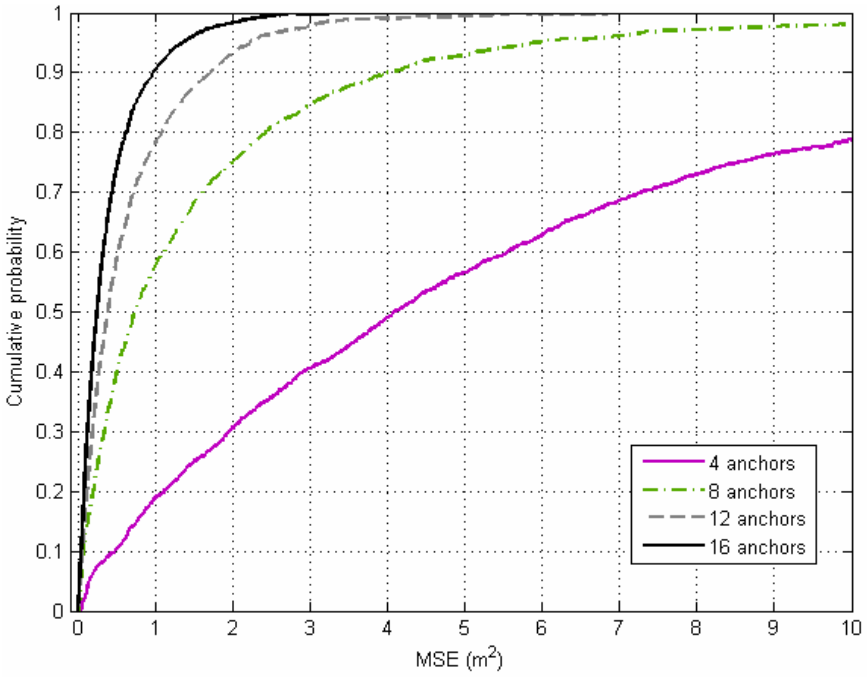

Figure 5.13: Localization Performance as a function of number of anchors.

It is evident that having only 4 anchors results in unacceptable localization performance. As the number increases to 16 anchors, 90% of the time the MSE is less than 1. This is very promising especially that the simulation results reflect the performance in Fuller building which is a harsh indoor environment. The increased number of anchors reduces the error in the initial nodes that transform into anchors and thus reduce error propagation.

Another important criterion for this type of cooperative localization scenario is the impact of large buildings on performance. In the next experiment 20 sensor nodes were deployed in an indoor environment and the building dimension was changed from 10 meters to 100 meters. In addition the number of anchors was changed from 4 to 16. 5000 Monte Carlo simulations were conducted with 100 topologies and 50 simulations per

topology. Figure 5.14 shows the percentage of un-localized nodes as a function of building dimension with different number of anchors.

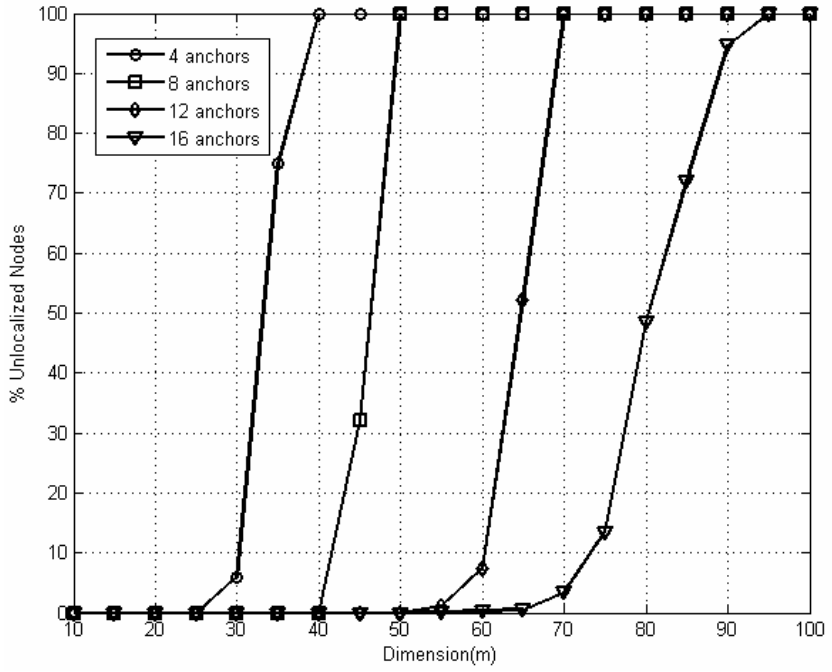

Figure 5.14: CLOQ – % of un-localized nodes as a function of building dimension.

A brief discussion regarding the practicality of CLOQ algorithm is necessary. There is a design consideration between convergence time and localization error, where the former refers to the time it takes the entire network to localize. The convergence time is essentially controlled by the method in which nodes transform into anchors. As mentioned earlier in CLOQ algorithm, anchors nominees that have large variation from the 1-hop neighbors withdraw from the localization process. An alternative method could be that only anchor nominees with the best position variance transform into anchors. Although this seems like a positive direction in controlling error propagation, simulation studies have shown that if in each iteration only one anchor nominee becomes an anchor both the convergence time and final location error increases. This occurs mainly because it takes more time to localize the entire network since a minimum number of anchor

nodes are transformed in each iteration. The increase in localization error is due to the enhanced impact of geometry induced errors on the localization process. Less anchors at each stage means a higher chance of nodes having “bad” geometry according to the GDOP mentioned earlier. This means that in each iteration it is important to maximize the number of node-anchor transformation. Even newly transformed anchors with high position variance can help to reduce geometry errors and overall position errors through the WLS approach.

Chapter 6 Conclusion & Future Work

6.1. Conclusion

In this dissertation we have described a comprehensive UWB measurement and modeling campaign that was aimed to characterize the spatial behavior of indoor TOA-based ranging. In addition we provided an analysis of cooperative localization bounds for WSNs based on empirical models of UWB TOA-based OTI and ITI ranging in indoor multipath environments. Finally we integrated the channel information and developed a novel cooperative localization algorithm CLOQ that is specifically suitable for the indoor WSNs.

The measurement and modeling involved spatial characterization. This involved analyzing and modeling the coverage and accuracy of ranging in indoor environments. The measurement involved four different building environments: residential, old office, modern office and manufacturing floor and three different ranging scenarios ITI, OTI and RTI. We showed that ranging coverage is inversely related to the bandwidth of the system and the harshness of the ranging scenario and environment. In addition, ranging error can be modeled as normal and lognormal in the presence and the absence of the DP, respectively. Furthermore, the modeling parameters are affected by the ranging scenario, environment and system bandwidth. The modeling results in this dissertation provide an experimental analysis of the physical constraints imposed by the dense cluttered indoor environments on TOA-based UWB ranging. In addition the models should help

researchers obtain localization bounds specific to indoor environments which are important to assess and evaluate the limitations facing different localization algorithms. As for cooperative localization we verified the need for such technology in applications where indoor sensor nodes lack sufficient coverage to outdoor anchor nodes. We also verified that in addition to extending coverage, cooperative localization has potential for improving accuracy. In addition we provided a comprehensive evaluation of the limitations imposed by the indoor multipath environment on cooperative localization performance in multi-hop WSNs.

Simulation results showed that increasing node density improves localization accuracy and can improve performance in indoor multipath channels. Increasing the number of anchors however has greater impact in harsh indoor environments such as office buildings due to shorter ranging coverage, i.e. less inter-node connectivity. For the ranging model parameters, localization is constrained by the ranging coverage, statistics of ranging error, probability of NLOS, probability of DP blockage and bandwidth. In general, office building structures introduce higher probability of NLOS/DP blockage and shorter ranging coverage (higher DP penetration loss and pathloss exponent) which means higher localization error. Manufacturing floors and residential buildings on the other hand exhibit better performance due to "lighter" indoor channel conditions. Also, increasing the system bandwidth, although reduces ranging coverage, has the effect of improving accuracy. The localization performance in office buildings exhibited less sensitivity to changes in bandwidth because the range measurements faced harsher obstacles such as metallic doors, vending machines and elevators. As for the cooperative localization application for firefighter or military operations, it is clear that in order to

improve accuracy numerous nodes must be deployed in the indoor environment alongside those attached to the personnel. In addition to providing the necessary network density required for effective localization, these stationary nodes can constantly provide ranging/localization information which further improves performance in dense cluttered environments.

Finally simulation results of the CLOQ algorithm showed that incorporating the quality of the range and position estimation can substantially improve the localization performance in WSNs.

6.2. Future Work

As we have seen throughout the dissertation, TOA-based ranging and localization face many challenges in indoor environments. Potential applications that require high localization accuracy need novel techniques in localization. One of the most promising alternatives is cooperative localization in WSNs using UWB signals. The UWB signals have shown to be able to combat multipath error in indoor environments, while cooperative localization mitigates the channel impairments and further extends the coverage of the anchor nodes.

Future work in this area should continue the measurements and modeling in order to analyze the ranging error beyond ranging coverage. Specifically the behavior of the biases and measurement time variations with distance must be evaluated for different ranging scenarios and environments. In addition the analysis of cooperative localization must extend the analysis to 3-dimensions where RTI ranging can provide coverage extension to multi-floor buildings.

Also research in localization algorithms for indoor-specific WSNs is needed to identify and mitigate NLOS biased range measurements in order to achieve acceptable localization performance. It would be therefore pertinent for nodes to be able to range and localize with precise information regarding the channel conditions.

Another important research direction is analyzing and characterizing error propagation in WSN localization. One of the major problems to accurate localization in iterative distributed algorithms is error propagation. Algorithms must therefore be able to incorporate methodologies which can help in controlling or even reducing error propagation so that nodes on the edge of networks do estimate reliable position information.

References

[Aky02] I. Akyildz, W. Su, Y. Sankarasubramaniam and E. Cayirci, "A survey on sensor networks", *IEEE Communications Magazine,* vol. 40, no. 8, pp. 102-114, Aug. 2002.

[Ala03a] B. Alavi, K. Pahlavan, "Bandwidth effect on distance error modeling for indoor geolocation", *IEEE Proceeding on Personal, Indoor and Mobile Communications,* vol. 3, pp. 2198-2202, Sept. 2003.

[Ala03b] B. Alavi, K. Pahlavan, "Modeling of the distance error for indoor geolocation", *IEEE Wireless Communications and Networking Conference (WCNC),* vol. 1, pp. 668-672, March 2003.

[Ala05] B. Alavi and K. Pahlavan, "Analysis of undetected direct path in time of arrival based UWB indoor geolocation", *in Proceedings of the IEEE Vehicular Technology Conference,* vol. 4, pp. 2627-2631, Dallas, TX, USA, September, 2005.

[Ala06] B. Alavi, K. Pahlavan, "Modeling of the TOA-based distance measurement error using UWB indoor radio measurements", *IEEE Communications Letters,* vol. 10, no. 4, pp. 275-277, April 2006.

[Alb01] J. Albowicz, A. Chen and L. Zhang, "Recursive position estimation in sensor networks", in *Proc. of 2001 IEEE International Conference on Network Protocols* (ICNP'01), Riverside, CA, pp. 35-41, Nov. 2001.

[Alj04] S. Al-Jazzar, "Algorithms and parameter estimation for radiolocation in NLOS environments", Ph.D. dissertation, University of Cincinnati, Cincinnati, OH, 2004.

[Als06a] N. Alsindi, K. Pahlavan, B. Alavi and X. Li, "A novel cooperative localization algorithm for indoor sensor networks", in *Proc. of 2006 IEEE International Symposium on Personal Indoor and Mobile Radio Communications* (PIMRC '06), Helsinki, Finland, pp. 1-6, Sept. 2006.

[Als06b] N. Alsindi, K. Pahlavan, B. Alavi, "An error propagation aware algorithm for precise cooperative indoor localization", *in Proc. of IEEE Military Communications Conference* (MILCOM), Washington D.C., pp. 1-7, October, 2006.

[Als07a] N. Alsindi, B. Alavi, K. Pahlavan, "Empirical pathloss model for indoor geolocation using UWB measurements", *IEE Electronic Letters,* vol. 43, no. 7, pp. 370-372, March 2007.

[Als07b] N. Alsindi, B. Alavi, K. Pahlavan, "Spatial characteristics of UWB TOA-based ranging in indoor multipath environments" in *Proc. of IEEE International Symposium on Personal Indoor and Mobile Radio Communications (PIMRC) '07,* Athens, Greece, pp. 1-6, Sept. 2007.

[Als08a] N. Alsindi, B. Alavi, K. Pahlavan, "Measurement and modeling of UWB TOA-based ranging in indoor multipath environments", accepted manuscript to be published in *IEEE Transactions on Vehicular Technology*, 2008.

[Als08b] N. Alsindi, K. Pahlavan, "Cooperative localization bounds for indoor ultra

wideband sensor networks", *EURASIP ASP special issue on Cooperative Localization in Wireless Ad Hoc and Sensor Networks*, vol. 2008, article ID 852509, pp. 1-13, April 2008.

[Als08c] N. Alsindi, M. Heidari and K. Pahlavan, "Blockage identification in indoor UWB TOA-based ranging using Multi Band OFDM signals", *in Proc. IEEE Wireless Communications and Networking Conference,* Las Vegas, NV, April 2008.

[Als08d] N. Alsindi and K. Pahlavan, "Node Localization", *Wireless Sensor Networks: A Networking Perspective,* Wiley – IEEE Press, to appear, 2008.

[Bah00a] P. Bahl and V. Padmanabhan, "RADAR: an in-building RF-based user location and tracking system," in *Proceedings of 19th Annual Joint Conference of the IEEE Computer and Communications Societies (INFOCOM),* vol. 2, Tel Aviv, Israel, March 2000, pp. 775-784.

[Bah00b] P. Bahl, V. Padmanabhan and A. Balachandran, "*Enhancements to the RADAR User Location and Tracking System,"* Tech. Rep. MSR-TR-00-12, Microsoft Research, Feb. 2000.

[Ber04] J. Berlant, Y. Goegebeur, J. Segers, J. Teugels, *Statistics of Extremes: Theory and Applications,* Wiley, 2004.

[Bet04] A. Betra, et. Al, Multi-band OFDM Physical Layer Proposal for IEEE 802.15 Task Group 3a, Sept. 2004.

[Bot04] C. Botteron, A. Host-Madsen and M. Fattouche, "Effects of system and environment parameters on the performance of network-based mobile

station position estimators", *IEEE Transactions on Vechicular Technology,* vol. 53, no. 1, pp. 163-180, Jan. 2004.

[Cha06] C. Chang and A. Sahai, "Cramer-Rao-type bounds for localization", *EURASIP Journal on Applied Signal Processing*, vol. 2006, article ID 94287, pp. 1-13, 2006.

[Caf98] J. Caffery and G. Stuber, "Subsriber location in CDMA cellular networks", *IEEE Transactions on Vehicular Technology,* vol. 47, no. 2, pp. 406-416, May 1998.

[Cas88] E. Castillo, *Extreme Value Theory in Engineering,* New York: Academic, 1988.

[Che99] P. –C Chen, "A non-line-of-sight error mitigation algorithm in location estimation," *IEEE Wireless Communications and Networking Conference (WCNC' 99)*, New Orleans, LA, USA, Sept. 1999, pp. 316-320.

[Cho05] C.-C. Chong, S.K. Yong, "A generic statistical-based UWB channel model for high-rise apartments", *IEEE Transactions on Antennas and Propagation,* vol. 53, no. 8, pp. 2389-2399, Aug. 2005.

[Chu03] W.C. Chung and D. Ha, "An accurate ultra wideband ranging for precision asset location", *IEEE Conference on Ultra Wideband Systems and Technologies (UWBST),* pp. 389-393, Nov. 2003.

[Den04] B. Denis, and N. Daniele, "NLOS ranging error mitigation in a distributed positioning algorithm for indoor UWB ad-hoc networks", in *Proc. of IEEE International Workshop on Wireless Ad-hoc Networks (IWWAN),* pp. 356-360, Oulu, Finland, May-Jun. 2004.

[Dum94] L. Dumont, M. Fattouche and G. Morrison, "Super-resolution of multipath channels in a spread spectrum location system", *IEE Electronic Letters,* vol. 30, no. 19, pp. 1583-1584, Sept. 1994.

[Dur98] G. Durgin, T.S. Rappaport and H. Xu, "Measurements and models for radio pathloss and penetration loss in and around homes and trees at 5.85 GHz", *IEEE Transactions on Communications,* vol. 46, no. 11, pp. 1484-1496, Nov. 1998.

[Fal06] C. Falsi, D. Dardari, L. Mucchi and M.Z. Win, "Time of arrival estimation for UWB Localizers in realistic environments", *EURASIPJournal on Applied Signal Processing,* vol. 2006, article ID 32082, pp. 1-13, 2006.

[Fon02] R. J. Fontana and S. J Gunderson, "Ultra-wideband precision asset location system", in *Proc. of IEEE Conference on UWB Systems and Technolgies (UWBST),* Baltimore, MD, May 2002, pp.147-150.

[Gha04] S.S. Ghassemzadeh, R. Jana, C.W. Rice, W. Turin and V. Tarokh, "Measurement and modeling of an ultra-wide bandwidth indoor channel", *IEEE Transactions on Communications,* vol. 52, no. 10, pp. 1786-1796, Oct. 2004.

[Ghav04] M. Ghavami, L.B. Michael and R. Kohno, *Ultra-wideband Signals and Systems in Communication Engineering,* Wiley, Hoboken, NJ, 2004.

[Guv07] I. Guvenc, C.-C. Chong and F. Watanabe, "NLOS identification and mitigation for UWB localization systems" *IEEE Wireless Communications and Networking Conference (WCNC) '07,* pp. 1571-1576, Hong Kong, China, March 11-15 2007.

[Gez05] S. Gezici, Z. Tian, G.B. Giannakis, H. Kobayashi, A.F. Molisch, H.V. Poor and Z. Sahinoglu, "Localization via ultra-wideband radios: a look at positioning aspects for future sensor networks," *IEEE Signal Processing Magazine,* vol. 22, no. 4, pp. 70-84, July 2005.

[Hat06] A. Hatami, K. Pahlavan, M. Heidari and F. Akgul, "On RSS and TOA based indoor geolocation – a comparative performance evaluation", *in Proceedings of the IEEE Wireless Communications and Networking Conference (WCNC),* vol.4, pp. 2267-2272, Las Vegas, NV, USA, April 2006.

[Hei07] M. Heidari, F.O. Akgul and K. Pahlavan, "Identification of the absence of direct path in indoor localization systems" in *Proc. IEEE International Symposium on Personal Indoor and Mobile Radio Communications (PIMRC) '07,* Athens, Greece, pp. 1-6, Sept. 2007.

[How90] S. J. Howard and K. Pahlavan, "Measurement and Analysis of the indoor Radio Channel in the Frequency Domain", *IEEE Transactions on Instrumentation and Measurements,* no. 39, pp. 751-55, Oct. 1990.

[Jai01] R. Jain, A. Puri, and R. Sengupta, "Geographical routing using partial information for wireless ad hoc networks," *IEEE Personal Communications Magazine,* vol. 8, no. 1, Feb. 2001, pp. 48-57.

[Jou06b] D.B. Jourdan, D. Dardari and M.Z. Win, "Position error bound and localization accuracy outage in dense cluttered environments", in *Proceedings of IEEE International Conference on Ultra-Wideband,* pp. 519-524, Boston, MA, USA, Sept. 2006.

[Jou06a] D.B. Jourdan, D. Dardari and M.Z. Win, "Position error bound for UWB localization in dense cluttered environments", in *Proceedings of IEEE Int'l Conf. on Commun. (ICC) '06,* vol. 8, pp. 3705-3710, Istanbul, Turkey, June, 2006.

[Kap96] E.D. Kaplan, *Understanding GPS: Principles and Applications,* Artech House, Norwood, MA, 1996.

[Kay93] S.M. Kay, *Fundementals of Statistical Signal Processing: Estimation Theory,* Prentice Hall, Upper Saddle River, New Jersey, 1993.

[Ko98] Y. Ko and N.H. Vaidya, "Location-aided routing (LAR) in mobile adhoc networks," in *Proceedings of the Association for Computing Machinery (ACM)/IEEE Mobile Computing and Networking (MOBICOM),* Dallas, TX, Oct. 1998, pp. 66-75.

[Koo98] H. Koorapaty, H. Grubeck and M. Cedervall, "Effect of biased measurement errors on accuracy of position location methods", in *IEEE Global Communications Conference (GLOBECOMM) '98,* vol. 3, pp. 1497-1502, 1998.

[Kos00] H. Koshima and J. Hoshen, "Personal locator services emerge", *IEEE Spectrum,* vol. 37, no. 2, Feb. 2000. pp. 41-48.

[Kri99] P. Krishnamurthy and K. Pahlavan, "Radio propagation modeling for indoor geolocation applications," in *Proceedings of IEEE Personal, Indoor and Mobile Radio Communications, PIMRC'99*, Kyoto, Japan, pp. 446-450, Sept. 1999.

[Lar04] E.G. Larsson, "Cramer-Rao bound analysis of distributed positioning in

sensor networks", *IEEE Signal Processing Letters,* vol. 11, no. 3, pp. 334-337, March 2004.

[Li04] X. Li and K. Pahlavan, "Super-resolution TOA estimation with diversity for indoor geolocation", *IEEE Transactions on Wireless Communications*, vol. 3, no. 1, pp. 224-234, Jan. 2004.

[Lee02] J.-Y. Lee and R.A. Scholtz, "Ranging in a dense multipath environment using an UWB radio link", *IEEE Transactions on Selected Areas in Communications,* vol. 20, no. 9, pp.1677-1683, Dec. 2002.

[Lee06] J.-Y. Lee and S. Yoo, "Large error performance of UWB ranging in multipath and multiuser environments", *IEEE Transactions on Microwave Theory and Techniques,* vol. 54, no. 4, pp. 1887-1895, April 2006.

[Low05] Z.N. Low, J.H. Cheong, C.L. Law, W.T. Ng and Y.J. Lee, "Pulse detection algorithm for line-of-sight (LOS) UWB ranging applications", *IEEE Antennas and Wireless Propagation Letters,* vol. 4, pp. 63-67, 2005.

[Mar05] S. Markose, A. Alentorn, "Option pricing and the implied tail index with the generalized extreme value distribution", *Computing in Economics and Finance*, 396, Society for Computation Economics, 2005.

[McG02] J. McGeough, "Wireless location positioning based on signal propagation data", White Paper, http://www.wirelessdevnet.com/software/, 2002.

[Mis02] P. Misra and P. Enge, *Global Positioning System: Signals, Measurements and Performance,* Ganga-Jamuna Press, Lincoln, MA, 2002.

[Mol05] A.F. Molisch, "Ultrawideband propagation channel-theory, measurement and modeling", *IEEE Transactions on Vehicular Technology,* vol. 54, no.

5, pp. 1528-1545, Sept. 2005.

[Muq06] A. Muqaibel, A. Safaai-Jazi, A. Attiya, B. Woerner and S. Riad, "Path-loss and time dispersion parameters for indoor UWB propagation", *IEEE Transactions on Wireless Communications,* vol. 5, no. 3, pp. 550-559, March 2006.

[Nic01] D. Niculescu and B. Nath, "Ad-hoc positioning system", in *Proc. of 2001 IEEE Global Communications Conference* (Globecomm '01), San Antonio, TX, pp. 2926-2931, Nov. 2001.

[Opp04] I. Oppermann, M. Hamalainen and J. Iinatti, *UWB Theory and Applications,* Wiley, Hoboken, NJ, 2004.

[Pah98] K. Pahlavan, P. Krishnamurthy and J. Beneat, "Wideband radio propagation modeling for indoor geolocation applications," *IEEE Communications Magazine*, vol. 36, no. 4, pp. 60-65, April 1998.

[Pah00] K. Pahlavan, P. Krishnamurthy, A. Hatami, M. Ylianttila, J. Makela, R. Pichna and J. Vallstrom, "Handoff in hybrid mobile data networks (invited paper)," *IEEE Personal Communications Magazine,* vol. 7, no. 2, Apr. 2000, pp. 34-47.

[Pah02] K. Pahlavan, X. Li, and J. Makela, "Indoor geolocation science and technology," *IEEE Communications Magazine*, vol. 40, no. 2, pp. 112-118, Feb. 2002.

[Pah05] K. Pahlavan, A. H. Levesque, *Wireless Information Networks*, 2nd edition, John Wiley, 2005.

[Pah06] K. Pahlavan, F.O. Akgul, M. Heidari, A. Hatami, J.M. Elwell and R.D. Tingley, "Indoor geolocation in the absence of the direct path", *IEEE Wireless Communications Magazine,* vol. 13, no. 6, pp. 50-58, Dec. 2006.

[Pat03] N. Patwari, A.O. Hero, M. Perkins, N.S. Correal and R.J. O'Dea, "Relative location estimation in wireless sensor networks", *IEEE Transactions on Signal Processing,* vol. 51, no. 8, pp. 2137-2148, August, 2003.

[Pat05] N. Patwari, J.N. Ash, S. Kyperountas, A. O. Hero, R. L. Moses and N. S. Correal, "Locating the nodes: cooperative localization in wireless sensor networks", *IEEE Signal Processing Magazine,* vol. 22, no. 4, pp. 54-69, July 2005.

[Por03] D. Porcino and W. Hirt, "Ultra-wideband radio technology: potential and challenges ahead", *IEEE Communications Magazine,* vol. 41, no. 7, pp. 66-74, July 2003.

[Pot00] G.J. Pottie and W.J. Kaiser, "Wireless integrated network sensors," *Communications of the Association for Computing and Machinery (ACM),* vol. 43, no. 5, May 2000, pp. 51-58.

[Qi06] Y. Qi, H. Kobayashi, H. Suda, "Analysis of wireless geolocation in a non-line-of-sight environment", *IEEE Transactions on Wireless Communications*, vol. 5, no. 3, pp. 672-681, March 2006.

[Roo02a] T. Roos, P. Myllymaki, H. Tirri, P. Miskangas and J. Sievanen, "A probabilistic approach to WLAN user location estimation," *International*

Journal of Wireless Information Networks, vol. 9, no. 3, Jul. 2002, pp. 155-164.

[Roo02b] T. Roos, P. Myllymaki and H. Tirri, "A statistical modeling approach to location estimation," *IEEE Transactions on Mobile Computing,* vol. 1, no. 1, pp. 59-69, Jan. 2002.

[Sav05] A. Savvides, W.L. Garber, R.L. Moses and M.B. Srivastava, "An analysis of error inducing parameters in multihop sensor node localization", *IEEE Transactions on Mobile Computing,* vol. 4, no. 6, pp. 567-577, Dec. 2005.

[Savr01] C. Savarese, J.M. Rabaey and J. Beutel, "Locationing in distributed ad-hoc wireless sensor networks", in *Proc. of 2001 International Conference on Acoustics, Speech and Signal Processing* (ICASSP'01), Salt Lake City, UT, May 2001, pp. 2037-2040.

[Savr02] C. Savarese, K. Langendoen, and J. Rabaey, "Robust positioning algorithms for distributed ad-hoc wireless sensor networks", in *Proce. Of USENIX Technical Annual Conference,* Monterrey, CA, Jun. 2002, pp. 317-328.

[Shi01] D. Shin, T. Sung, "Analysis of positioning errors in radionavigation systems", *in Proceedings of IEEE Intelligent Transmission Systems Conference,* pp. 156-159, Oakland, CA, USA, August 2001.

[Siw03] K. Siwiak, H. Bertoni, and S.M. Yano, "Relation between multipath and wave propagation attenuation", *IEE Electronic Letters,* vol. 39, no. 1, pp. 142-143, Jan. 2003.

[Sma00] A. Smailagic and D. Koan, “Location sensing and privacy in a context-aware computing environment,” *IEEE Transactions on Wireless Communications,* vol. 9, no. 5, Oct. 2000, pp. 10-17.

[Spi01] M. Spirito, “On the accuracy of cellular mobile station location estimation,” *IEEE Transactions on Vehicular Technology,* vol. 50, no. 3, May 2001, pp. 674-684.

[Tar06] Z. Tarique, W.Q. Malik and D.J. Edwards, “Bandwidth requirements for accurate detection of direct path in multipath environment”, *IEE Electronic Letters,* vol. 42, no. 2, pp. 100-102, Jan. 2006.

[Van68] H.L. Van Trees, *Detection, Estimation and Modulation Theory, Part I.* John Wiley & Sons, Inc., 1968.

[Ven07a] S. Venkatesh and R.M. Buehrer, “NLOS mitigation using linear programming in ultra wideband location-aware networks”, *IEEE Transactions on Vehicular Technology,* vol. 56, no. 5, pp. 3182-3198, Sept. 2007.

[Ven07b] S. Venkatesh and R.M. Buehrer, “NLOS identificaiton in ultra-wideband systems based on received signal statistics”, *IET Microwave, Antennas and Propagation,* vol. 1, no. 6, pp. 1120-1130, Dec. 2007.

[Wei05] W. Wei, X. J.- Yu, Z. Z.- Liang, “A new NLOS error mitigation algorithm in location estimation”, *IEEE Transactions on Vehicular Technology,* vol. 54, no. 6, pp. 2048-2053, Nov. 2005.

[Wer98] J. Werb and C. Lanzl, “Designing a positining system for finding things and people indoors,” *IEEE Spectrum,* vol. 35, no. 9, Sept. 1998, pp. 71-78.